ALPINE AND SUBALPINE LANDSCAPE RESPONSE TO POST-GLACIAL CLIMATE CHANGE IN THE SAN JUAN MOUNTAINS: A COMPARISON OF NEW LANDSCAPE AND CLIMATE RECORDS

by

Bradley Gordon Johnson

A dissertation submitted to the faculty of
The University of North Carolina at Charlotte
in partial fulfillment of the requirements
for the degree of Doctor of Philosophy in
Infrastructure and Environmental Systems

Charlotte

2010

_____
Martha Cary Eppes

_____
John A. Diemer

_____
Matthew W. Parrow

_____
Matthew D. Eastin

_____
Kent E. Curran

ABSTRACT

BRADLEY GORDON JOHNSON. Alpine and sub-alpine landscape response to post-glacial climate change in the San Juan Mountains: A comparison of new landscape and climate records. (Under the direction of DR. MARTHA CARY EPPES)

Post-glacial interactions between climate, landscapes, and soils remain poorly understood, especially in alpine and sub-alpine areas. Here, I aim to increase understanding of the dynamic interactions between climate, landscape evolution, and soil development by compiling detailed records of all three. First, pollen assemblages, diatom assemblages, and sedimentology from Cumbres Bog in the southern San Juan Mountains of Colorado provide a record of climate change since the end of the Last Glacial Maximum (LGM, 16-22 ka regionally). Next, geomorphic mapping in the upper Conejos River Valley of the San Juan Mountains provides evidence of incision and aggradation that has occurred since the end of the LGM. Lastly, nineteen soils, examined for particle size, Fe extractions, and organic carbon, provide a chronosequence across multiple parent materials.

The Cumbres Bog record provides strong evidence of: cooling during the Younger Dryas (~12.8-11.5 ka), generally warm, stable climate until 6 ka, and cooler, more variable climate after 6 ka. Additionally, pollen ratios and fossil diatoms indicate that cold periods generally match with previously identified periods of rapid climate change and occurred at 10.6, 8.7-7.9, 7.0-6.9, 5.4–5.2, 3.3–3.0, 2.3, 2.0 and 1.5 ka. This record also adds resolution to previous regional records and indicates that the periodicity of climate change changed from 2,000-3,000 years during the interval from 11.5-6 ka to 700-1,100 years for the interval from 6-3.5 ka, then to <500 years after 3.5 ka. These changes correspond with increased El Niño-Southern Oscillation (ENSO) activity after the mid-Holocene (~6 ka).

The upper Conejos River Valley appears to have undergone three distinct periods of aggradation. The first occurred during the Pleistocene-Holocene transition (~12.5 – 9.5 ka) and is interpreted as paraglacial landscape response to deglaciation after the LGM. Evidence of the

second period of aggradation is limited but indicates a small pulse of sedimentation at ~ 6 ka. A third, more broadly identifiable period of sedimentation occurred in the Late Holocene (~2.2 – 1 ka). The latest two periods of aggradation are concurrent with the ENSO related increases to the frequency of climate change. This suggests that Holocene alpine and sub-alpine landscapes respond more to rapid ENSO-driven changes in climate than to large singular climatic swings. More specifically, it is likely that landscapes respond to the strengthened ENSO indicated by increased frequency of climate change. Soil development and radiocarbon dating indicate that hillslopes were stable during the Holocene even while aggradation was occurring in valley bottoms. Thus, we can conclude that erosion does not occur equally throughout the landscape but is focused above headwater streams, along tributary channels, or on ridgetops.

Lastly, the soil chronosequences indicate that ratios of oxalate/dithionite Fe extractions exhibit a robust trend with age for all soils. The relationship between extractable iron and time is in contrast with other soil properties, such as reddening, profile thickness, and clay content, which are not good indicators of age. Variation in eolian deposition and parent material sedimentology likely led to the observed variability in soils of similar age.

ACKNOWLEDGEMENTS

I want to thank everybody for making this dissertation what it is and supporting me since I started college 11 years ago. Christa, thanks for your all your support through 6 years of degrees and marriage. You have rarely hesitated when I have asked for support of moving, field work, working weekends, etc. Thanks again. Mom and Dad, thanks for all of your support of Christa and me as we have progressed through the early stages of our live together. Thanks for all you have done.

I also want to thank my dissertation committee. The final product presented here would not have been well developed had it not been for discussion and debates between Missy and myself. I also thank Missy for providing solutions to problems when work was at its most frustrating. John needs to be thanked for the many times he has sat quietly and listened to months of work synthesized into arguments in order to provide thoughtful, clear feedback. I want to thank Matt and Matt for sticking by this project even when I disappeared for weeks or months at a time. Thanks to Kent for joining this committee at the last minute so that the project could proceed.

Support during some of the mapping was provided by Jessica Jelacic and also by my wife, Christa. Soils were examined was the extensive assistance of Joshua Link. My dog, Tasha, spent all of every single day in the field with me. Extensive laboratory assistance was provided by Jon Watkins and Melanie Felts who processed hundreds of samples between them. Samples were also run and/or processed by Amanda Cuer, Amanda Roth, and Dylan Williams. Claire Chadwick is the laboratory coordinator for the Department of Geography and Earth Science and provided logistical and technical support throughout.

Lastly, this project could not have been completed without the generous financial support of numerous organizations. Mapping was supported by USGS EDMAP grant #07HQAG0051 while additional funding was provided by the Geological Society of America Student Grant

program, The Colorado Scientific Society, UNC-Charlotte Geology Scholars Program, and UNC-Charlotte Faculty Research Grant. Cores were split, described, and stored at LacCore with extensive help from the staff there. Lodging and food in Chama, New Mexico was provided by the extremely generous Chama Institute of Arts and Sciences, an organization focused on fixing up old houses in historic Chama.

TABLE OF CONTENTS

CHAPTER 1 – INTRODUCTION

Decades of paleoclimate research have resulted in a clear record of glacial-interglacial climate changes throughout the Quaternary (e.g., Petit et al., 1999). The coarse temporal and spatial resolution of global records means that the timing and magnitude of regional and less-severe millennial scale climate changes remain poorly understood. This is despite the fact that these smaller-scale climate changes are potentially more analogous with current documented global climate change (IPCC, 2007). Furthermore, few studies have focused on how landscapes respond to millennial scale climate variability which has been dominant since the end of the last glacial maximum (LGM). In order to address these gaps in our knowledge of latest Pleistocene and Holocene climate change and landscape evolution, this project has two primary goals: (1) to characterize the magnitude and timing of climate change in the San Juan Mountains since the end of the end of the LGM and (2) to attempt to correlate those changes with periods of landscape evolution as mapped in the upper Conejos River valley of the southern San Juan Mountains of Colorado

Importance of Forming Climate Records

Recent climatic warming has increased the need for understanding Holocene climate, which is dominated by millennial scale changes and not the longer term Milankovic Cycles that dominate Pleistocene climate change. Since Bond et al.'s (1997) identification of millennial scale climate cycles, little has been resolved about them in terms of global severity and spatial distribution. This is mainly because few high resolution records exist and large spatial gaps exist between those that have been established (Mayewski et al., 2004). This low spatial resolution of

records makes understanding the spatial distribution of millennial scale climate change virtually impossible to understand.

Holocene climate records are also the foundation of climate models used in predicting future global climate change. As current climate models attempt to forecast the impacts of global climate change they are biased by concentration of data near the poles where ice cores are available. Yet the majority of the world's population lives in the mid-latitudes making it more important that we understand the future of climates in these areas. Thus, it is important to continue to develop high resolution mid-latitude terrestrial climate records which will improve our ability to forecast how climate change will influence people.

Global climate change may also influence the evolution of landscapes by changing moisture regimes and altering ecosystems that stabilize landscapes. It is difficult to assess how landscapes may evolve in the future as a result of climate change. This is partially because the majority of research on modern landscape evolution focuses on the effect of humans on natural systems (e.g., Gergel et al., 2002) and not on climate influences on modern systems. Holocene landscape response to climate variability should provide a useful proxy for how landscapes may respond to global climate change but information on landscape evolution in the Holocene is nearly absent from the literature (e.g., Slaymaker et al., 2003).

Approach and Field Area

The absence of ancient ice at mid-latitudes, with the exception of some high altitude sites (e.g., Thompson et al., 1998), means that we must turn to other proxies for high resolution climate records. High elevation bog and lake cores have been shown to provide good proxies for Holocene climate for a number of reasons (Blackford, 2000). They are relatively easy to obtain and can be examined for valuable sedimentological data and paleoecologic data such as diatom and pollen assemblages. Additionally, alpine areas have been shown to be particularly reactive to climatic changes. This is because alpine or arctic environments tend to be in a more tenuous equilibrium and warm more quickly during periods of climate change than low altitude, low

latitude environments (IPCC, 2007). Thus, when climate change occurs, the landscape is more likely to react and these reactions are recorded in bogs as a change in sediment composition and quantity. In addition to geologic changes, ecotones at high elevation comprise narrow, altitude-controlled, bands of species. Small changes in climate can affect plant communities resulting in changes in pollen and diatom assemblages (e.g., Jiménez-Moreno et al., 2008; Stone and Fritz, 2006). Thus, examining high elevation bog cores from mid-latitudes could provide a high resolution climate record over geologically short time scales.

Research on the climate and geomorphology of the southeastern San Juan Mountains is extremely limited. Surficial mapping in the area is limited to the classic Atwood and Mather (1932) maps which are at a low spatial resolution and lack age control. Recent LGM glacial studies have been done to the north (Brugger, 2006; Brugger, 2007) and west (Guido et al., 2007) while evidence for Holocene climate change was examined to the south in the Sangre de Christo Mountains (Armour, 2002). These studies leave a large area where neither the surficial geology nor the evidence for paleoclimatology have been examined at high resolution. Additionally, modern climate in the area is significantly affected by the North American Monsoon (Adams and Comrie, 1997) and paleoclimatic records may provide insights into historic variations of the monsoon. The El Niño-Southern Oscillation (ENSO) also influences climate in the region. During El Niño periods (sometimes called the warm phase), winters in the San Juan Mountains tend to be wet and somewhat colder than normal (from NOAA collected data). In contrast, La Niña periods (cold phase) tend to produce warm, dry conditions in the San Juan Mountains.

Specific mechanisms that create modern landforms are poorly defined in most landscape settings. In particular, the interactions between climate, erosion, aggradation, and the development of landforms are poorly documented for alpine areas during the Holocene (e.g., Coulthard et al., 2002). Large sedimentary sequences deposited at the end of the Last Glacial Maximum (LGM) have resulted in a clear understanding of landscape response to Milankovic Cycle scale climate change (e.g., Ritter et al., 1993). However, the understanding of landscape

response to millennial scale climate change is more limited (e.g., Harvey et al., 1999), especially in alpine and subalpine areas. Since it has been shown that cold Pleistocene climates lead to significant erosion and subsequent deposition (Ritter et al., 1993), it has been assumed that the same would be true during the Holocene. However, the assumption that cold climates are simply correlated with increased sedimentation is likely misguided because of the different erosive processes acting in different magnitudes of climate change. In other words, without extensive glacial activity associated with glacial/interglacial climate change, large post-glacial alluvial fans are unlikely to form simply via cold temperatures (Nichols et al., 2007; Pierce and Scott, 1982; Ritter et al., 1993). Furthermore, the assumption that cold periods are also wet periods is not always supported as authors typically compare periods of landscape change to global climate records and not regional ones (e.g., McDonald et al., 2003). Landscapes may be more likely to respond to differences in precipitation and vegetative stability than to slight cooling (Bull, 1991; Langbein and Schumm, 1958; Marston, 2010). In fact, post-glacial landscapes may respond to climate in exactly the opposite way that glacial/interglacial landscapes do since wetter, colder periods in the Holocene could have increased the vegetation and stabilized landscapes while warmer, drier times could have reduced vegetative cover and led to increased erosion and deposition (similar to Bull, 1991). Recent mapping of surficial landforms in the upper Conejos River Valley (Johnson et al., 2010; Chapter 3) shows that Holocene age depositional landforms exist in the form of (1) stream terraces incised into valley moraines and large alluvial fans formed during the Pleistocene immediately after the LGM and (2) smaller, Holocene alluvial fans graded to those terraces and set into the larger post-LGM fans. Thus, we can compare the age of these fans and terraces to changes in climate recorded in bog cores to determine what aspects of regional climate correspond with Holocene deposition.

The initial hypotheses for this study were: 1) changes in regional climate would have been recorded and preserved in Cumbres Bog, 2) the changes seen in the Cumbres Bog core will correspond with deposition in the upper Conejos River Valley, and 3) these two records would

show that deposition during the Holocene occurs in response to wet/cool periods, dry/warm periods, or during the transition between the two.

Methodology

To test these hypotheses, a high resolution, late Pleistocene and Holocene climate record was derived from cores from Cumbres Bog in the southeastern San Juan Mountains of Colorado (Figure 1.1; Chapter 4). The record was created by examining the cores for changes in sedimentology, magnetic susceptibility (MS), and organic content as well as changes in paleoecologic indicators such as diatom and pollen assemblages. Surficial mapping in the upper Conejos River Valley (Figure 1.2, Chapter 3) was undertaken and the ages of landforms were determined via AMS dating of available carbon samples found in the subsurface of units. A soil chronosequence was then created by examining soils of 19 landforms throughout the field area (Chapter 6). Relative soil development was used to examine landscape evolution and expand the few carbon dates that were processed. Once the recent history of the upper Conejos River Valley was known, it was compared with the paleoclimate record to determine timing of landscape instability (Chapter 5).

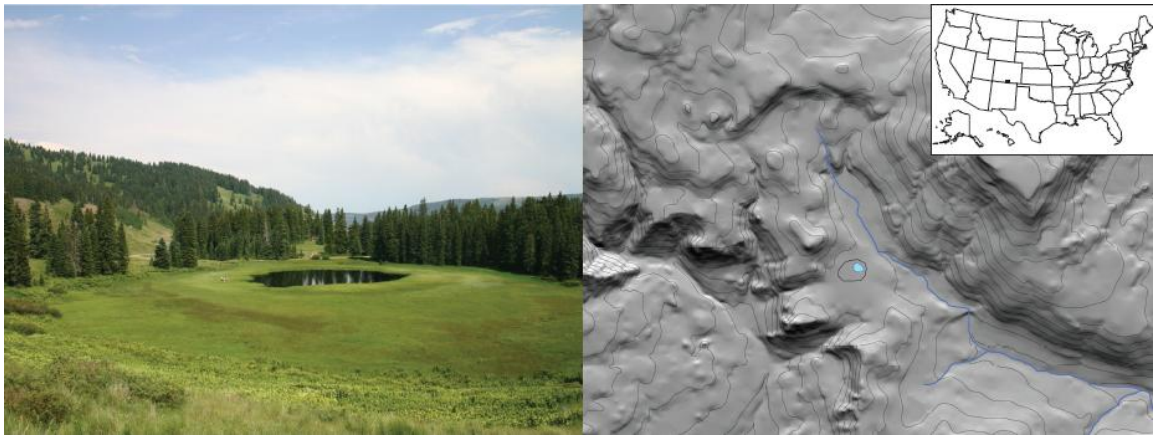

Figure 1.1 Location map for Cumbres Bog in the southern San Juan Mountains of southern Colorado (37°1'18"N, 106° 27'W). The section of open water is ~50 m across. Contour interval in the inset map is 10 m.

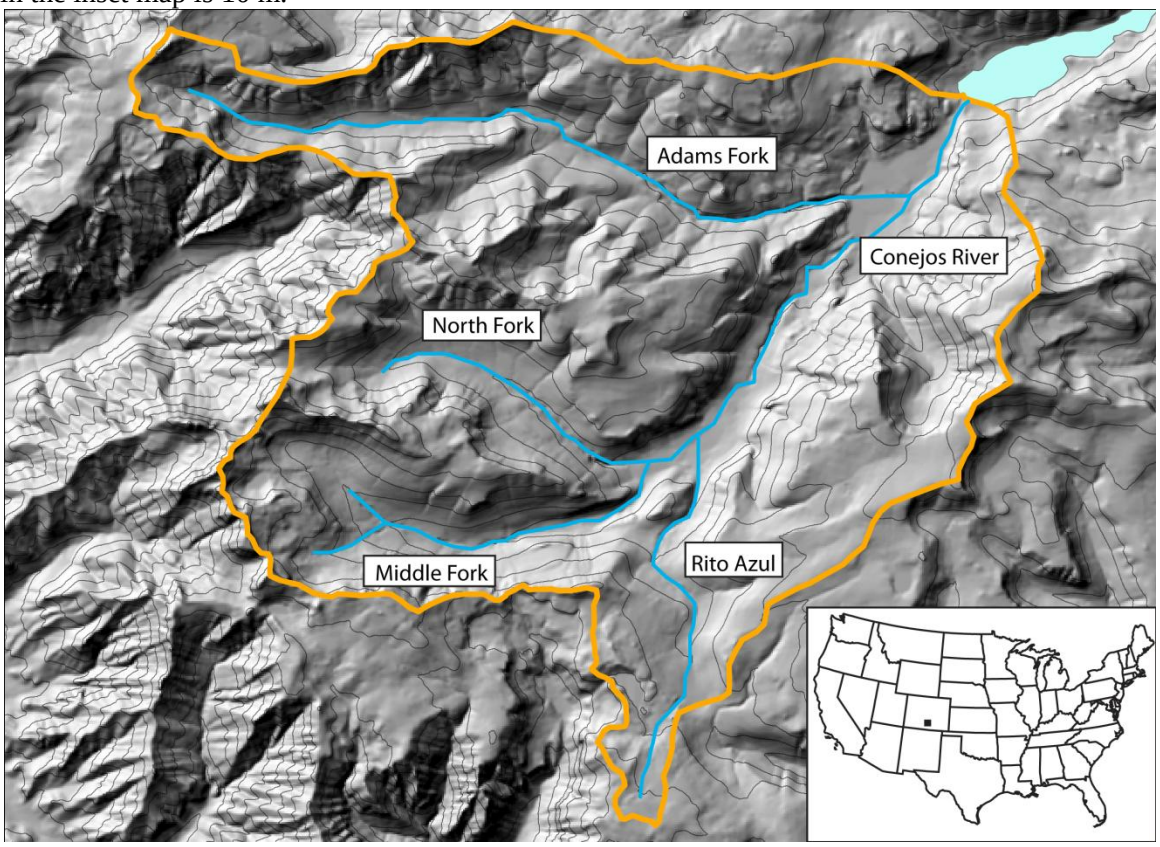

Figure 1.2 Map showing the layout for the upper Conejos River Valley in the San Juan Mountains of southern Colorado. The Conejos River and its tributaries are labeled and the contour interval is 100 m.

CHAPTER 2 – METHODS

This chapter comprises the general methology for the entirety of the dissertation. The methods described here are generally more detailed than journal formats allow therefore some of the information is repeated in the following manuscript chapters. Detailed laboratory procedures are located in Appendix A

Field Methods for Mapping (modified from Johnson et al., 2010, Chapter 3)

Prior to field work, the upper Conejos River watershed was examined using aerial photographs. The resolution of available photographs was insufficient for mapping complex interactions between landforms in valley bottoms and all mapping was completed in the field. Detailed field mapping was completed over a 1:24,000 base-map derived from merging parts of four USGS 7.5 minute quadrangles. In some areas, particularly valley bottoms, the basemap was enlarged to 1:12,000 for more detailed mapping.

Map Unit Identification

In the field, map units were examined in the field and described in terms of landform morphology, sedimentology, soils and stratigraphic relationships as described below. The results from these landform descriptions were then interpreted and landforms were named based on inferred genetic origins of landforms. For example, rounded, well sorted gravels mapped above the modern channel would be interpreted as a fluvial terrace deposit.

Field Descriptions (modified from Johnson et al., 2010, Chapter 3)

Not all units mapped could be described because of time constraints. Thus, unit description efforts were focused on depositional units thought to be indicative of landscape response to climate change. Units described in the field were as follows: Hft2 (Holocene fluvial

terraces, 6 locations), Paf1 (Pleistocene alluvial fan, 5), Haf2 (Holocene alluvial fan, 2), Hla (Holocene lacustrine, 3), Pgt (Pleistocene glacial terrace, 11 because till and glacial terraces were later combined), Hgm (Holocene glacial moraine, 3), PHcol (Pleistocene-Holocene colluvium, 3), Htal (Holocene talus, 4), Pgm (Pleistocene glacial moraine, 3), Pot (Pleistocene outash terrace, 1), Haf3 (Holocene alluvial fan, 1) Hfp (Holocene floodplain, 1), and Hfc (Holocene fluvial channel, 1). Each description included the following information: 1) description of landform morphology (i.e. shape, surface relief, level of dissection and extent), 2) stratigraphic relations to other units, 3) sedimentology, including matrix (<2mm) texture, clast sorting, rounding, average clast size, minimum clast size, maximum clast size, and percent clasts (>2mm), 4) bedding and unit thickness, 5) degree of lichen cover and pitting on boulders, 6) local bedrock type, and 7) soil color at 30 cm depth.

Radiocarbon Sampling

Carbon was sampled whenever it was found in a deposit (12 total) and five carbon samples were chosen for dating based on location importance and quality of the sample. Samples were taken by isolating carbon from the soil using a soil knife. These were then placed in aluminum foil pouches to avoid contamination. Samples were cleaned in the laboratory to remove as much mineral sediment as possible. Radiocarbon samples were run on an Accelerator Mass Spectrometer at the University of Georgia Center for Applied Isotope Studies. These radiocarbon ages, combined with stratigraphic relationships and soil chronosequence data, provide age control for map units.

Digitizing of Map

The field map was digitized directly into ArcMap 9.3 without the creation of a paper office map. Individual units were reassessed during digitizing and photographs were consulted. Areas not inspected directly in the field were interpolated based on surrounding units and were marked with queried contacts. Contacts that were hidden or gradual were identified with dashed, approximate lines. Contacts that were previously located in the field were identified by solid

contacts. The Map Units file in ArcMap is a polygon file and while that file includes an attribute table that includes contact information, contacts were digitized separately in a polyline file. This allowed all contacts to be created individually and prevent lumping of contact types together.

The map was exported and used numerous times for submission to EDMAP and on GSA posters. Most commonly, the map was exported as a raster which often sacrificed quality when blown up. The final copy of the map, which was published in the *Journal of Maps* (Johnson et al., 2010, Chapter 3), was exported as a pdf so that vectors could be individually edited within Adobe Illustrator. This is in line with the requirements of the journal, which asks that maps be submitted as vector files to preserve quality during enlargement and minimize file size. The USGS background, originally exported from iGage Mapbox, was converted to vector from raster by ArcMap during exportation with uneditable results.

Soil Description Methods

Nineteen soil pits were dug to the c horizon (where possible) on various surfaces throughout the field area (Johnson et al., 2010, map). Each pit was described using the techniques described in the *Field Book for Describing and Sampling Soils* (Schoeneberger et al., 2002). The pits varied from 1.0-1.5 meters in depth and each horizon was sampled for future laboratory analyses such as particle size. The individual locations of pits were chosen to minimize the effects of microtopography and microclimates so that small, non-representative features such as erosive channels or overly thick organic deposits could be avoided. Thus, pits were generally located on flat, treeless areas in the middle of landform surfaces and were assumed to be representative of the surface as a whole.

Description Procedure

Pits were dug to either the depth of unweathered material or until the hole could not be deepened because of rocks, water, or difficulty in extending the hole. The National Forest Service permits that allowed us to dig soil pits specified that sod above pits be removed in large,

intact pieces so that they could be replaced at the end of the day to minimize disturbance. All pits were refilled the same day that they were dug and described.

Once the pit was dug, the profile wall was cleaned and examined for horizonation. Joshua Link then sieved each horizon to determine rough gravel percentages. He also determined moist colors for each horizon and, when possible, laid samples out to dry so that dry colors could be taken. Meanwhile, each horizon was described for structure (type, grade, and size), wet consistence (stickiness and plasticity), moist consistence, porosity (occurrence for each size), roots (occurrence for each size), texture, clay films (amount, distinctness, and location), and boundary type (distinctness and topography) in accordance with Birkeland (1999).

Soils were sampled for each horizon and not by depth intervals. The intent of this method was to ensure that all horizons were sampled and to determine whether or not horizonation noted in the field could be confirmed by lab work. Horizons thicker than ~ 30 cm were double sampled with the first sample coming from the top half and the second sample coming from the bottom half of the interval.

Core Extraction Methods

Documenting historical climate change must be done via proxies since direct observations of climate are limited to, at most, the last 200 years. Researchers have used many different indicators for climate but the most accurate come from ice cores. However, the majority of ice old enough to be of value to paleoclimatologists is located at high latitudes and it is not always clear what the relationship is between climate change near the poles and climate change in the mid-latitudes and low-latitudes where the majority of Earth's population lives. The majority of researchers working in the mid-latitudes have examined climate by looking at variations in climate proxies found in various types of sediment cores including ocean cores, lake cores, bog/fen cores, and cores from meadows. The essential premise is to sample sediment from depositional environments where depth can be correlated to age.

Numerous cores were taken in the southern San Juan Mountains and after initial descriptions of all cores it was determined that the best results came from Cumbres Bog which is on the border between New Mexico and Colorado. The Cumbres Bog core (extracted by John Diemer, Missy Eppes, Jake Armour, and myself) contains sediment from as deep as 12 meters below the surface (Plate 2). The core was taken using a Livingston square rod corer with a Bolivia adapter which allowed cores to be taken directly into polycarbonate tubing and was thus cores were not exposed to the open environment during extrusion. Livingston corers are hand driven corers (to minimize sediment disturbance) which uses a piston (essentially a plug) to prevent material from entering the corer until desired. This is accomplished by a cable which is attached to the piston which is allowed to be slack while the corer is put into position. Then, as the core drive begins the cable is held taught while the corer is pushed down. This holds the piston in place while the core barrel is driven past the piston. The piston creates suction and helps keep the core in place.

Lab Methods for Processing Core

A core by itself is not an indicator of past climate and so data about the nature of historic climates must be derived from proxies contained within the core. Proxies that were examined include organic content, particle size, diatom content, and pollen content. Organic content was examined using a total carbon analyzer because the method has higher precision than the more typical loss on ignition procedure. Particle size analysis is a multi-step procedure beginning with the removal of organic material from the sample. This is done by adding 30% hydrogen peroxide to the sample and placing it in a hot water bath until all of the organics are dissolved. The resulting samples were diluted and analyzed in dispersing agent using a Sedigraph. See Appendix A for more detailed lab methods.

Core Processing at LacCore

Cores were shipped from Chama, NM to the LacCore facility at the University of Minnesota in Minneapolis via FedEx, the preferred method of LacCore. Upon arrival at LacCore

the cores were run through a Geotek standard multi-sensor core logger which recorded approximate gamma density, p-wave velocity, electrical resistivity, and magnetic susceptibility through the walls of the core tubing. They were then stored in LacCore's refrigeration system until myself and John Diemer could be present to open the cores. Upon arrival, the cores were cut along the sides using a cast saw designed to cut through the polycarbonate tubing without disturbing the sediment. Each core was then split using fishing wire and/or piano wire. After splitting, the archive halves, which were not disturbed in any way, were photographed using a GeoTek Geoscan-III digital linescan camera and examined for magnetic susceptibility at 1 cm resolution using a Geotek XYZ multi-section automated split core logger.

The other half of each core was described for color, sedimentary structures, organic content, texture, and any changes in sedimentology. Samples of organic material for radiocarbon dating were taken during the description process and smear slides (< 1 mm^3 of wet sediment on glass slides) were made at 10 cm intervals. Once the description was completed, the half cores were cut in half again with one quarter of the original core being preserved for future sampling and the other quarter being cut into 2 cm intervals and brought back to UNC-Charlotte for particle size analysis and organic content determination (Appendix A).

Radiocarbon Sampling and Dating

Carbon was sampled throughout the core for radiocarbon dating. Samples were taken with even distribution in mind and when high quality, intact, organic fragments were found. Samples were taken by isolating carbon from the core using a knife or tweezers. These were then placed in glass vials to avoid contamination. Five samples (details in Chapter 5) were chosen for dating based on the quality of the samples with the intent of having dates spread throughout the entire core. Radiocarbon samples were run on an Accelerator Mass Spectrometer at the University of Georgia Center for Applied Isotope Studies. Once the results from the first 5 samples were received, more samples were selected to increase resolution of areas deemed climatologically important. A total of 8 radiocarbon samples from the core were analyzed.

Particle Size

Determining particle size for samples from a sediment core is difficult because of the small amount of material recovered. A laser particle counter (LPC) was used to determine particle size for samples because it requires less material than other typical methods such as a Sedigraph or pipette method. The method sacrifices accuracy and precision but is the only known method that can determine sediment size with < 1 g of sediment. Organic material is removed from each sample before analysis using hydrogen pyroxide. Specific laboratory procedures are located in Appendix A.

Pollen Preparation and Diatom Sampling

Sixteen sediment samples (1mL each) were taken from the core for pollen analysis. The distribution of these samples was determined with the goal of obtaining data from the entire core. However, there was some sampling bias towards the bottom of the core where sedimentary changes were obvious. Later, ~60 additional pollen samples were taken at 10 cm intervals throughout the core and shipped directly to Gonzalo-Jimenez Moreno at the University of New Mexico for analysis. Dr. Moreno completed pollen isolation and identification at Northern Arizona University using the Faegri and Iverson (1989) methodology. A 1mL polystyrene microsphere spike was used to estimate pollen losses.

Diatoms were examined on smear slides which were made during the initial analysis of the core. Initial examination of these samples showed significant changes in species assemblages and diatom abundances. Thus, roughly 350 samples were taken at 2 cm intervals for the entire core with the goal of further diatom examination. Due to time constraints roughly 40 of these samples were examined and diatoms were counted by Jeffery Stone at the University of Nebraska. The results of that analysis are contained in the manuscript presented in Chapter 5.

Lab Methods for Soil Processing

General laboratory procedures are mentioned below. Specific laboratory techniques are located in Appendix A.

Sieving and Splitting

Samples taken from the soil were laid out to dry in a laboratory where they would not be disturbed. After drying, the samples were split using a standard soil splitter. One half of the sample was then stored in its original state while the other half was sieved. The sediment greater than 2mm in diameter was label and stored while the finer material was bagged and set aside for the procedures described below.

Particle Size Examination

Sediment was isolated from organic material using digestion. Samples were saturated with water and hydrogen peroxide and placed in a hot water bath until digestion was complete. The samples were then diluted and run through a Spectrex Laser Particle counter to determine particle size distribution. Details are located in Appendix A.

Organic Content

Organic content was measured using standard Loss on Ignition (LOI) procedures. Samples were weighed and then placed in crucibles. The crucibles were placed in a furnace with a temperature between 550 degrees C and 650 degrees C for at least one hour or until all organic material had burned off. Samples were then reweighed to determine the percentage of material lost. Since only organic materials is known to burn off at these low temperatures, it is used as a proxy for organic percentage.

Iron Extraction (Modified from Chapter 6)

Obtaining extractible iron values allows us to examined the ratio of Fe_o to Fe_d which reduces over time as amorphous iron (measured by Fe_o) converts to goethite and hematite (measured by Fed, Alexander, 1974). Iron extraction was done using the dithionite-citrate (Fe_d) method (Mehra and Jackson, 1960) and the oxalate extraction (Fe_o) method (McKeague and Day, 1997, Appendix A).

Data Manipulation

Creation of Age Model

Radiocarbon dates taken from throughout the core presented an age model for its entire length. Sections between dates were interpolated and at the bottom of the core, the age model was extrapolated based on the sedimentation rate of the nearest section. The same was done at the top, where the projected age of the top of the core is remarkably near modern age. Later, the age model was annualized using XlXtrFun, which is an add-on for Microsoft Excel 2003. XlXtrFun automatically creates interpolated ages for each year between data points.

Time Series Analysis

The climate records were also examined statistically to determine if reoccurring periodicities exist that are not obvious to the naked eye. Such statistics allow the derivation of the frequency of important climatic events including drought (Stone and Fritz, 2006), El Nino/Southern Oscillation (ENSO; Ariztegui et al., 2007; Rodbell et al., 1999), and variations in monsoon strength (Duan and Yao, 2003). Since the southern San Juan Mountains are affected by all three of these climatic cycles it may be possible to search the core proxies for such signals.

Data used as input into time series analysis functions must be in a format whereby equal time periods exist between data points. Annualized data was then imported from Excel 2007 into the statistics program JMP 8 (File → Open) and analyzed for spectral density (Model → Time Series). JMP then presents the results as a graph comparing spectral density with period with high spectral density for a particular period indicating its reoccurrence (Figure 4.4).

CHAPTER 3 – SURFICIAL MAPPING IN THE CONEJOS VALLEY

Introduction

Only recently has the importance of landscape response to modern climate change been recognized. Consequently, landscape response to millennial scale climate change has been only sparsely documented and is not well understood despite its obvious relevance to modern climate change. Alluvial fans and fluvial terraces related to glacial-interglacial cycles have been well documented worldwide (e.g., Bull, 1991). However, these landforms are notoriously difficult to date and the precise timing of relevant sedimentation is less well understood (e.g., Ritter et al., 1995), particularly for the Holocene (Slaymaker et al., 2003). Our lack of understanding stems from the difficulty in differentiating between recent landscape evolution and inherited surface morphology. Fortunately, alpine landscapes, such as those in the western United States provide a natural laboratory for expanding our understanding of landscape response to millennial scale climate change (Bond et al., 1997) for numerous reasons. First, the erosive power of alpine glaciation during the Last Glacial Maximum (LGM) cleared the landscape of remnant landforms and sediments in these systems. Thus, alpine areas were renewed leaving subsequent landscapes to evolve over the next ~ 15 ka. Additionally, alpine environments hold important clues as to how landscapes respond to large-scale events such as deglaciation. Furthermore, studies investigating the timing of climate-driven sedimentation events have traditionally focused on range-front alluvial fans while few, if any, studies have examined the sedimentation history of headwater systems. Finally, alpine environments are ideal for examining the evolution of fluvial systems since they are particularly responsive to the factors discussed above including climate change, hillslope stability, and changes in local base level. In an effort to document the evolution

of a post-LGM landscape in an alpine system, it was the objective of this project to map the surficial geology of the headwaters of the Conejos River, a major drainage in the San Juan Mountains of southern Colorado.

The upper Conejos River watershed located above Platoro Reservoir is about 80 km^2 and forms the headwaters for the Conejos River, a 5^{th} order stream that flows into the Rio Grande River in the San Luis basin. Platoro Reservoir marks the lowest point in the field area and lies at an elevation of 3039 m. Conejos Peak is the highest point in the watershed with an elevation of 4015 m. The upper Conejos River watershed consists of four main tributaries (the Adams Fork, the North Fork, the Middle Fork, and the Rito Azul) which flow into the main stem of the Conejos River. Each tributary is characterized by unique topography and geomorphology that is described below. Human influence on the field area is minimal and much of the area is designated as wilderness. The surface mapping of Atwood and Mather (1932) provides an accurate record of the maximum San Juan Ice Sheet extent (LGM in age), but does little to describe surficial deposits other than terminal moraines. More recent mapping by Lipman (1974) provides a detailed record of the bedrock geology as well as some general descriptions of surficial units. The area is underlain by a variety of Tertiary volcanics, including lahar flow deposits and numerous ignimbrites (Lipman, 1974).

Methods

Prior to field work, a preliminary map of landforms in the upper Conejos River watershed was created using stereographic aerial photographs. The resolution of available photographs was insufficient, however, for detailed mapping of landforms in the valley bottoms. Detailed field mapping was completed using a 1:24,000 basemap derived from merging parts of four USGS 7.5-minute quadrangles. In some areas, particularly valley bottoms, the basemap was enlarged to 1:12,000 for more detailed mapping. In the field, map units were differentiated based on landform morphology, sedimentology, soils, and stratigraphic relationships.

Each unit was described in detail at no fewer than three localities. Each description included the following information: 1) description of landform morphology (i.e., shape, surface relief, level of dissection, size, and distribution), 2) stratigraphic relationships to other units, 3) sedimentology, including matrix (<2mm) texture, clast sorting, rounding, average clast size, minimum clast size, maximum clast size, and percent clasts (>2mm), 4) bedding and unit thicknesses, 5) degree of lichen cover and pitting on boulders, 6) local bedrock type, and 7) soil colors at 30cm depth (approximate depth to B horizon).

In addition, nineteen soil pits were dug to the C horizon (where possible) on various surfaces throughout the field area (see map). Each pit was described using the techniques described in Schoeneberger et al. (2002). The pits varied from 1.0-1.5 meters in depth and each horizon was sampled for future laboratory analyses such as particle size. The individual locations of pits were chosen to minimize the effects of microtopography and microclimates so that small, non-representative features such as erosive channels or thick, organic rich soils could be avoided. Thus, pits were generally located on flat, treeless areas in the middle of landform surfaces and were assumed to be representative of the surface as a whole.

Carbon was sampled whenever it was found in a deposit (12 total) and five carbon samples were chosen for dating with the goals of dating a maximum number of landforms and dating the highest quality samples. Radiocarbon samples were run on an Accelerator Mass Spectrometer at the University of Georgia Center for Applied Isotope Studies. These radiocarbon ages, combined with stratigraphic relationships and soil chronosequence data, provide age control for map units.

Conclusions

Observations of soils and stratigraphy (see detailed descriptions located on the main map) provide evidence that erosion and resultant sedimentation have occurred episodically throughout the field area since LGM deglaciation. We find that the upper Conejos River watershed is characterized by at least three distinct periods of hillslope, alluvial fan, fluvial, and glaciofluvial

aggradation adjacent to and in the valley bottoms. Between these periods of aggradation are periods of incision which are poorly constrained. The first period of aggradation, which presumably occurred immediately following ice retreat, is represented by large (up to 5000 m^2) alluvial fans (Paf1) which grade to a bedrock valley-bottom surface that lies ~ 2 – 5 meters above the modern fluvial channel. These surfaces (which include Paf1, Pgt, and Pft1) are mantled by relatively mature soils characterized by strong structure and relatively bright colors (more oxidation). Colluvial hillslopes (Pcol) are mantled by similarly mature soils and are common throughout the field area. These sediments have been dated to 9837 +/- 71.5 and 9567 +/- 67 calibrated radiocarbon years BP (Table 3.1). The gap in dated landforms between ~9500 ybp and ~2000 ybp suggests that sedimentation stopped and landscapes stabilized during the Early Holocene.

The next period of deposition is characterized by the formation of relatively smaller fill terraces and alluvial fans. The alluvial fan unit (Haf2) is generally characterized by fans < 50 m^2 in size that are stratigraphically set into the older fans (Figure 3.1). The related terrace (Hft2) has a tread which lies 1 – 2 meters above the modern stream channel. The soils on these surfaces are generally similar to Hft2 (AC-AB-Bw-C horizonation and duller hues) providing evidence for their syndeposition. Both units often contain weakly-developed buried soils or evidence for cummulic development. Furthermore, these two units grade to one another throughout the field area and display similar radiocarbon ages. Hft2 has been dated to 1217 +/- 45.5 and 1904 +/- 32 calibrated radiocarbon years BP at different depths of the same outcrop (Figure 3.2), while Haf2 has been dated to 2065 +/- 55 cal. ybp.

The third period of active deposition appears to be modern (sparsely vegetated sediments with no soil development) and is restricted to the upper Adams Fork drainage. There, high basin relief and ash rich bedrock lead to high rates of debris production via rockfall. This rockfall, along with 1st order fluvial processes, created alluvial fans (Haf3) which are genetically similar to debris fans. Since these fans occur only locally and not throughout the field area, we infer that

they formed independently of climate or changes in base level, and that they are a result of easily erodible bedrock and topography.

One deposit which was dated outside of the three periods of deposition is an alluvial fan that was stratigraphically between Paf1 and Haf2. It was dated to 5384 +/- 65 calibrated years BP. However, no other unit in the area correlates stratigraphically to the landform and it is thought to be a local feature.

In the upper Conejos River watershed, relatively flat u-shaped valley floors now lie 1-100 meters above the modern fluvial channels (Figure 3.3). We call these surfaces "glacial terraces" as they are abandoned surfaces, but are glacial in origin rather than fluvial. These glacial terraces are characterized by 1-2 meters of glacial till underlain by bedrock although glaciofluvial facies occur locally. The bedrock bases of these glacial features high above the valley floor provide a reference point against which to measure stream incision that has occurred since the LGM. Fluvial tributaries to the main stem of the Conejos River would have flowed in the bottom of hanging valleys as ice retreated upstream and water would have emptied into the main valley via significant knickpoints at the valley junctions. Subsequent to this time, these knickpoints have retreated up the tributaries from the junctions. However, the long profile morphologies produced by the retreat varies for each of the four tributary valleys (Figure 3.4). The Adams Fork has deviated more than any other tributary from its post-LGM hanging valley longitudinal profile, both in the headward direction (4500 m) and in the vertical (100 m), resulting in a fairly linear longitudinal profile with a slope of ~ 2º. The North Fork and the Rito Azul tributaries both have well preserved glacial terraces. The modern channel has incised only a few meters into this surface, therefore steeply cascading knickpoints are still preserved upstream of the valley junctions (~ 1 - 1.5 km for each). The glacial knickpoint of the Middle Fork has retreated in the headward direction (~ 3 km) and survives today as a ~40 m waterfall at a bedrock contact between soft lahar deposits and harder lava flows (Figure 3.5; Lipman, 1974). I hypothesize that the observed variability in stream morphologies to be the result of differences in bedrock type and

stream flow (discharge) in each of the tributary watersheds. Presumably, the Rito Azul, North Fork, and Adams Fork tributaries all occur in relatively weak bedrock (volcaniclastic facies including lahar breccias and conglomerates weakly cemented with ash matrices) but the Adams Fork has a basin area of ~ 27 km^2 compared with ~ 13 km^2 for the North Fork and ~ 9.5 km^2 for the Rito Azul. I therefore suggest that higher discharge in the Adams Fork tributary has caused faster incision. The Middle Fork has an intermediate basin area (14 km^2), but the resistant bedrock (volcanic vent facies, Lipman, 1974) appears to dominate the stream profile morphology, not drainage area. The modern knickpoint runs along a contact where the more resistant vent facies has prevented additional headward erosion.

Glacial deposits throughout the field area are generally less than 2 m thick. This is in contrast to areas down-valley from Platoro Reservoir where till often fills the valley floor with deposits as thick as 20 m and moraines can rise up to 10 m from the valley bottom. While it is difficult to determine the reason for the thin nature of the deposits within the map area, it seems that the uppermost parts of the Conejos River Valley were primarily erosional during the LGM. We infer that the deposits that do exist were deposited during a rapid deglaciation leaving only thin deposits of till. Furthermore, moraines (Pgm) in the field area are recessional and their small sizes were likely determined by the short amount of time they were active. Lastly, some of these moraines may have been surrounded and partially buried by sediment during the creation of Paf1 resulting in moraines that appear small.

In conclusion, the upper Conejos River watershed is a relatively stable landscape under modern climate conditions and modern base level. Only a small percentage of the field area (estimated to be ~10%) exhibits evidence of ongoing erosion or deposition, the vast majority of which is in the upper Adams Fork. Since the LGM, knickpoints in tributary streams have incised into their former glacial valley bottoms to varying degrees depending on rock strength and basin area. Also, since the LGM, the area has been subjected to three discrete periods of significant historic geomorphic activity, one beginning with ice retreat and ending around 9500 years BP, the

second between 1000 years BP and 2000 years BP, and the third being modern activity limited to the Adams Fork.

Ongoing research aims to compare the sedimentological record presented here with climate information derived from an 11-meter bog core taken south of the field area. That core appears to contain a full record back to deglaciation about 11,000 years BP. The combination of these two records should provide further insight into the complex relationship between the latest Quaternary climate record and landscape evolution.

Figures

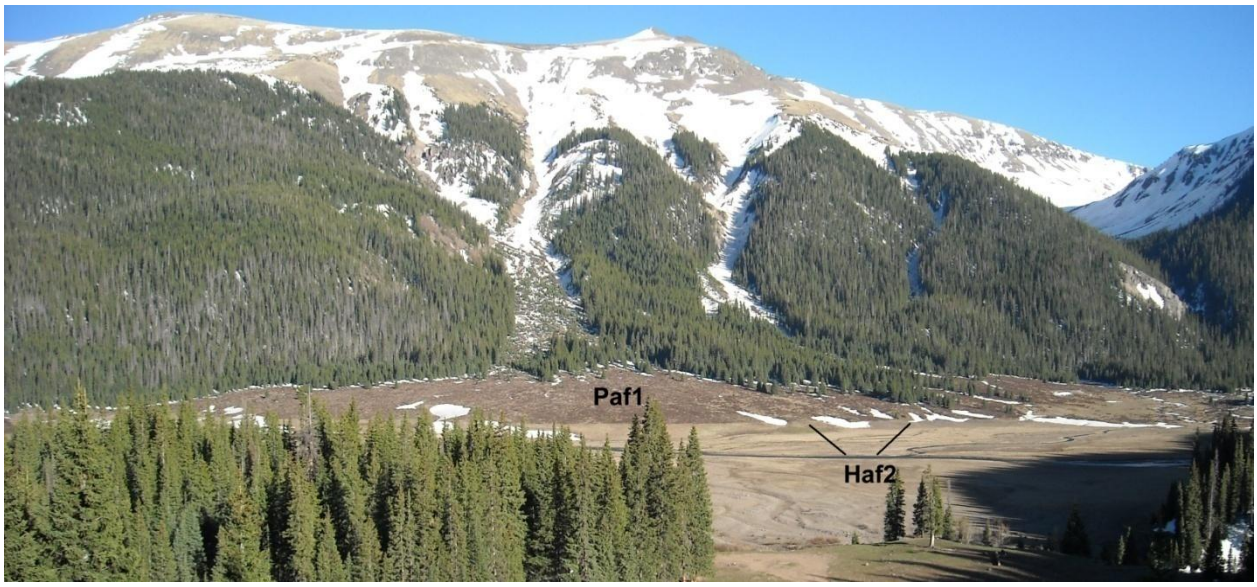

Figure 3.1 Large late-Pleistocene alluvial fans (Paf1) are obvious throughout the field area, occurring where intermittent channels reach the main valley floor. Smaller, inset Holocene alluvial fans (Haf2) are less prominent, but are still common in the mapped area. The large alluvial fan is ~600m wide for scale.

Figure 3.2. Cut bank along the North Fork of the Conejos River exposing a section of the Holocene terrace (Hft2). Radiocarbon samples CVS1 and CVS2 were taken from depths of 65 cm and 110 cm respectively. The dates here are calibrated ages (see Table 3.1 for uncalibrated ages). Inset image displaying soil development was taken a year later when the lower sampling site was under water.

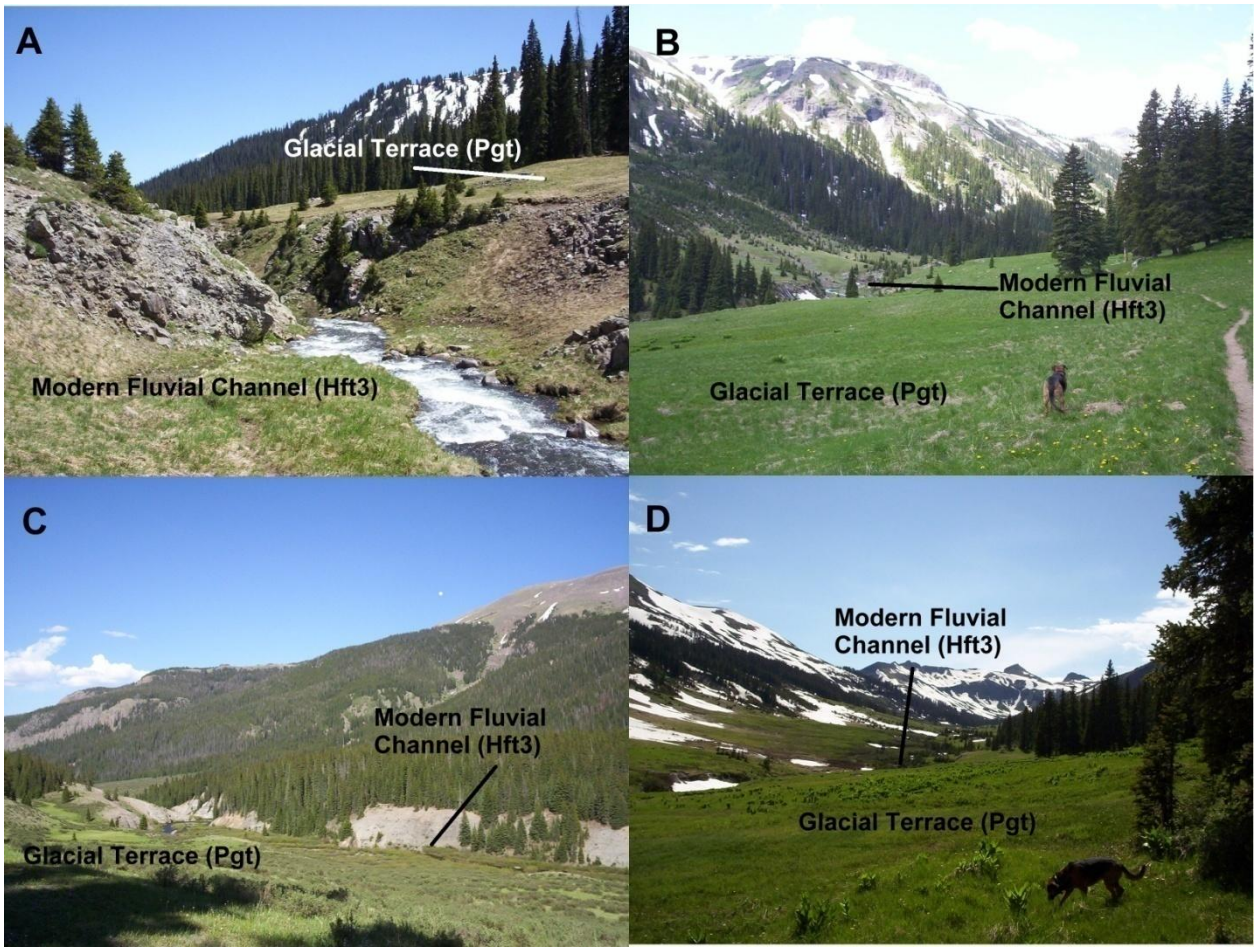

Figure 3.3. Stream incision into former glacial valley bottoms varies by magnitude and morphology throughout the field area. Incision from four locations is listed above as follows: (A) North Fork, (B) upper Adams Fork, (C) main stem of the Conejos River, and (D) Middle Fork. In each location, the LGM U-shaped valley floor (Pgt) is clearly distinguishable from the inset fluvial channel (Hft3).

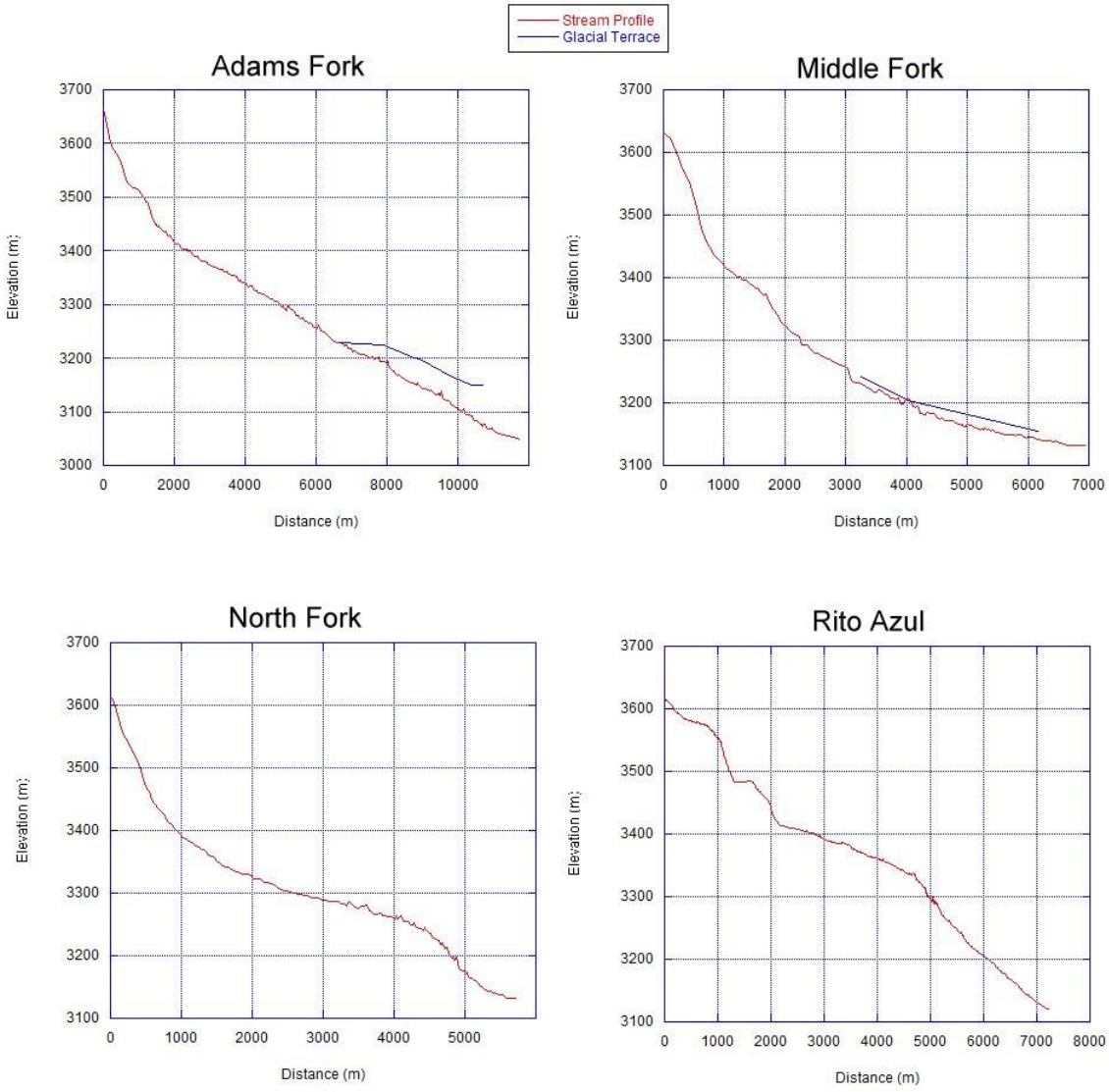

Figure 3.4. Stream profiles were derived from USGS digital elevation models (DEMs). Each tributary would have flowed across a hanging valley knickpoint immediately after the LGM. This is most obvious in the Adams Fork and the Middle Fork where remnants of the U-shaped valley floor bottom are preserved high above the modern valley bottom (blue lines). Minor inaccuracies in stream profiles are due to the size (10 m) of the pixels in USGS datasets. Termination of the long profiles is coincident with entrance into the main stem of the Conejos River.

Figure 3.5. Conejos Falls is the modern morphological expression of the knickpoint that has migrated upstream since deglaciation of the Middle Fork Valley. Above the falls is a U-shaped valley floor which appears to have extended ~3 km down valley towards the confluence with the Rito Azul and the North Fork. The modern knickpoint is located at the bedrock contact between weak volcanic breccia and stronger welded ash flow deposits. The person to the right of the waterfall is ~1.8 m tall for reference.

Table 3.1. A list of carbon sampled and dated within the mapped area. Calibrations were calculated using CalPal Online version 1.5. Error is presented to the 1 sigma level.

Sample ID	Location	C14 Age	+/-	Cal Age	+/-
CVS1	Middle Fork Hft2	1950	30	1901	32
CVS2	Middle Fork Hft2	1250	30	1217	45.5
CVS3	Paf1 Along Main Fork	4650	30	5384	65
CVS6	Adams Fork Mouth Colluvium - PHcol	8810	30	9837	71.5
SJ-7-07-3Char	Adams Fork Colluvium - PHcol	8520	30	9567	67
SJ-7-07-4B	Adams Fork Haf2	2100	30	2065	55.5

CHAPTER 4 – THE CLIMATIC RECORD DERIVED FROM CUMBRES BOG SEDIMENTS

Introduction

High-resolution paleoclimate records are necessary for interpreting past climate variability as well as predicting anthropogenic climate change. Holocene climates varied globally over millennial time scales (e.g., Bond et al., 1997; Denton and Karlen, 1973; Mayewski et al., 2004), however in many continental interiors, including the southern Rocky Mountains, a paucity of paleoclimate records makes it difficult to accurately compare regional with global records. Glacial or periglacial records exist (Armour et al., 2002; Benedict, 1973; Refsnider and Brugger, 2007), but are specific to small, north-facing cirques, which may be more responsive to local microclimates than to global forcing (Johnson et al., 2007). Paleoecological records (Carrara et al., 1984; Fall, 1997; Feiler et al., 1997; Markgraf and Scott, 1981; Reasoner and Jodry, 2000; Toney and Anderson, 2006; Vierling, 1998) are generally of higher resolution, but are nevertheless insufficiently detailed to discern between regionally-absent short-lived climate events and a simple lack of data. Furthermore, most available records do not cover the entire post- Last Glacial Maximum (LGM). The spatial resolution of paleoclimate records in the southern Rocky Mountains is also generally low, especially compared with the density of records in adjacent physiographic provinces (Anderson et al., 2000). Increasing the spatial and temporal resolution of paleoclimate records is critical in illuminating influences of El Niño-Southern Oscillation (ENSO), the North American Monsoon, and the Pacific Decadal Oscillation (PDO) on complicated local climates of the southern Rocky Mountains. This study examines lacustrine deposits for changes in sedimentology and paleoecological indicators in order to determine the timing of post-LGM climate variability. The resulting record increases regional spatial resolution

and is also of sufficient temporal resolution to compare with globally-synchronous events as identified in Mayewski et al. (2004).

Study Site and Approach

The San Juan Mountains are part of an ~25,000 km^2 complex of intermediate to felsic volcanic rocks of Oligocene to Pliocene age (Lipman et al., 1996). The range was covered by an ice cap during the LGM (Atwood and Mather, 1932) leaving thin deposits of till and alluvium above ~3000 m and 0-20 m of fluvial, outwash, and till deposits in valley bottoms (Johnson et al., 2010).

The southern San Juan Mountains are characterized by mean annual temperatures of ~0.5°C at 3350 m elevation. The range is also subject to intense and frequent summer monsoonal storms (Adams and Comrie, 1997), although variability in monsoon strength since the LGM is poorly understood (Asmerom et al., 2007). Late spring and early summer are driest (June avg. 25 mm/month; avg. from Lily Pond SNOTEL station) before monsoonal rains begin in mid-July (peaking at ~80 mm/month) followed by relatively wet fall, winter and spring (~80-100 mm/month). Decadal-scale climate of the region is significantly influenced by ENSO and PDO activity (Grissino-Mayer et al., 2004).

Cumbres Bog (37°1'18"N, 106° 27'W) lies at 3,050 m (~ 500 m below modern tree line) and is surrounded by subalpine coniferous species (Weber, 1976, Supplemental Data). The bog is ~ 150 m across with ~50 m of open water. A 3-4 m thick peat mat covers the majority of the bog's surface. The basin is elevated (~2-3 m) above the adjacent Cumbres River, and no significant channels flow into Cumbres Bog. Field observations show that little groundwater flows into the bog and most water flows directly into the bog from adjacent hillslopes.

We extracted a core to 12 m depth from Cumbres Bog using a Livingston square rod piston corer. From the surface down we encountered 4 m of unconsolidated peat, 1 m of water below the peat mat, and 7 m of sediment. Cores were split, described and sub-sampled at the LacCore facility at the University of Minnesota, analyzed for particle size and organic content (2

cm intervals), magnetic susceptibility (1 cm intervals), pollen (10 cm intervals), and diatoms (20 cm intervals; Supplemental Methods for details), and dated (7 14C samples; Figure 4.1).

Results and Discussion

The Record of Climate Change

The core's age model includes ~20 ka of extrapolated record (Figure 4.1). Sedimentation rates in Cumbres Bog remained between 0.2 and 0.4 mm/yr for 6 of the 7 intervals bracketed by the age data. The sedimentation rate between 2.3 and 1.4 ka is 1 mm/yr.

Basal gravels and mapping provide evidence that Cumbres Bog was dammed by an LGM terminal moraine (Atwood and Mather, 1932) and was still glaciated at ~20 ka. Thus, this study supports the notion (e.g., Benson et al., 2005; Guido et al., 2007) that deglaciation began in the San Juan Mountains and the intermountain west shortly after 20 ka. The post-glacial Pleistocene is characterized by low *Picea*/*Artemisia* (-0.7 to -0.92) and *Pinus*/*Artemisia* (< 0) ratios implying significantly colder temperatures than the Holocene (0.22 to -0.8 and -0.2 to 0.8 respectively; Figure 4.2). Gradual warming after 18 ka was punctuated by a brief warmer interval at ~15.5 ka, which could correspond to the Bølling warm period. The absence of fossil diatoms prior to ~17 ka (Figure 4.3) suggests that the basin was occupied by a low-nutrient and/or low-light water environment, which may have been ice-covered or too turbid to allow for significant productivity (Engstrom and Fritz, 2006). Benthic and small colonial fragilarioid diatoms became a significant component of the sediment at ~16.5 ka, suggesting some weathering of sediment within the basin, and at least periodic ice-free conditions, indicating a shift toward warmer climate (Lotter and Bigler, 2000). Organic percentages prior to 14 ka, during the post-glacial cold period, were the lowest in the core and increased along with temperature during the Allerød interstadial (14-13 ka). Rhythmically-bedded clay-rich layers alternating with layers of sandy silt characterized bog deposition between 20 and 13 ka. A highly variable (0-300 SI units) MS record during this period indicates high clastic content variability. Around 14.5 ka, the fossil diatom record transitioned to a well-developed planktonic community, more representative of lake conditions

than those of a shallow bog, suggesting warm, nutrient-rich waters with significant ice-free periods (Lotter and Bigler, 2000; Lotter et al., 1998). Diatoms recorded peak temperatures at ~13.5 ka, when the assemblage briefly shifted toward planktonic fragilarioid species, commonly associated with stronger thermal stratification, and then began to regress toward cooler conditions thereafter (Kilham et al., 1996). By ~12.5 ka, the fossil plankton assemblage began to be replaced by small colonial fragilariod species, suggesting a return to cooler conditions (Figure 4.3).

The Younger Dryas (YD; 12.8 – 11.5 ka) is marked by temperatures generally warmer than during deglaciation but still cooler than the Holocene and Allerød interstadial. Increased *Picea*/*Artemisia* and *Pinus*/*Artemisia* pollen ratios as well as a switch to thermocline-associated plankton indicate warming immediately after the YD, during which there was an abrupt transition from clastic-dominated sediment to organic-dominated sediment, and a significant decrease in the variability of MS data (down to ~5 SI units). The increase in organic content indicates a more biologically productive environment after 11.5 ka that we interpret as a crossing of a temperature threshold for productivity and not a filling of the bog. The fossil diatom record before 10.6 ka is dominated by small fragilarioid diatoms, suggesting a short ice-free period.

Pollen ratios indicate that temperatures at Cumbres Bog were cold during numerous intervals in the Holocene including: 8.7-7.9, 7.0-6.9, 5.4–5.2, 4.1–3.8, 3.3–3.0, 2.3, 2.0 and 1.5 ka. Between 10 and 6 ka the cold periods had very little impact on organic content implying that biologic productivity in the pond was relatively constant despite changes in climate and vegetation on adjacent slopes. The diatoms for the early Holocene were increasingly dominated by plankton that thrived in open, thermally-stratified water, matching the general rise in temperature shown in the pollen ratios. Cooler periods during the Holocene are indicated by the repeated transitions in dominance from planktonic *Fragilaria* to *Aulacoseira* species (Fritz et al., 1990; Kilham et al., 1996). After 6 ka, periods of cold temperature generally correlated with low organic percentages (i.e. at ~ 5.2, 4.0, 3.0, 2.0, and 1.5 ka) although an apparent lag existed for

each period except 2.0 ka. The fossil diatom record indicates a gradual change in water level, transitioning to shallower and more acidic, bog-like, benthic-dominated conditions by ~5 ka. In the late Holocene, periods interpreted as cool are often represented in the diatom record as a shift toward *Aulacoseira* dominance and warmer periods as a shift toward *Eunotia* dominance, suggesting frequent and often abrupt transitions in water depth. Clay content was relatively uniform throughout the entire Holocene section.

The frequency of climate variations evident in the core increased significantly after 6 ka and again after 3.5 ka (Figure 4.2). A simple frequency analysis of the data identified that the periodicity of climate variability (measured from warm peak to warm peak) was ~2,700 years between ~11.5 ka (the end of the YD) and 6 ka, ~1,100-1,200 years between 6 and 3.5 ka, and ~ 400-600 years after 3.5 ka (Figure 4.4). An analysis of pollen ratios resampled at even intervals indicates that the frequency increase is not an artifact of higher sedimentation rates. Additionally, the magnitude of climate variability before 6 ka appears moderated when compared with climate after 6 ka, which is characterized by higher and lower peaks in pollen ratios.

Comparisons with other records

YD cooling generally affected southwestern alpine areas (Reasoner and Jodry, 2000), however, its spatial variability is not well understood (Figure 4.5). A shift in plant species in the Cumbres Bog core confirms strong YD cooling in the southern San Juan Mountains (Figure 4.3). The Bolling-Allerod interstadial is represented in the core by an isolated period of organically-dominated sediment, suggesting that post-LGM warming was of significant magnitude in the southern San Juan Mountains. The core record generally conforms to the warm early and middle Holocene followed by a cold Late Holocene that has been documented by others (Figure 4.5), and also adds evidence of significant climate variability during these periods, especially during the Late Holocene. Rapid shifts in climate are consistent with other records showing brief periods of late Holocene glacial re-advance (Benedict, 1973; Miller, 1973; Refsnider and Brugger, 2007).

Mayewski et al. (2004) identified periods of rapid climate change that occurred globally during the Holocene, however, the majority of the intermountain western United States is without representation in the study. In the Cumbres Bog record (Figure 4.3), each period, excepting 600-150 cal yr BP, of rapid climate change noted by Mayewski generally corresponds with a cold period, or a transition in or out of a cold period, as shown by pollen ratios from the Cumbres Bog core. While these correlations are not perfect we interpret the differences to be within margin of error for the age model.

The progressive increase in the frequency of climate variability during the Holocene matches well with published records showing an increase in the strength of ENSO during the mid- to late-Holocene. Schulmeister and Lees (1995) found that modern ENSO-dominated precipitation patterns began roughly 4 ka in Australia while Rodbell et al. (1999) reported the establishment of modern ENSO frequencies in Ecuador at 5 ka. More recently, Riedinger et al. (2002) found that ENSO events occurred between 7.1 and 3.1 ka but were low in frequency. After 3.1 ka, a more rapid frequency was established, which appears to be consistent through today. In the American southwest, Menking and Anderson (2003) noted extreme drought between 7.8 ka and 6.2 ka followed by a rise in water tables after 6.2 ka attributed to increased ENSO strength. While the timing of increased ENSO frequency and strength varies regionally, the pattern of increased ENSO strength throughout the Holocene is unmistakable and is supported by modeling (Liu et al., 2000). We see similarly timed changes in the Cumbres Bog core including a change in periodicity from 2,000-3,000 years before 6 ka, to 700-1,100 years from 6 ka to 3.5 ka, and a change to 400 years after 3.5 ka. Similarly, the organic content has very little variability prior to 6 ka and then becomes highly variable, on a 700-1,000 year period, after 6 ka. The MS periodicity also increases significantly at 6 ka. Sedimentation rates increased after 6 ka indicating higher bog productivity related to ENSO activity. Therefore, we conclude that the change in frequencies of the various proxies in the core is closely linked to the increased strength

of ENSO (Rodbell et al., 1999). This is supported by an increased sedimentation rate in the late-Holocene.

In modern climates, ENSO warm phases (El Niño) increase winter precipitation in the San Juan Mountains while cold phases (La Niña) lead to warm, dry winters. Thus, a stronger ENSO cycle increases the inter-annual winter precipitation variability by providing alternating years of high magnitude, wet and dry winters. It is possible that during the Holocene, periods of strong ENSO warm phases led to increased spring and summer snowpack and cool, dry summers in the San Juan Mountains while periods of strong cold phase ENSO events led to warm winters and long, wet summers. This could occur because low spring snowpack allows convective heating during the monsoonal summer and increasing precipitation. The resulting record would be characterized by short, intense periods of cold intermixed with intense periods of warm, wet conditions. The proxies presented here are stronger indicators of temperature than precipitation. Thus, future research may benefit from a focus on the variability of precipitation during the Holocene. This would increase understanding of how ENSO influenced climate periodicity and may also explain the inferred fluctuations in water levels observed in the fossil diatom record after 6 ka.

Conclusion

The record indicates that climate in the southeastern San Juan Mountains was cool during the YD (~12.8-11.5ka), then generally warm until ~ 6 ka, and cool again from 6 ka until the present. Additional cool periods occurred at 10.6, 8.7-7.9, 7.0-6.9, 5.4–5.2, 3.3–3.0, 2.3, 2.0 and 1.5 ka. The periodicity of climate change shortened after 6 ka, and shortened after 3.5 ka. The timing of these shortened periodicities correspond with records of increased ENSO strength (Liu et al., 2000; Rodbell et al., 1999; Tudhope et al., 2001) indicating that the strength of ENSO influences the rate at which climate varies in the region. The mechanism by which this occurs is difficult to determine without paleo-precipitation data for the region. The increased frequency of

short, cool periods after 6 ka, and again after 3.5 ka, may account for the general cooling trends in the Late Holocene identified by previous authors.

Figures

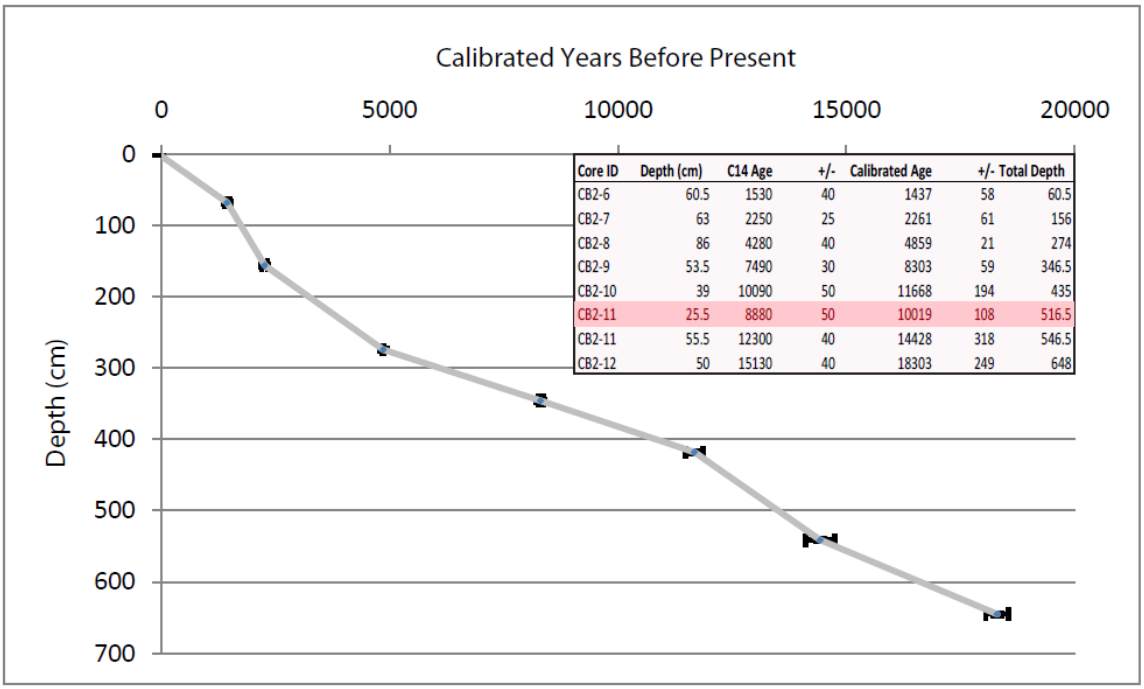

Core ID	Depth (cm)	C14 Age	+/-	Calibrated Age	+/-	Total Depth
CB2-6	60.5	1530	40	1437	58	60.5
CB2-7	63	2250	25	2261	61	156
CB2-8	86	4280	40	4859	21	274
CB2-9	53.5	7490	30	8303	59	346.5
CB2-10	39	10090	50	11668	194	435
CB2-11	25.5	8880	50	10019	108	516.5
CB2-11	55.5	12300	40	14428	318	546.5
CB2-12	50	15130	40	18303	249	648

Figure 4.1 Age model for the Cumbres Bog core, San Juan Mountains, Colorado. The highlighted age was not used in the creation of the age model as it was determined to be contaminated. Samples were analyzed at the University of Georgia Center for Applied Isotope Studies and calibrated using Quickpal 2007 version 1.5.

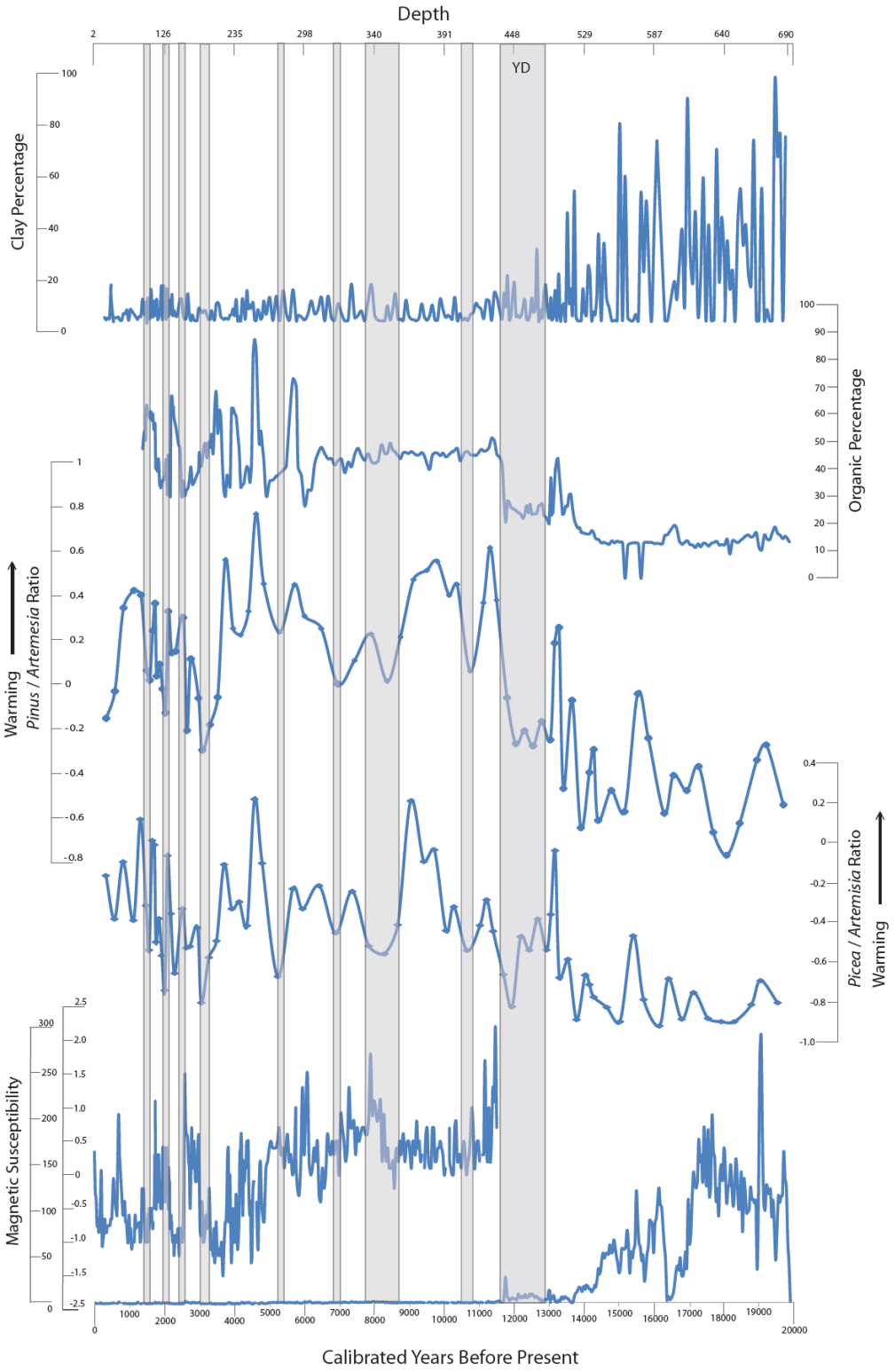

Figure 4.2 Paleoclimate proxy data from Cumbres Bog. Highlighted intervals include the YD and all of the zones of rapid climate change identified in the text. Pollen percentages were calculated as well as ratios of *Pinus*/*Artemisia* (Pi-A/Pi+A) and *Picea*/*Artemisia* (P-A/P+A).

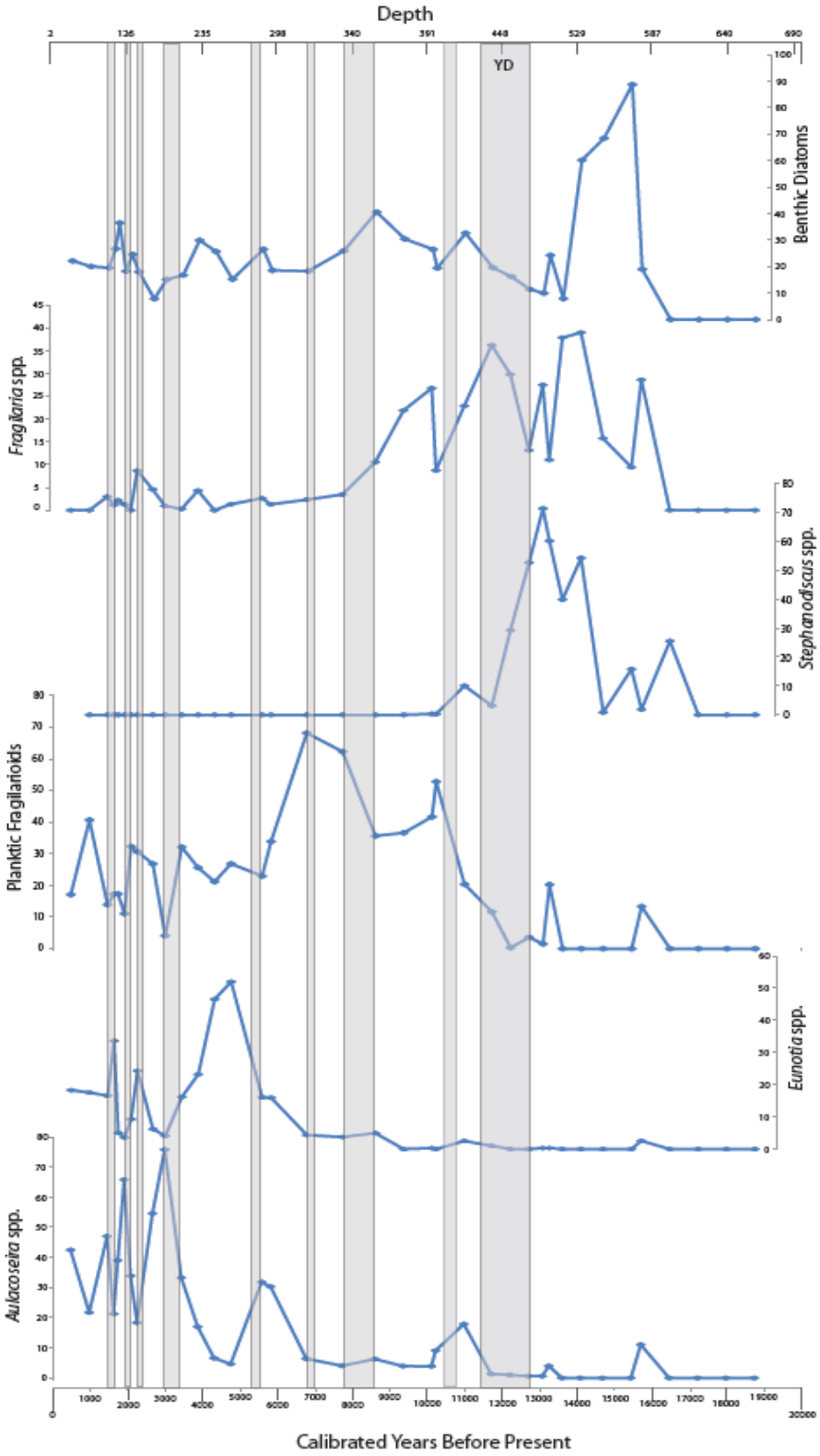

Figure 4.3 Diatom proxy data from Cumbres Bog. Highlighted intervals match those in Figure 4.2.

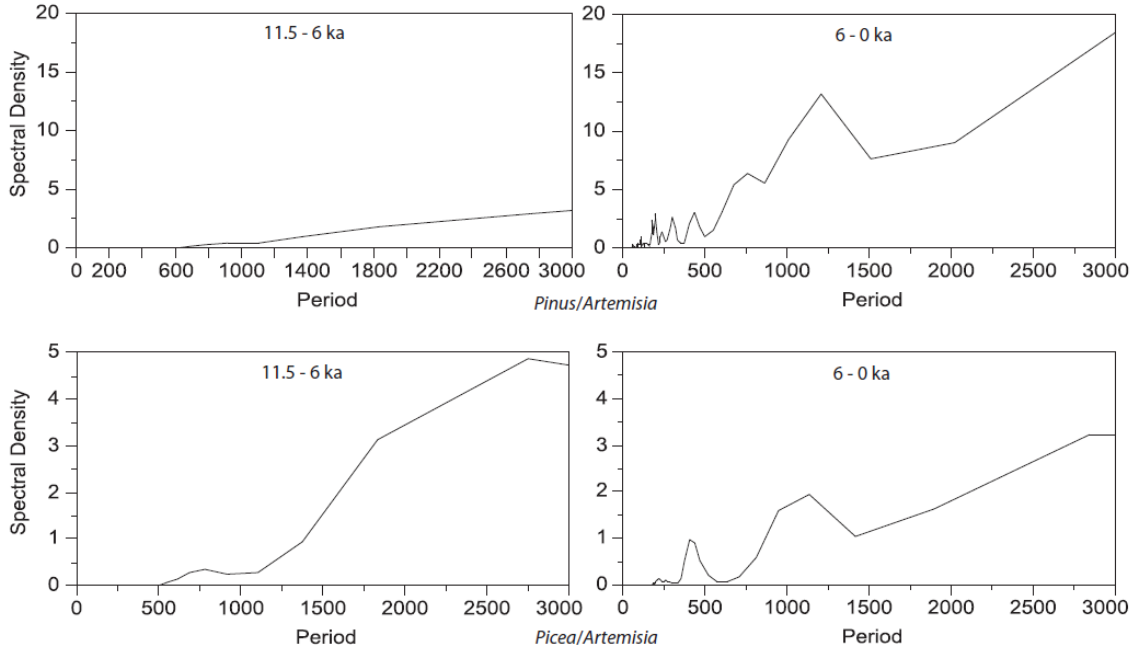

Figure 4.4 Frequency analysis for the two pollen ratios presented in Figure 4.3 presented as the relationship between periodicity (P=1/frequency) and spectral density. Between 11.5 and 6 ka the only notable periodicity is ~2700-3000 years. Between 6 and 0 ka additional periodicities occur including one at ~ 1200 years and others below 500 years including one strong signal at 400 years. We interpret these shorter periodicities to be the result of increased climate variability after 6 ka (~1200 year periodicity) and again after 3.5 ka (~400 year periodicity). These shorter frequencies appear to be superimposed on the underlying periodicity of ~3000 years.

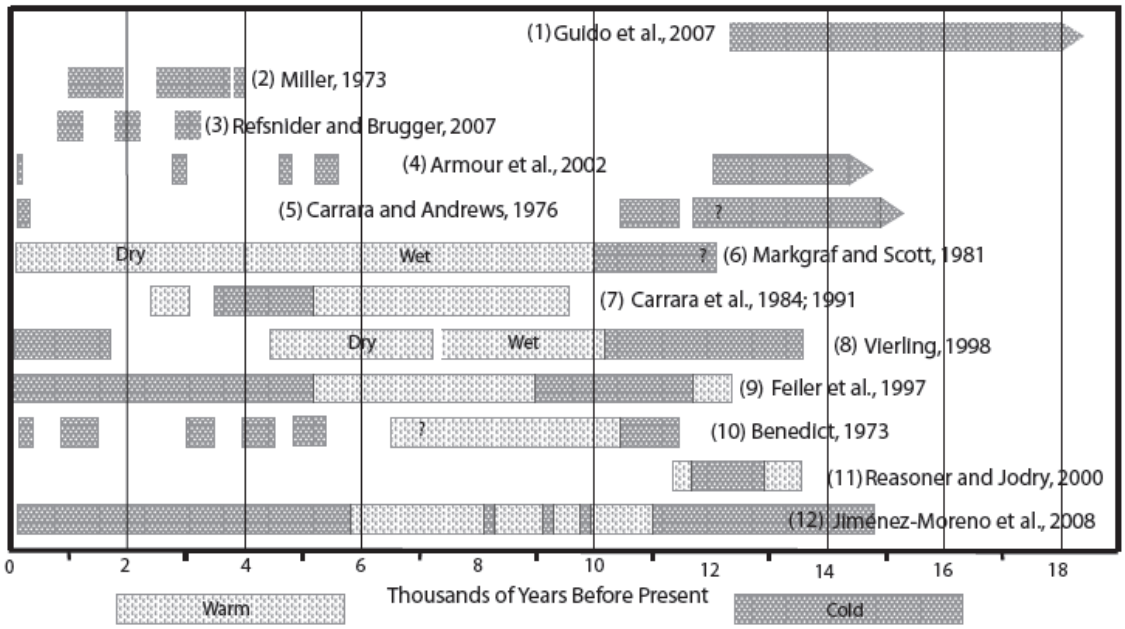

Figure 4.5 A summary of paleoclimate records from the southern Rocky Mountains. Locations of the records are as follows: (1) San Juan Mountains, Colorado (2) Sawatch Mountains, Colorado, (3) Elk and Sawatch Mountains, Colorado, (4) Sangre de Christo Mountains, New Mexico, (5) San Juan Mountains, Colorado, (6) Elk Mountains, Colorado, (7) San Juan Mountains, Colorado, (8) Front Range, Colorado, (9) White River Plateau, Colorado, (10) Front Range, Colorado, (11) Front Range and San Juan Mountains, and (12) Sangre de Christo Mountains, New Mexico.

CHAPTER 5 - THE RELATIONSHIP BETWEEN CLIMATE AND POST-GLACIAL LANDSCAPE EVOLUTION IN THE SOUTHERN SAN JUAN MOUNTAINS

Introduction

The timing and nature of climate-related landscape evolution is not well understood (Dixon et al., 2009) despite an increased focus on Critical Zone processes over the last decade (Marston, 2010; Riebe et al., 2001; Roering et al., 2001; von Blanckenburg, 2005). This uncertainty is amplified in alpine and subalpine areas where few post-Last Glacial Maximum (LGM) landforms have been precisely dated leading to a poor understanding of the processes by which erosion and aggradation influence landscape evolution. Mountainous environments which were glaciated during the LGM are often dominated by large, paraglacial landforms (Ballantyne, 2002; Marston, 2010) yet Holocene aged landforms, including talus slopes, rock glaciers, inset alluvial fans, and terraces, are common in alpine areas (e.g., Curry and Morris, 2004; Johnson et al., 2010; Johnson et al., 2007; Matsuoka and Sakai, 1999). Determining the climatic conditions during which erosion and aggradation occurs in alpine and subalpine areas is critical in understanding the processes that influence the evolution of alpine and subalpine landscapes. Furthermore, many studies of fluvial systems make inferences about sediment supply fluctuations from the contributing alpine portions of their basins without determining the erosional history of those basins.

Understanding landscape evolution in mountainous environments requires local records of erosion, aggradation, and paleoclimatic change. In the absence of regional paleoclimate records, authors generally compare records of erosion and sedimentation with global paleoclimate records (McDonald et al., 2003; Wells et al., 1987). However, robust regional paleoclimate records are critical to understanding the influence of climatic forcing on local landscapes. Having

a local climate record is especially important when examining landscapes in the southern Rocky Mountains because climate is the result of complex interactions between Southwestern climate to the south and Rocky Mountain climate to the north (Mann and Meltzer, 2007). To summarize, the evolution of alpine and subalpine landscapes is not well understood from previous work because 1) the timing and evolution of post-LGM landscapes is poorly constrained, and 2) regional paleoclimate records are not always available to compare with landscape evolution records.

In the southern San Juan Mountains, a series of small, Holocene alluvial fans and terraces inset into larger post-glacial landforms have been identified. These features imply that erosion and aggradation after the LGM were episodic and related to changes in climate since the area is tectonically inactive (Lipman, 1974). It is my goal to document the timing of landscape evolution in the uppermost part of the Conejos River Valley and compare it with a paleoclimate record derived from a core extracted from the nearby Cumbres Bog (Chapter 4). Comparing these two records will provide a direct link between local climatic conditions and post-LGM landscape change. From this record, we should be able to better understand the causes of erosion and sedimentation in alpine and subalpine landscapes since the LGM. Source area landscape evolution records will ultimately aid researchers examining alluvial fans and sedimentation rates in large basins (e.g., San Luis Basin) by increasing understanding of sediment supply and discharge. This could lead to better prediction of water use and sedimentation in populated basins throughout western North America.

Field Area

The field area is located in the southeastern San Juan Mountains of southern Colorado (Figure 5.1). The site is at the intersection of a variety of climatic and geologic regimes. To the immediate east is the arid San Luis basin, which is the uppermost section of the Rio Grande Rift and is bounded to its east by the Sangre de Cristo Mountains. To the immediate north and west is the bulk of the San Juan Mountains with the central Rocky Mountains lying farther to the north.

To the west and southwest is the desert southwestern extension of the Basin and Range with numerous mountain ranges bounded by flat, dry valleys and playas. The Jemez Mountains and Sonoran Desert lie directly to the south.

The Continental Divide runs through the eastern San Juan Mountains, which are characterized by generally high elevations with relatively low relief. Valleys typically lie at ~ 2900 meters while peaks reach as high as 3900 meters. Mapping by Atwood and Mather (1932) showed that the San Juan Mountains were covered by the second largest alpine ice mass in the continental United States during the LGM, after only the Yellowstone ice cap. According to their maps, the area contained two separate ice domes that were connected by individual valley glaciers, with an ice mass centered along the continental divide. U-shaped glacial valleys, erratics in high elevation valleys and plateaus (~3350 meters), and large volumes of glacial sediment in mountain valleys is also present (Johnson et al., 2010), providing further evidence for the ice-covered landscape that Atwood and Mather mapped in the eastern San Juan Mountains.

The research presented here focuses on deposits in the uppermost Conejos River Valley, an area that lies entirely above 3050 m. During the LGM, only ridgetops (~3,800 m and higher) were exposed above the San Juan Ice Cap (Atwood and Mather, 1932). The main valley of the upper Conejos River trends north and is fed by 4 major tributaries (Figure 5.1). The lowest extent of the field area is marked by the Platoro Reservoir, which was created when the Conejos River was dammed in 1951. Post-LGM incision has cut V-shaped notches into the U-shaped glaciated Conejos valley floor in many locations (Johnson et al., 2010). In addition to mapping completed in the Conejos River Valley, a paleoclimate record was derived from a core taken from Cumbres Bog, which lies ~40 km south of the upper Conejos River Valley, and is situated near the headwaters of the Cumbres River (Chapter 4). The small basin containing the bog is elevated slightly above the Cumbres River with no fluvial inputs. The bog is dammed by a recessional moraine formed by the Cumbres Glacier during the LGM. The dominant sources of clastic

sediment input into the basin are likely colluvium from the surrounding hillslopes and windblown dust.

Previous Work

Little is known about how alpine and subalpine landscapes respond to millennial scale climate change during post-LGM times, including the Holocene. The majority of previous work has focused on processes of headwall retreat, talus production, and transport of materials by rock glaciers. Curry and Morris (2004) examined talus production after deglaciation in south Wales and found the majority (~84%) of headwall retreat occurred during the Late Glacial (~13 ka – 10 ka) while the remaining 16% occurred during the Holocene. They interpret this retreat to result from both diurnal freeze/thaw during the Late Glacial (possibly the Younger Dryas) as well as general headwall instability resulting from deglaciation. Humlum (2000) determined that the volume of rock glaciers in cirques in West Greenland could be correlated to the weathering rate of the cirque headwalls, leading to the conclusion that the presence of rock glaciers in cirques significantly increased headwall erosion during the Holocene. Both of these high latitude studies demonstrated that landscape evolution was not necessarily driven by Holocene climate change but rather by ongoing landscape adjustments to Late Pleistocene glacial processes such as physical weathering by glaciers and rock glaciers. At lower elevations in northeastern New Mexico, valley-fill has provided evidence that incision occurred during periods of wet summers while aggradation occurred during periods of summer drought although more complicated mechanisms are difficult to accesses (Mann and Meltzer, 2007).

Alternately, in arctic landscapes, glacial landforms and sediments were slowly replaced by paraglacial fluvial and mass wasting landforms (Lønne and Lysså, 2005). These conclusions have similar implications to the above-mentioned studies, whereby a large transition between glacial and interglacial conditions dominates the evolution of landscape morphology.

Previous work on lake sediments in northern Sweden found that mineral input into lakes varied significantly during the Holocene (Rubensdotter and Rosqvist, 2003). The early Holocene

was characterized by high amounts of clastic input from fluvial sources and was followed by lower, steady sedimentation rates during the middle Holocene. The late Holocene was characterized by higher sedimentation rates associated with climate deterioration. From this, the authors inferred that hillslopes were active during the early and late Holocene while they were stable during the middle Holocene.

Holocene alluvial fans provide evidence about the relative stability of adjacent hillslopes and channel heads. Perhaps the most regionally and climatologically relevant paper on Holocene landscape evolution examined Holocene alluvial fan deposition in central Nevada (Miller et al., 2001). The research focused on upland watersheds, which received roughly 50% of the annual precipitation of the field area. The authors examined the relationship between Holocene climate and landscape processes on hillslopes and in streams and found that a shift in climate towards drier and warmer conditions at 2500 – 1300 YBP correlated to hillslope erosion and subsequent deposition. Once hillslopes and alluvial surfaces restabilized, the primary landscape response was for streams to incise (after 1900 YBP, Miller et al., 2001). Desert alluvial fans, which are more widely studied than alpine ones (e.g., Bull, 1991; Eppes et al., 2002; Wells et al., 1987), have been shown to be active during the Holocene (Eppes and McFadden, 2008). This investigation showed multiple periods of post-LGM aggradation but a lack of datable material made it difficult to determine the cause of erosion despite strong local paleoclimate records (Enzel et al., 1989). More recent research has showed that desert alluvial fans in the Sonoran Desert aggraded between 3,300 and 2,300 years BP due to an increase in effective moisture caused by a strengthened El Niño-Southern Oscillation in the late Holocene (Bacon et al., 2010).

Previous authors have discussed the conditions under which post-glacial erosion, hillslope instability, and subsequent deposition occur in lower elevation areas of mountain belts. Langbein and Schumm (1958) first reported a link between climate and sediment yield in a given area. Their study concluded that sediment yield increased with effective precipitation until it reached a threshold between 25 and 35 cm of precipitation per year where the sediment yield

decreased significantly. They reasoned that an increase in vegetation with an increase in precipitation beyond the threshold would stabilize the surface and prevent erosion. While slightly generalized, the study included evidence collected from all areas of the United States and compared measured sediment yield with annual precipitation. This early study provided a basis for investigations over the next 50 years into how landscapes respond to climate change. Bull and Schick (1979) examined interactions between climate, lithology and colluvium remobilization in southern Israel. They found that rock type significantly affected how colluvium was mobilized and deposited which, in turn, affected whether or not colluvium was reactivated during periods of minor climate change. More generally, they concluded that it was likely that the majority of erosion and sedimentation occurred during a change towards a warmer and/or drier climate.

The literature on Pleistocene alluvial fan evolution is more extensive and can be used to make inferences about hillslope processes. Wells et al. (1987) found that when slopes mantled by colluvium stabilize, sheet flow is increased on lower surfaces causing erosion in the piedmont. The study showed that this migration of sites of erosion created new fans inset into the channels of the older fan. Focusing more on climatic interactions, Pierce and Scott (1982) found that Late Pleistocene alluvial fan deposition occurred in unglaciated drainages as well as glaciated drainages. From this they inferred that the alluvial fans were formed during the LGM because of increased snowpack, a more concentrated runoff season, and surface water dominated systems, and not because of increased sediment supply from glacial erosion. They did not account for the changes in vegetation during climate change that could have caused the observed sedimentation.

Alluvial fans in central Idaho are characterized by four distinct periods of deposition (Ritter et al., 1993; Ritter et al., 1995). The first two periods of deposition are associated with Bull Lake and Pinedale glaciations. The other two periods occurred during the Holocene although none of the periods of deposition are well dated. The authors infer from stratigraphic relationships that deposition occurred during glaciation.

Riebe et al. (2001) found that when climates are stable through time, there is very little difference in sedimentation across a mountain range despite significant changes in precipitation. From this, they inferred that climate only weakly regulates erosion in non-glacial systems. However, they did not account for the fact that modern climates are relatively static over human time scales and that it may be the transition periods between warm and dry to cool and wet climates in which landscapes are unstable. Kirchner et al., (2001) examined erosion over three different time periods and found that erosion rates over decadal time scales are significantly lower than erosion rates over 10 ka and 10 ma time scales. From this they inferred that the majority of erosive work must be done by episodic mass movements that are not necessarily common over human (decadal) time scales. However, episodic deposition may also be the result of erosion that occurred during climatic transitions and erosion rates measured during times of relative stability are likely to be lower.

It is likely that landscapes respond to climate change because the geologic record shows episodic sedimentation in areas that are tectonically inactive. However, the precise timing of these sedimentation episodes remains more enigmatic. The difficulty associated with dating alluvial deposition means that most episodes of sedimentation are poorly constrained. The majority of studies discussed here support the idea that sediment mobilization and deposition may occur during transitions between climatic regimes (Bull, 1991) and yet many authors support the notion that aggradation occurs primarily during wet periods (McAuliffe et al., 2006; McDonald et al., 2003). These two viewpoints represent the two dominant, and opposing, viewpoints on the relationship between climate and landscape stability. It is difficult to identify which mechanism drives erosion and sedimentation in the San Juan Mountains for a couple of reasons. First, the magnitude of any climate change that occurs during the Holocene will be different than the magnitude of climate change that occurred in the Pleistocene, and secondly, the thresholds for erosion may be very different in alpine and subalpine areas during the relatively stable post-glacial period.

Methods

The surficial geology of the Conejos River valley was mapped above Platoro Reservoir in the southern San Juan Mountains of Colorado (Johnson et al., 2010). Mapping was completed at a 1:24,000 scale with key sections of valley bottom mapped at a 1:12,000 scale. Landforms were identified and differentiated in the field and then described based on morphology, sedimentology, soil development and stratigraphic relationships (Johnson et al., 2010). Additionally, 17 soil pits were dug throughout the area and an additional two pits were dug on recessional moraines outside the field area. These soil pits were described using methods described in Birkeland (1999) and Schoeneberger et al. (2002). Data from soil pits were used to determine relative ages of landforms which were then combined with radiocarbon dates to create calibrated ages (Chapter 6).

An ~7 m core obtained from Cumbres Bog (~3,100 m asl) contains a possible record of paleoclimate for the southern San Juan Mountains (Chapter 4). The core was opened and described at the LacCore facility at the University of Minnesota. Samples were taken from the core to determine the sediment, organic, diatom and pollen contents. Sediment samples were run on a Spectrex Laser Particle Counter to determine sediment size, and organic content was determined using loss on ignition. Pollen was extracted using standard chemical protocol (Faegri and Iversen, 1989). Pollen ratios were calculated as *Pinus*/*Artemisia* (Pi-A/Pi+A) and *Picea*/*Artemisia* (P-A/P+A).

Results

Landscape Evolution

The landscape of the high elevations of the southeastern San Juan Mountains is dominated by LGM-aged erosional and depositional features, such as glacially-carved bedrock ridges, as well as moraines and glacial outwash formed during retreat of the Conejos Glacier. Valley floors are typically U-shaped in cross section and are mantled by thin deposits of till emplaced during glacial recession (Pgt, full unit descriptions in Johnson et al., 2010). Upslope

from the glacial valley bottoms are large alluvial fans (Paf1) that either grade to the valley floor or slightly overlie it (Figure 5.2). Soil development and stratigraphic relationships (Johnson et al., 2010) suggest that deposition of the alluvial fans began immediately after deglaciation and lasted until the early Holocene. This is supported by radiocarbon dates from colluvial deposits (PHcol, 9837 +/- 72 and 9567 +/- 67 calibrated years B.P., see Table 1 for all dates) that grade to these large alluvial fans. The Pleistocene glacial till and outwash along with Pleistocene to early Holocene colluvium and Pleistocene-Holocene aged alluvial fans and bedrock exposures, cover the vast majority (>90%) of the landscape in the Conejos River Valley.

Throughout the field area, the Conejos River has incised into the floor of the glacial valley (Johnson et al., 2010). The incision has eroded through Pleistocene depositional features and exposed bedrock in many areas. This incision is commonly 1 – 4 meters but locally the Conejos River and its tributaries are incised as much as 100 m. For example, the mouth of the Adams Fork, formerly a hanging valley, now grades to the modern Conejos Valley floor. Incision has isolated the Pleistocene glacial deposits (Pgt) and alluvial fans (Paf1) of the upper Adams Fork well above the modern channel at the confluence of the Adams Fork with the Conejos River (Figure 5.2).

Inset into the larger late Pleistocene alluvial fans (Paf1), till (Pgt1), and colluvium (PHcol) are Holocene units. Holocene alluvial fans and fluvial terraces, although small in extent, are common throughout the field area. Along incised reaches of the Conejos River, there are fluvial terraces (Hft2) that are situated 1 -2 meters above the modern channel. These terraces have been dated to 1217 +/- 45.5 and 1904 +/- 32 cal yr BP (Table 1, Figure 5.3). Small, Holocene alluvial fans (Haf2), inset into the larger alluvial fans (Paf1), grade to the Holocene terraces (Figure 5.4). These small alluvial fans have been dated at 2065 +/- 55.5 cal yr BP. An additional alluvial fan that is stratigraphically between the ~2 ka fans and the Pleistocene fans was dated at 5384 +/- 65 cal yr BP. While only one alluvial fan of this age has been identified in

the area, the timing of deposition does match the formation of terraces and alluvial fans below Platoro Reservoir (Layzell, 2010).

Paleoclimate

The core taken from Cumbres Bog extended 12 m down from the surface of the peat mat that covers the surface of the bog. The first 4 m of the core were unconsolidated peat containing little or no clastic material. The 5th meter of the core was open water containing no sediment and very little organic material indicating that the 4 m thick peat mat is floating. The last 7 meters of the core, discussed herein, comprise sediments from below the lake floor and these were recovered in 1 meter sections. Generally, sediment in the upper 3 m of the core is organic-rich and is made up of finely laminated (<1 mm thick) muddy sediment with varying amounts of organic matter. The next 3 m of the core are composed of finely laminated (< 1 mm thick) muds, which become progressively less organic-rich down section. The basal 1 m of the core comprises thinly bedded (~1 cm) muds that are rhythmically bedded overlying cm-scale graded beds composed of sands and muds interpreted as varves. A more detailed assessment of the core and the pollen record is discussed elsewhere (Chapter 4, Jiménez-Moreno et al., in prep; Johnson et al., in review). However, those results are critical to this work and we present here relevant findings from that research.

Pollen data were analyzed as ratios between species known to be indicative of climate in mountainous areas of the western United States (Jiménez-Moreno et al., 2008). *Pinus*/*Artemisia* and *Picea*/*Artemisia* ratios were found to be the best proxies for climate in the core (Figure 5.5). Since *Pinus* currently grows at elevations below Cumbres Bog, pine pollen in the core is an indicator of cooler periods when those pines could have grown at higher elevations. Similarly, modern *Picea* tends to be dominant at elevations near Cumbres Bog. Alternatively, high *Artemisia* percentages (*Artemisia* is currently found at elevations above Cumbres Bog) indicate either the expansion of tundra near the bog or an increase in transported *Artemisia* pollen from lower elevations (due to decreased forest around the bog). Thus, when both ratios are high,

climate is interpreted as being warm, due to the upslope migration of *Picea* and *Pinus*. Alternatively, when both rations are low, *Artemisia* has migrated downslope to the vicinity of the bog.

Both pollen ratios indicate that temperatures were colder than those of the Holocene from the LGM through about 14 ka, with the exception of a short, warm interval at 15.5 ka (Figure 5.5). After 14 ka, pollen indicates that temperatures rose rapidly until the onset of the Younger Dryas (12.8 to 11.5 ka) when temperatures cooled and stayed cool through 11.5 ka. Climate between 11.5 ka and 6 ka was characterized by a relatively warm interval during which temperature variations occurred over 1 – 2 ky periods. After 6 ka, climate not only became slightly colder but also became more variable in terms of frequency and magnitude of temperature oscillations (Chapter 4). Specifically, climate changes in the second half of the Holocene occured more rapidly (400 year periods) and at greater magnitudes than changes that occurred in the first half of the Holocene (Figure 5.6).

The magnetic susceptibility (MS) record from the core varies to a greater degree during the Pleistocene (0 – 300 SI units) than it does during the Holocene (-1.5 – 2.5 SI units). Generally high MS values during the Pleistocene are indicative of the high clastic content in the sediment of that age. The highest MS values are present in layers where the sand content is high. After 12 ka, MS values decreased to near 0 SI units and remained relatively constant through 5.5 ka. Between 5.5 ka and the present, MS values fluctuated between 1.5 and -1.5 on roughly 500 to 1000 year time scales. During this period, MS values appear to anti-correlate with organic content implying that MS could be indicative of changes in the organic content of the sediment.

Clay percentages vary considerably during the Pleistocene section of the core (bottom 3 m; nearly 0 – 100%). While the method used in this study has a high error rate (the Spectrex LPC calculates a low clay percentage by mass when measuring samples rich in coarse silt), the maximum values are indicative of the clay-rich nature of the core bottom. Above the Younger Dryas interval (4.3 to 4.8 m depth), clay values are low and vary much less than below the

Younger Dryas interval, implying fairly stable sources of clastic material in the upper part of the core.

Discussion

The comparison of the record of landscape evolution with the record of regional paleoclimate provides us with a record of how landscapes respond to specific climatic events. It is reasonable to assume that rates of sedimentation were extremely high in valley bottoms immediately after deglaciation as hillslopes would have lacked vegetative cover. Poorly stabilized hillslopes combined with a wet climate and glacial meltwater would have provided transport mechanisms for sediment both on hillslopes and in valley bottoms. The earliest dates (9567 and 9837 cal yr BP) from the field area were taken from colluvium and suggest that valleys in the San Juan Mountains took ~2.5 ky to adjust to non-glacial conditions based on the timing of regional deglaciation (onset at 19.4 ka and completion by 12.3 ka) documented in Guido et al. (2007). The stabilization of hillslopes during the paraglacial adjustment period (~12.3-9.8ka) likely involved complicated interactions between the erosion of loose sediment, the relaxation of slope angles, and the reestablishment of vegetation over time (Ballantyne, 2002; Marston, 2010). The high sedimentation rates on hillslopes during the 3 ky paraglacial period likely led to the large alluvial fans (Paf1, Johnson et al., 2010) visible in the field area today. However, there are no significant, continuous fill terraces implying that Conejos River discharges were sufficient to move sediment supplied by hillslope processes out of the upper Conejos River Valley. The paraglacial alluvial fans (Paf1) currently grade to an elevation 1 – 5 meters above the active fluvial channel.

Colluvium (PHcol) in the Conejos River Valley, generally lying near the angle of repose, is unconsolidated, and is subject to erosion by extreme summer monsoon rain events (Adams and Comrie, 1997). These observations suggest that the hillslopes are actively eroding. However, age dates and the degree of soil development on hillslopes show that colluvium was stable, at least locally, throughout the Holocene, despite the factors mentioned above. The long term

stability of colluvium during the Holocene is in contrast to many published models for hillslope erosion (Dixon et al., 2009), which assume that weathering of colluvium, and underlying bedrock, is constant and steady through time. While is it unknown whether this is a local phenomenon or can be expanded to other regions, the stability of these hillslopes is an important insight into alpine and subalpine landscape evolution.

The fact that hillslopes have remained stable for nearly the entire Holocene is not to say that they are completely inactive. The two early Holocene radiocarbon dates in colluvium imply that large quantities of sediment have not been removed via mass wasting as has been shown in other areas (Pierce et al., 2004). However, the consistently well-developed soil profiles also indicate that neither significant aggradation (which would produce buried soils within the profile) nor erosion (which would produce weakly developed profiles) has occurred since the hillslopes stabilized. That said, the steep slope of the landscape makes it likely that some amount of sediment is being transported downslope from the ridgetops to the valley bottom. The transported material is apparently insufficient to create landforms along the valley bottom as modern aggradational features are generally absent. From this, we infer that the hillslopes are most likely in a steady-state equilibrium and are neither aggrading nor eroding.

The period beginning with hillslope stabilization (~9.8 ka) and running through the middle Holocene is noteworthy for its lack of depositional landforms in the field area. While it is possible that alluvial fans and terraces were deposited between 10 ka and 6 ka and subsequently eroded, it is more likely that no significant deposition occurred. The Cumbres Bog climate record indicates that climate was warm during the first half of the Holocene (excepting the short lived 8200 year cooling event) and varied over lower frequencies than climate did in the late Holocene (Figure 5.6). These observations correspond well with other regional paleoclimate records, which suggest a warm, and sometimes wet, climate between 10 ka and 6 ka in the Southwestern U.S. (Carrara et al., 1984; Carrara et al., 1991; Feiler et al., 1997; Jiménez-Moreno et al., 2008; Markgraf and Scott, 1981; Vierling, 1998). The local landscape stability during this time period

suggests that San Juan Mountain landscapes were stable during intervals of to warm regional temperatures and climate variability occurring over longer, 2 – 3 ka timescales. This interpretation is generally in agreement with similar research at lower elevations in northeastern New Mexico which documented that landscape were stable or incising during the early Holocene (Mann and Meltzer, 2007).

The oldest Holocene depositional feature observed in the field area is an alluvial fan dated at 5.4 ka BP. The alluvial fan is stratigraphically younger than the large Pleistocene alluvial fans but older than the alluvial fans dated to 1 – 2.2 ka (see below). While this is the only identifiable alluvial fan of mid-Holocene age identified in the Conejos River headwaters, dating of terraces downstream of the field area have indicated the creation of a fill terrace at around 5.4 ka BP (Layzell, 2010). The timing of formation of this mid-Holocene alluvial fan correlates with a drop in temperatures indicated by the pollen record in the Cumbres Bog core as well as the earliest period of Holocene glacial activity in the Front Range noted by Benedict (1973). This period also corresponds with a change in the frequency of major climate shifts in the core record (from a 2,000 – 3,000 years frequency before 6 ka, to a 1,000 years frequency between 6 ka and 3 ka). It is difficult to determine what could have caused a short period of aggradation during the Holocene but it is likely that erosion and subsequent deposition were caused by the combination of cold climate and an increase in the frequency of climate variability (discussed below).

Both alluvial fans and streams terraces were deposited along radial channels in the headwaters of the Conejos River between ~2.2 ka and ~ 1 ka +/- 100 years (Haf2 and Hft2). Additionally, mapping downstream has identified a set of terraces of similar age and morphology (Layzell, 2010). Furthermore, lower elevation investigations indicate regular periods of deposition and incision throughout the mid to late Holocene (Mann and Meltzer, 2007). The resolution of the pollen record makes it possible to recognize at least 3 and perhaps 4 warm/cold cycles that occurred during late Holocene. From this record, we infer that it is not warm or cold periods during the Holocene that initiated the strongest response from this landscape but rather

that it was the rapid alternation of the climate between warm and cold periods. The Late Holocene period of rapid climate change that is documented in the core may be caused by an increase in El Niño-Southern Oscillation (ENSO) strength after 6 ka and further increased after 3.5 ka (Bacon et al., 2010; Rodbell et al., 1999). A strengthened ENSO cycle could provide additional winter snowpack and spring runoff during warm cycles (El Niño) and a higher frequency of summer storms and rain events during cold cycles (La Niña). Thus, high discharge values basin-wide may cause sediment mobilization and downstream aggradation to occur. This is supported by recent research suggesting that an intensified ENSO cycle led to extreme summer storm events which caused aggradation on alluvial fans in the Sonoran Desert (Bacon et al., 2010) and by research showing a decrease in the periodicity of depositional patterns after ~6.8 cal yr BP in northeastern New Mexico (Mann and Meltzer, 2007). However, at this point we cannot preclude that rapid changes in climate may have destabilized surfaces because vegetation was unable to adapt and ecological succession was too slow to stabilize all landforms.

The most recent period of deposition presents a paradox whereby material is aggrading in valley bottoms (Haf2 and Hft2) but adjacent hillslopes (PHcol) are thought to be generally stable during the Holocene. The three most likely sources of sediment in the system are tributary headwaters, ridge-top colluvium, and previous generations of alluvial fans and terraces (Figure 5.7). If the sediment mainly comes from tributary stream headwaters, this would imply that tributary streams are eroding headwardly. Alternatively, the aggrading sediment may simply be from previous generations of alluvium within the existing fluvial system. For example, in the few locations where they exist, the mid-Holocene (5.5 ka) alluvial fans formed within channels incised into Pleistocene alluvial fans. The Late Holocene fans formed slightly downstream of these mid-Holocene fans. Thus, the Late Holocene fans may have formed when high discharge caused by increased ENSO strength reworked sediments from the mid-Holocene fan surfaces and deposited them on the Late Holocene fans formed at the mouths of tributary stream channels.

This would further explain why mid-Holocene alluvial fans are rare and, when present, are incised into by modern fluvial channels.

It is also possible that sediment was sourced from the uppermost hillslopes within the stream headwaters. This ridge-top colluvium was not examined and may be easily eroded because of a lack of vegetation on ridge-tops combined with increased snowpack. Thus, it is possible that sediment on these high elevation surfaces was more easily mobilized than sediment at lower elevations along the Conejos River and its major tributaries.

Whatever the source of sediment for Late Holocene aggradation, it is clear that erosion was not occurring basin-wide but rather was occurring in localized zones of rapid erosion. This is an important distinction because standard methodology in measuring basin-wide erosion rates assumes equal erosion over the entire area (Bierman and Steig, 1996). This assumption may still be accurate over longer timescales but it is clear that over Holocene timescales erosion rates were spatially variable.

Conclusions

Landscapes in alpine and subalpine regions of the southern San Juan Mountains underwent a 2.5 ka paraglacial adjustment period after the LGM. This adjustment was characterized by the aggradation of large alluvial fans and widespread colluvial mobility, followed by the eventual stabilization of hillslopes and fans at ~9.5 ka. The landscape appears to have remained relatively stable from ~9.5 ka until a mid-Holocene period of sediment mobilization at ~5.5 ka. The core extracted from Cumbres Bog indicates that cooling occurred at ~5.5 ka. This period of sedimentation is likely not well expressed in the field area because it is not well preserved. However, there is a set of terraces dated to ~5.5 ka farther down the Conejos River Valley and outside the field area (Layzell, 2010). The most significant sedimentation event to occur in the Conejos River Valley during the Late Holocene occurred between ~2.2 ka and ~1 ka +/- 100 yr. This period of deposition corresponds not with a discrete cold period but rather with a period of rapid climate oscillation between warm and cold temperatures. I have correlated

that period of rapid climate switching to increased ENSO strength (Chapter 4) implying that sedimentation may actually be the result of climate instability where erosion occurs during both wet winters (ENSO warm phase) and wet summers (ENSO cold phase).

The sources of sediment deposited in valley bottoms during the Holocene are difficult to identify. However, radiocarbon dates implying that hillslopes have been stable since the Early Holocene suggest that erosion rates are not equal throughout the basin. Understanding how erosion varies throughout stream drainages is important in understanding how landscapes evolve over relatively short time scales. Specifically, landscapes are likely to evolve differently over Holocene timescales than they would during glacial-interglacial (i.e. Quaternary) timescales. The results of this study provide some of the first evidence that alpine and subalpine landscapes evolve during the Holocene as a result of high frequency climate instability and not as a result of generally cool climates. Future work should focus on determining whether this result is specific to regions affected by ENSO cycles or if other regional climate mechanisms (e.g., PDO, Asian Monsoon) play a similar role in the evolution of high elevation landscapes of other areas.

Table 5.1. Radiocarbon Samples taken from throughout the field area.

Sample ID	Location	14C Age	+/-	Calibrated Age	+/-	Material
CVS1	Middle Fork Hft2	1950	30	1901	32	Charcoal
CVS2	Middle Fork Hft2	1250	30	1217	45.5	Charcoal
CVS3	Main Fork Haf2	4650	30	5384	65	Charcoal
	Adams Fork Mouth					
CVS6	PHcol	8810	30	9837	71.5	Charcoal
SJ-7-07-3Char	Adams Fork Phcol	8520	30	9567	67	Charcoal
SJ-7-07-4B	Adams Fork Haf2	2100	30	2065	55.5	Charcoal

Figures

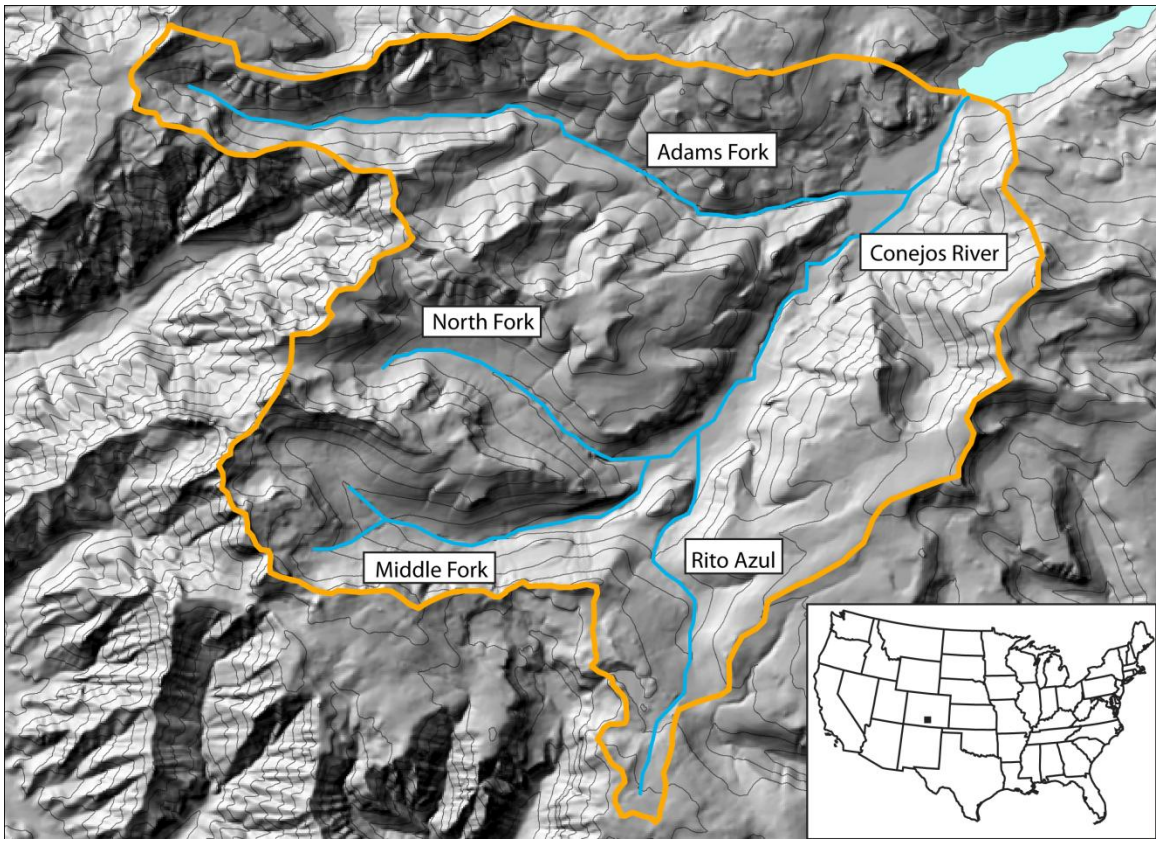

Figure 5.1 A hillshade of the Upper Conejos River Valley created from a 10 m digital elevation model. The three main tributaries to the Conejos River are labeled and the contour interval is 100 m. Platoro Reservoir, which marks the bottom of the field area is located in the upper right (NE) corner.

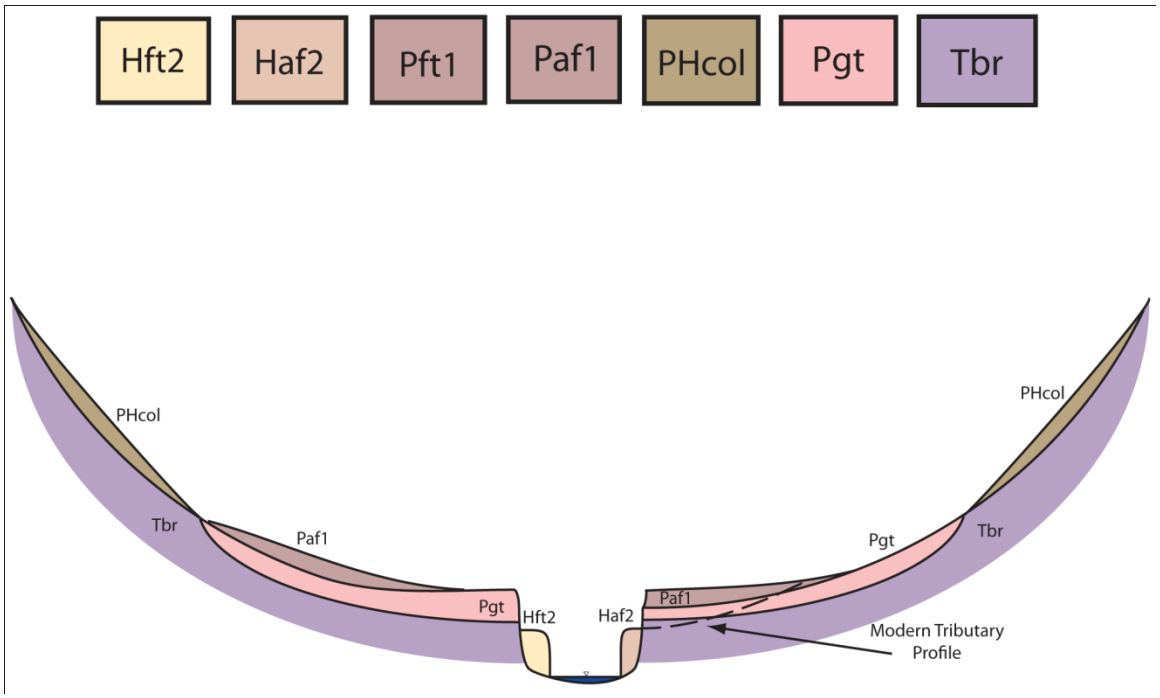

Figure 5.2 Representative cross-section of the upper Conejos River and its tributaries. Valley bottom is vertically exaggerated to emphasize the various elevations of fluvial terraces and alluvial fans. The map units identified are described in full in previous work (Johnson et al., 2010).

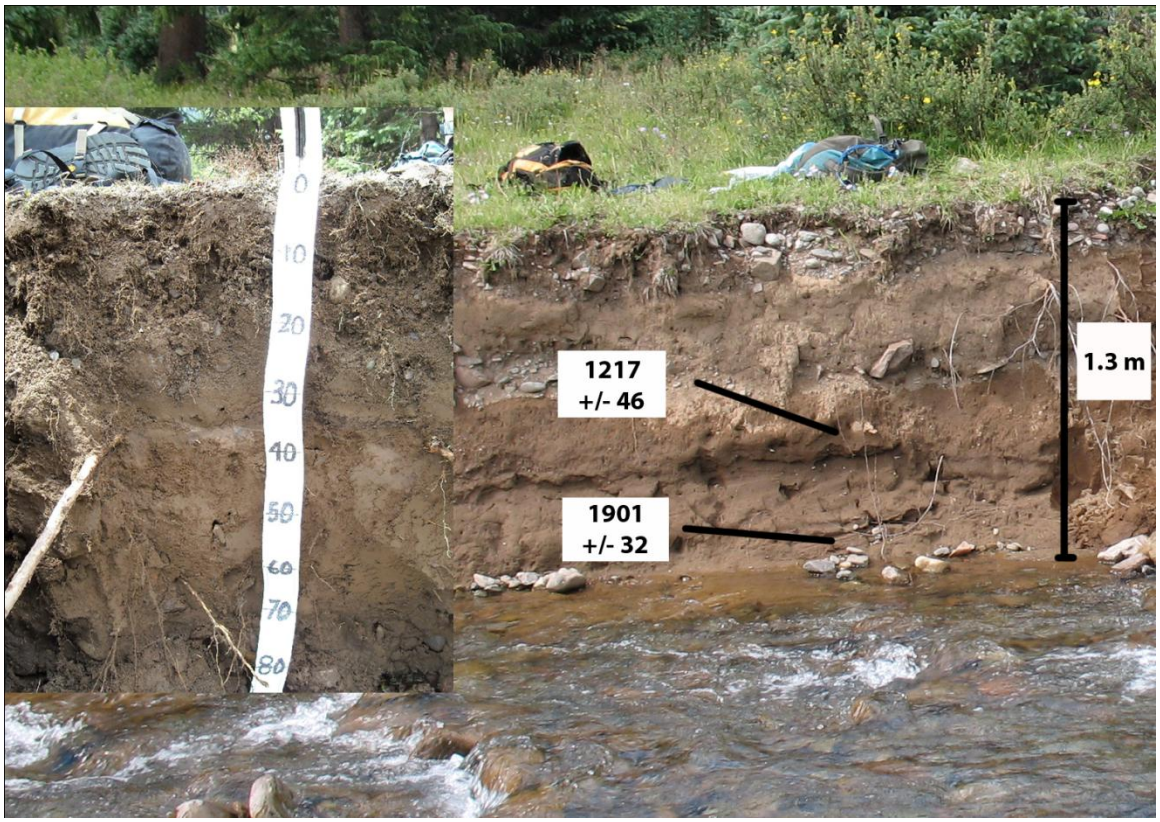

Figure 5.3 A cut-bank exposure of the Holocene fluvial terrace (Hft2) unit where charcoal fragments were sampled for radiocarbon dating (CVS1 and CVS2, see Table 1 for details). The sediment comprises gravels and sands and soil texture varies from sandy loam to loam. The inset image shows a detailed view of the soil profile.

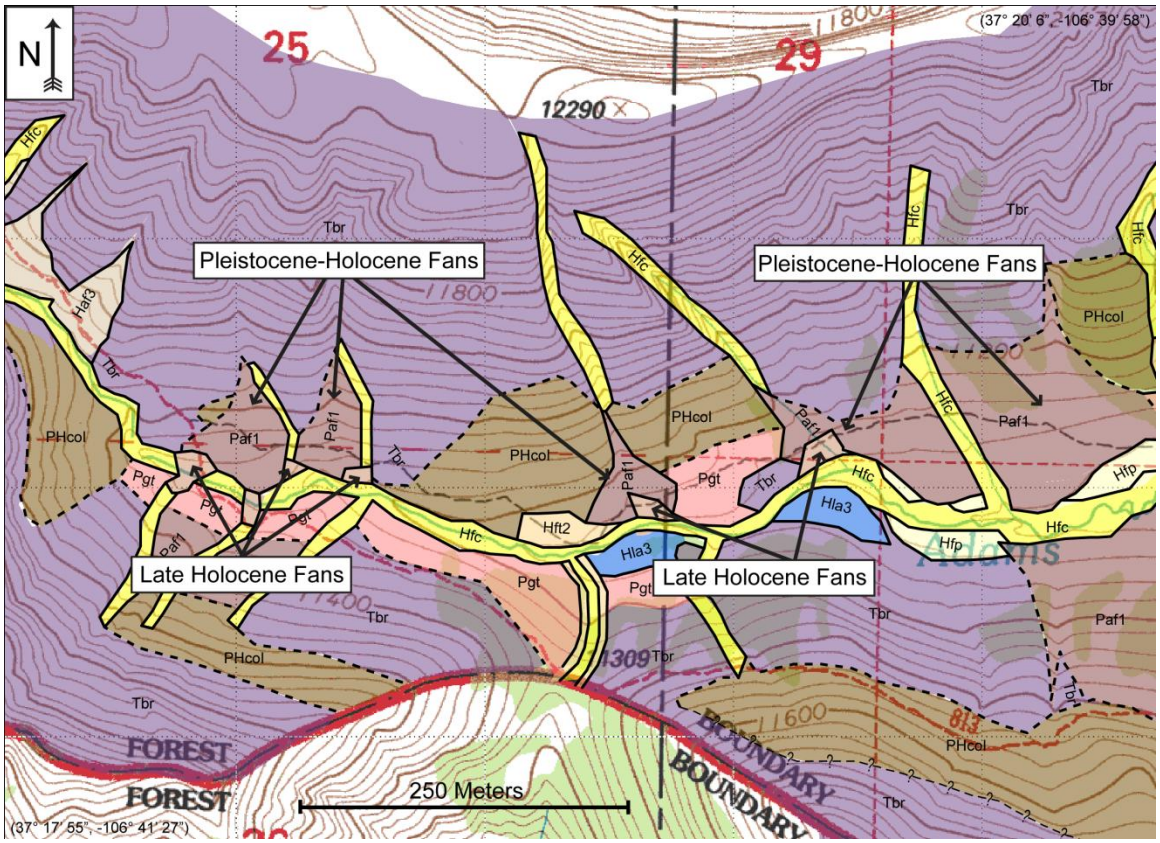

Figure 5.4 A detailed geologic map of the surficial deposits of a valley-bottom section of the Upper Conejos River drainage (Johnson et al., 2010) showing typical stratigraphic relationships between Holocene alluvial fans and Pleistocene-Holocene alluvial fans. The highlighted section was taken from the Adams Fork and is ~ 1 km in length.

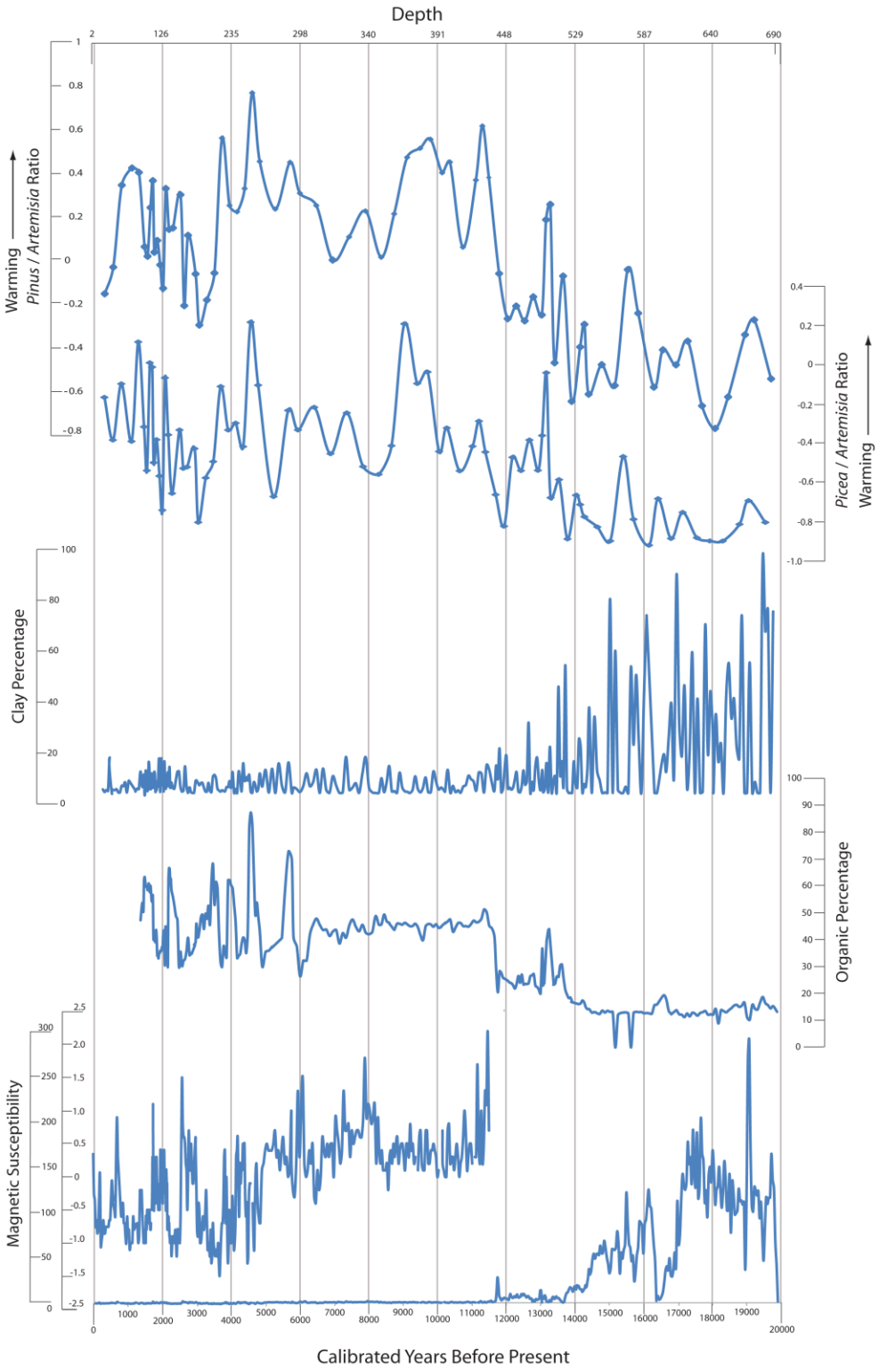

Figure 5.5 Paleoclimate proxies from the Cumbres Bog core plotted against an age model derived from seven radiocarbon dates from throughout the core (Chapter 4). Pollen ratios were calculated as *Pinus*/*Artemisia* (Pi-A/Pi+A) and *Picea*/*Artemisia* (P-A/P+A).

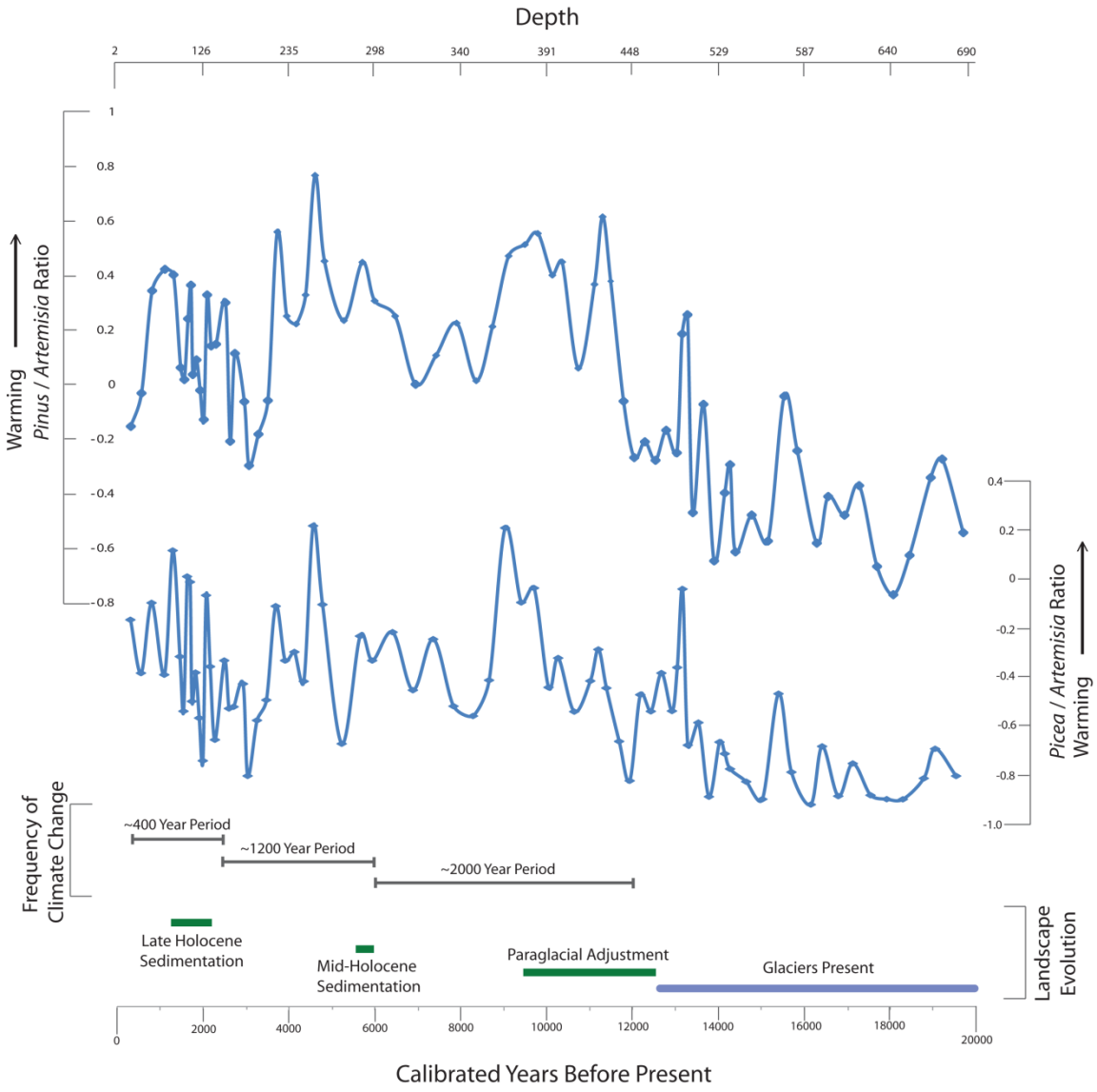

Figure 5.6 A comparison of the timing of climate change (pollen ratios), the frequency of climate change, and aggradation identified by mapping in the field area. The frequency of climate change was calculated using frequency analysis (Chapter 4) while the periods of aggradation are interpreted based on radiocarbon dates, stratigraphy, and relative soil development. The timing of deglaciation is estimated based on glacial retreat ages in the western San Juan Mountains (Guido et al., 2007).

Figure 5.7 Photographs of likely sources of sediment aggraded in Conejos River valley bottom: (A) Headward incision of first order streams , (B) Lateral and vertical reworking of sediment located along main fork tributaries incised into the Pleistocene alluvial fans, or (C) Erosion along exposed ridgetops throughout the field area.

CHAPTER 6 – SOILS IN THE CONEJOS VALLEY

Introduction

Soils develop as a result of climate, organisms, relief, parent material and time (Jenny, 1941, 1980) and soil geomorphologists have often used soils as indicators of relative age of deposits when other factors can be considered relatively stable through time. These soil geomorphological studies create chronosequences which can provide strong relative age data during the mapping of geomorphic landforms. Previous authors have used chronosequences to examine the relative ages of many types of deposits including moraines (Berry, 1987; Birkeland and Burke, 1988; Douglass and Mickelson, 2007; Taylor and Blum, 1995), fluvial terraces (Eppes et al., 2008; McFadden and Weldon, 1987; Tsai et al., 2007), and marine terraces (Crittenden and Muhs, 1986; Kelsey and Bockheim, 1994). However, difficulty in identifying the separate influences of time and parent material on soil development has lead to few studies which attempt to create a soil chronosquence using soils in multiple Quaternary parent materials.

Quaternary sediments often make up the parent material in geomorphic studies and these sediments generally vary based on their mechanism for deposition. Determining the ages of landforms of different origins is a critical component of geomorphic mapping. For example, it is often necessary to compare the ages of alluvial fans and stream terraces in order to identify the source of sedimentation. However, comparing typical soil properties used as age indicators (e.g., clay content, structure) is difficult when comparing alluvial fans and terraces because of initial sedimentary differences (e.g., sediment size and sorting). Identifying soil properties which can be used as reliable age indicators across multiple subalpine parent materials would provide a valuable tool to geomorphic mappers.

Up to this point, very few alpine or subalpine chronosequences have been created in North America (Birkeland et al., 2003). This lack of previous work makes it difficult for authors to identify soil properties that change steadily through time. This is further complicated by the young nature of alpine and subalpine soils which have only begun forming in the last 15 – 20 ka.

In this study, I examine how soils may be used to provide relative and calibrated ages for geomorphic mapping in the subalpine southern Rocky Mountains, specifically the upper Conejos River Valley of the southern San Juan Mountains (Figure 6.1). The results from this study should be useful not only to future workers in this area but also to workers examining young, mountainous soil horizons in the intermountain United States.

Field Area

Geography

The Conejos River Valley is located in the southeastern San Juan Mountains in the southern Rocky Mountains (Figure 6.1). The river flows north from its headwaters in the center of the range before flowing east out into the San Luis Valley, draining roughly 2,300 km^2 in total. This study was undertaken in the upper Conejos River Valley which is the headwaters for the river and consists of 4 major tributaries (Rito Azul, North Fork, Middle Fork, and Adams Fork) and the main trunk of the Conejos River. The area now lies entirely above Platoro Reservoir (3,050 m) which was built in 1951. During the Last Glacial Maximum (LGM) the area was covered by the southern extent of the San Juan Ice cap which glaciated all but the highest peaks in the upper Conejos River Valley (Atwood and Mather, 1932). Large valley glaciers extended more than 40 km downstream from the center of the ice cap carving out large U-shaped valleys. In the eastern San Juan Mountains, the glaciers carved deeply into soft volcanic bedrock leaving a high relief landscape where peaks rise to nearly 4,000 meters and valley floors lie as much as 1,000 m below. The volcanic bedrock formed at ~ 30 m.a. and is thought to be associated with the end of the Laramide orogeny (Lipman, 1974; Lipman et al., 1970) . The eastern San Juan

Mountains appear to have been tectonically inactive since the end of Rio Grande Rift extension between 10 and 5 m.a. (Morgan et al., 1986).

Bedrock

Bedrock stratigraphy is characterized by volcanic conglomerates which are generally overlain by rhyodacite and andesite vent facies. Both of these units are locally overlain by volcanic breccias with high dips interpreted to be remnants of a volcanic cone (Lipman, 1974). The vent facies, which is the dominant bedrock type in the lower valley, is a cliff forming unit which varies in mineralogy laterally but remains erosion resistant throughout the field area. In contrast, the volcaniclastic conglomerate, which is characteristic of the valley walls and all upper valleys, varies significantly laterally. The conglomerate generally consists of large clasts suspended in a poorly welded ash matrix although the matrix is strongly welded and the unit is a cliff former in the upper reaches of the Adams Fork. The conglomerate is easily confused with glacial till as both consist of large clasts in a soft, ashy matrix.

Quaternary Geology

One goal for the examination of soils in the Conejos River Valley was to provide additional age control for surficial mapping (Johnson et al., 2010). Thus, soils were examined on depositional landforms relevant to the overall evolution of the landscape including glacial till, alluvial fans, stream terraces, and colluvium. Here I introduce those map units that were mapped and examined for soils (Johnson et al., 2010 for details). Two soils were examined on Last Glacial Maximum (LGM) terminal moraines which were mapped by Atwood and Mather (1932) and are not discussed here.

The oldest common deposits in the field area consist of glacial till lying 1-5 m above the modern stream channel. This material was deposited on the U-shaped valley floor during deglaciation and is now incised into by the modern stream channel. This unit is known as the glacial terrace (Pgt, Johnson et al., 2010) because of its elevation above the modern valley floor. While the glacial terrace has not been dated, it is thought to have formed between 12 and 13 ka

based on the regional timing of deglaciation (Guido et al., 2007). The glacial terraces are characterized by poorly sorted silty sands containing matrix-supported sub-angular to sub-rounded cobbles and boulders. This glacial material is graded to, and is sometimes overlain by, large alluvial fans (Paf1) that presumably formed during paraglacial landscape response to deglaciation. Alluvial fan sediment comprises clast- and matrix-supported gravels, cobbles, and boulders within a sandy matrix. Once again, these alluvial fans have not been dated but stratigraphic relationships suggest that they formed slightly before hillslopes stabilized. This constrains the age of the large alluvial fans (Paf1) as colluvial deposits (PHcol) have been dated to between 9.5 and 10 ka BP (Chapter 3). Thus, the large alluvial fans (Paf1) likely formed after ~12 ka and before 10 ka. Colluvium is characterized by poorly sorted, silt to gravel sized sediment that generally contains less than 25% gravel (although locally gravel can be as much as 65%). A unique Pleistocene fluvial terrace (Pft1) is located along the Adams Fork of the Conejos River. The thickness of the terrace (>5 m), the size of the largest clasts, and the lack of fine grained material in this clast-supported deposit indicate that discharge during deposition would have significantly greater than today. From this I infer that Pft1 deposition occurred as outwash during deglaciation. Thus, it is likely that it formed as outwash during deglaciation at ~ 12.5 ka BP or slightly thereafter.

Two distinct periods of aggradation occurred in the field area during the Holocene. First, a suite of small alluvial fans formed in the upper Conejos River Valley around 5.5 ka. It is difficult to determine how common these small, Middle Holocene alluvial fans were because they appear to be poorly preserved. However, downstream of the field area a thin bank deposit associated with a strath terrace was dated at ~ 5.5 ka (Layzell, 2010) indicating aggradation did occur in multiple locations. Later, a more extensive period of aggradation occurred that included small, inset alluvial fans and 1 m thick fill terraces adjacent to the modern stream channel. While the alluvial fans have not been dated they grade to fluvial strath terraces on the main fork of the Conejos River which have been dated to between 1.2 and 2.3 ka BP. The small, inset alluvial

fans consist of clast-supported gravels to boulders within a sandy matrix while their associated terraces are composed of clast-supported, rounded, and sub-rounded gravel and pebbles in a sand and silt matrix. The two generations of fans are difficult to differentiate in the field as they share similar morphologies. In addition, modern landforms exist throughout the field area and include floodplains, small, active alluvial fans, and lacustrine environments.

Climate

Climate in the San Juan Mountains is complicated as it is influenced by the North American Monsoon in addition to typical alpine microclimates (Adams and Comrie, 1997). Precipitation in the area also originates from mid-continental troughs and the sub-tropical jet stream. A SNOTEL station near the base of the field area monitors modern climate where annual mean temperature is ~ 1°C while average annual precipitation is ~ 45 cm. Most moisture fails either during the winter months or during the North American Monsoon which runs from mid-July through August. Maximum discharge occurs in the late spring (May and June) as temperatures warm and snowpack melts. Since these climate records are recorded at an elevation lower than the majority of the field area, the actual conditions are probably slightly cooler and wetter throughout the upper portion of the valley.

Climate is known to have changed in the San Juan Mountains since the LGM (Ariztegui et al., 2007; Carrara and Andrews, 1976; Carrara et al., 1984; Carrara et al., 1991; Fall, 1997; Guido et al., 2007; Jiménez-Moreno et al., 2008). However climate is assumed to have changed uniformly throughout the field area and thus would have influenced all soils equally. These changes in climate likely led to the periodic deposition of the sediment mentioned above (Chapter 4, Chapter 5, Layzell, 2010).

Methods

Variations in parent material significantly complicate the creation of a chronosequence for the field area. Generally, studies would attempt to minimize variations in parent material (Birkeland et al., 2003) when creating a chronosequence as variations in original sedimentology

can be difficult to differentiate from changes in soil texture through time. Furthermore, different parent materials may develop soils at different rates depending on initial conditions such as permeability and porosity. For instance, fluvial sediments which are rich in gravel may be characterized by a greater weathered depth than silt and clay rich glacial sediments. The focus on the evolution of the entire Conejos River Valley landscape, and not just on alluvial fans, means that pits have intentionally been dug on a variety of geomorphic surfaces. While this is advantageous in studying landscapes (Chapter 5), it makes the creation of a chronosequence more difficult.

Soil pits were dug on 17 surfaces throughout the field area with a goal of examining soils on surfaces with a variety of ages and parent materials (see Johnson et al., 2010 for pit locations). Two additional soil pits were dug on Last Glacial Maximum (LGM) terminal moraines (Atwood and Mather, 1932) which lie more than 40 km down-valley from the field area. The site of each of the 19 pits was selected to be representative of the surface of the individual feature. Pits were generally dug in flat, treeless areas where neither recent deposition nor erosion was apparent. This was done to avoid microtopographic influences on soil development. Pits were dug to the depth of the C horizon or until a barrier (a boulder or the water table) prevented further digging. The depth of pits varied from 1 - 2 m. Horizonation was identified in the field and each horizon was examined for percent gravel, moist color, dry color, structure, texture, roots, and pores in the field. Each horizon was sampled with horizons thicker than 30 cm double sampled to indentify changes within the thicker horizons.

Since the upper Conejos River Valley has significant variability in both elevation and aspect, it is important to examine soils in this light. For instance, annual precipitation likely varies with elevation while effective moisture likely varies by aspect (Franzmeier et al., 1969; Hunckler and Schaetzl, 1997). The influence of aspect was minimized by selecting soil pit locations which were flat and therefore had little or no dominant aspect. Pits dug in colluvium, which by definition must have an aspect, had aspects ranging from south facing to east facing. North

facing aspects were avoided because forest vegetation is thickest on north facing-slopes. Elevation was noted at each location so that any variations in soil development based on changes in climate with elevation could be identified.

The upper Conejos River Valley is generally high in relief with valley floors as low as 2,900 m and peaks as high as 3,900 m. However, the influence of relief was minimized by selecting flat locations for soil pits except for those dug in colluvium where pits were dug on slopes consistently near the angle of repose.

Organic material, mainly vegetation type and quantity, varies throughout the upper Conejos River Valley. The methods used in this study minimized the impacts of vegetation on soil development by selecting sites which were characterized by similar vegetation. Specifically, pits were not dug near large trees or in forested areas but instead were dug in open areas where grass and shrubs provided fairly uniform ground cover.

Samples were transported to the UNC Charlotte soil laboratory where they were dried and sieved to remove gravel. Finer grained materials were examined for organic content using loss on ignition and particle size using a Sedigraph. The most developed horizon from each pit was sub-sampled and processed to determine extractable iron content. The most developed horizon was identified using horizonation (as sub-sampled horizons were generally B and Bt horizons) and color. Iron extraction was done using both the dithionite-citrate (Fe_d) method (Mehra and Jackson, 1960) and the oxalate extraction (Fe_o) method (McKeague and Day, 1997). Obtaining both of these extractible irons values allows us to examined the ratio of Fe_o to Fe_d which reduces over time as amorphous iron (measured by Fe_o) converts to goethite and hematite (measured by Fed, Alexander, 1974, discussion below).

Fe was extracted from soil samples using both the oxalate (Fe_o) treatment method as well as the dithionite-citrate (Fe_d) treatment (Birkeland, 1999). The oxalate treatment generally removes ferrihydrite (sometimes referred to as amorphous iron) from soils. Ferrihydrite is a product of *in situ* weathering of parent material and forms as a coating on parent material either

via precipitation from water or bacterial fixation (Fortin and Langley, 2005). Ferrihydrite is a only a metastable mineral and will crystallize into goethite and then hematite over time (Schwertmann et al., 1999). A dithionite-citrate treatment will remove goethite and hematite as well as ferrihydrite and thus a ratio of Feo/Fed provides a measure of crystallization with numbers closer to zero being more crystallized (Birkeland, 1999; McFadden and Weldon, 1987). Birkeland (Birkeland, 1984) suggested that extraction procedures are less than precise in terms of removing known iron forms. As a consequence, extractable iron data will be discussed in terms of method and not necessarily the mineral form.

Relative ages for soil pits were calibrated with radiocarbon dates taken from the area during recent mapping (Chapter 5). Datable materials were recovered from small excavations, soil pit profiles, and exposed stream cuts. All samples were taken from more than 30 cm depth and were dated at the University of Georgia Center for Applied Isotope Studies using an AMS. Pits were numbered based on the order in which they were dug and all pit locations are labeled on the surficial geologic map of the Conejos River Valley (Johnson et al., 2010).

Results

Basic information about soil pits including sediment type and iron ratios are located in Table 6.1. All other raw soil data is located in Appendix C while profile photographs are located in Appendix D.

Last Glacial Maximum Terminal Moraines

Soils examined on LGM terminal moraines are characterized by consistent horizonation (typically A/AB/B/BC/C) and relatively deep weathering profiles (> 1 m). . The two pits excavated on LGM terminal moraines (pits 13 and 19) have very similar organic content profiles (Figure 6.2a). Both have generally low organic content throughout the profile (<20%) and are characterized by slightly higher organic content at the surface. Pit 13 increases in organic content two-thirds of the way down the profile before tapering off at the bottom while pit 19 simply tapers off with both containing less than 20% organic content throughout the entire depth profile.

Depth profiles of clay percentage are similar to each other as well with clay content increasing downward from the A into the AB and upper B horizons and then decreasing through the bottom of the profile (Figure 6.3a). B horizon moist colors are some of the brightest examined and range from 10 YR 5/3 to 7.5 YR 5/4. LGM soils also have the lowest extractable iron ratios of any soils examined (0.17 and 0.26).

Glacial Terrace

Glacial terraces (Pgt) soils are characterized by A/AB/B/C horizonation with Box horizons existing locally. The depths to C horizons range from 75 – 90 cm. Each profile decreases in organic content with depth and correlative horizons tend to have similar values (Figure 6.2b). A horizons are all characterized by organic contents between 12% and 27% while the bottom-most horizons for each pit contain less than 10% organic content. Clay content varies between pits (< 5% to 15 %) but shows a slight trend of increasing clay percentage in AB horizons followed by stable or slightly decreasing clay content through the bottom of the profile (Figure 6.3b). Moist soil colors from B horizons are characterized by relatively high chromas and values (and high intensity of color) which range from 10 YR 4/4 to 10 YR 3/2. Extractable iron ratios for the most developed horizons in glacial terrace soils range between 0.30 and 0.63.

Alluvial Fans

Latest Pleistocene alluvial fans (Paf1) are mantled by complicated, sometimes thick, soils that often contain evidence of buried soils within them. Horizonation varies between locations but can be generalized as A/AB/ABb/Bw/C although the C horizon is rarely observed as aggradational landforms tend to lead to thick soil profiles (see discussion). The depth to unweathered material varies depending on the number of buried soils present but ranges from ~ 1 m to >1.5 m. Pit 4 has a near uniform organic content throughout the entire profile with maximum values at 11% and minimum values at 7% (Figure 6.2c). In contrast, pit 11 is characterized by high organic content values at the top and bottom of the profile (14% and 20% respectively) with lower values in the middle (6%) indicating the presence of buried soils. The

clay content records for the soils mirror the organic content records with pit 4 having high clay content in the top and bottom of the profile while pit 11 has fairly consistent clay content throughout the profile (Figure 6.3c). Well-developed B horizons are not present on these surfaces, but moist colors of most developed horizons range from 10 YR 4/4 to 10 YR 4/2. Extractable iron ratios for the most developed horizons on large latest Pleistocene alluvial fans range from 0.53 to 0.70.

Holocene alluvial fans (Haf2) are also mantled by soils characterized by a combination of thin weathered profiles (25- 80 cm depth to unweathered zone) and thick weathered profiles incorporating buried soils (80 cm to >130 cm). Soil horizonation in thin soils is generally A/ABw/Bw/C while profiles containing buried soils are more commonly Aw/Bw/Ab/Bb. Pit 15 appears to be an outlier from these other soils and is characterized by A/AB/B/BC horizonation. Pit 10, which is the last landform dated to the Middle Holocene, is characterized by very high organic content values (Figure 6.2d) in the middle of the profile (up to 58% organic) and lower values in the top of the bottom of the profile (15% and 12% respectively). The three Late Holocene pits (pits 5, 15, and 16) are similar to each other, with generally decreasing organic values with depth. However, the magnitude of this decrease ranges from a large decrease in pit 16 (47% down to 3%) to a very small decrease in pit 5 (9% to 7%). Pits 5, 15, and 16 are also characterized by a relatively consistent, slightly decrease in clay content with depth (Figure 6.3d). Pit 10 is once again different and is characterized by relatively high clay content that increases through the middle of the profile and is lower but relatively constant in the bottom of the profile. Pit 10 was interpreted in the field to contain buried soils and the organic and clay content profiles support this interpretation. Moist colors for most developed horizons are relatively dark and range from 10 YR 4/2 to 10 YR 2/2. The extractable iron ratios for soils developed on Holocene alluvial fans range from 0.46 to 0.90.

Fluvial Terraces

The only Pleistocene age fluvial terrace (Pft1) soil examined (pit 7) is characterized by A/AB/B/BC horizonation and has a weathering profile > 1 m in thickness. The terrace is characterized by organic content variability throughout the profile. A peak in organic material (24%) occurs below the A horizon (in an AB horizon) and organic material then decreases below this point (to as low as 7%) before a slight increase in the bottom of the profile (9%, Figure 6.2e). Clay content decreases sharply with depth after relatively high clay percentages (Figure 6.3e) in the upper horizons (22% to < 5%). Moist color for the B horizon is a relatively dark 10 YR 3/3 and the extractable iron ratio for the horizon is 0.39.

Holocene fluvial terraces (Hft2) are mantled by generally thin (62 – 87 cm depth to unweathered zone) soils that commonly contain buried soil horizons. Soils containing buried soils generally have A/AB/Ab/Bb horizonation while Pit 9 has an A/B horizonation. Pit 6 has high organic content at the top of the profile (41%) with lower, but highly variable, content through the rest of the profile (Figure 6.2f). Pit 9 is characterized by similar variability except with significantly lower values near the surface (8%) and a peak two-thirds of the way down the profile (21%). Pit 12 is characterized by decreasing organic content with the exception of a large spike near the bottom of the profile (19%). Pit 6 has a relatively consistent clay content with depth while pit 9 increases with depth and pit 12 decreases with depth before a sharp increase in the lowest horizon (Figure 6.3f). Most soil colors are moderate and range from 10 YR 4/3 to 10 YR 3/4. Extractable iron ratios for soils on Holocene fluvial terraces range from 0.57-0.66.

Colluvium

Colluvial deposits (PHcol) are mantled by soils which are characterized by A/AB/B/C horizonation and 85 cm to over 120 cm depth to the unweathered zone in pits 3, 14, and 18. Two of the pits dug in colluvium (pit 14 and pit 18) share similar, generally decreasing, organic content depth profiles (Figure 6.2g). Pit 14 has a near-surface value of 16% and decreases to 10% while pit 18 contains 13% organics at the top and 5% at the bottom. Pit 3, on the other hand,

has an organic content peak one-third of the way down the profile. Clay percentages are also similar between pits (Figure 6.3g). Pit 14 has a near-surface value of 18% and shows a slight increase (in the B horizon) before decreasing to 12% while pit 18 contains 18% clay percentages at the top and 12% at the bottom. Pit 3, which has similar clay percentages as pit 14, shows a slight increase in clay percentages in the AB horizon before decreasing towards the bottom of the profile. Moist soil colors are amongst the brightest in the field area and range from 10 YR 4/4 to 2.5 Y 5/3. Extractable iron ratios for the most developed horizon of colluvial soils range from 0.35 – 0.48.

Discussion

Terminal Moraine Soils

The soils mantling LGM aged terminal moraines have the most developed horizonation of any pits (A/AB/B/BC/C). Both soils examined on terminal moraines have thick, established B horizons which are characterized by elevated clay contents and bright colors. The low extractable iron ratios provide additional evidence of significant soil development. Since the LGM moraines are known to be the oldest landforms examined, the soils on them provide a baseline with which to compare other soils in the area. The absolute age of the moraines is not known precisely but can be constrained by other studies in the area. The lowest date from Cumbres Bog, which is dammed by one of the moraines examined in this study, was measured as 18.3 ka BP +/- 250 years and should be considered a minimum age as it lies 0.5 m above glacial gravels. The Animas Glacier in the San Juan Mountains is thought to have abandoned its terminal moraine at 19.5 ka BP +/- 1.5 ka (Guido et al., 2007) and this is supported by research in the Sawatch Range suggesting the onset of deglaciation began at 19.5 ka BP +/- 1.8ka (Brugger, 2007). Earlier authors suggested that deglaciation in the central San Juan Mountains began at 16.8 ka +/- 0.3 ka although the majority of the data supported deglaciation beginning at 19 – 20 ka (Benson et al., 2005).

Glacial Terraces

It is difficult to discern how soil properties have changed through time on glacial terrace (Pgt) surfaces. Each soil mantling a glacial terrace has a well defined B horizon yet the soils have significant variation in extractable iron content, soil color, and overall horizonation (Appendix C). Variability in the rate of soil development through time may be the result of the intrinsic variability of glacial sediment (e.g., Evans and Benn, 2004). For instance, local initial differences in clay content may influence the hydrology of the soil and influence its weathering rate by altering the rate at which the soil absorbs water. Weathered depth is fairly consistent (76 - 86 cm) between sites although the weathered zone is not as thick as one would assume for deposits formed during the Pleistocene. The sediment is assumed to have been deposited ~12.5 ka BP based on glacial recession rates calculated in the Animas Valley of the western San Juan Mountains (Guido et al., 2007, see Chapter 1 for details) and the location of the glacial terraces approximately 40km up gradient from the terminal moraines discussed above.

Alluvial Fans

The large alluvial fans which formed in the latest Pleistocene (Paf1), and possibly into the Holocene, are mantled by soils which contain evidence of buried soils (pits 4 and 11). Buried soils are difficult to identify in the field because they were likely to be poorly developed when they were buried and are now overprinted by features forming in the modern B horizon. Analysis of organic contents, however, reveals the presence of buried soils at a number of different sites. Differences in the organic profiles between the two sites imply significantly different periods of soil development. Pit 4 has a consistent organic content with depth in the soil. In contrast, pit 11 increases in organic content with depth. This evidence for buried soils in pit 11implies that the fan may have been created by pulses of aggradation while the fan in which pit 4 is located was created by long-term, consistent aggradation. Similar trends in organic content have been used for identifying buried soils in other studies (McDonald and Busacca, 1990). The increase in clay content with depth also indicates a buried soil in pit 11 while a smaller increase in pit 4 provides

evidence of a buried B horizon possible formed during a brief period of stability. The extractable iron ratio (0.70) at pit 4 is much higher than other landforms that were deposited around the Pleistocene/Holocene transition indicating that the surface of the fan may have received sediment throughout the Holocene (Table 6.1). Furthermore, the AC horizon on top of pit 4 indicates that sedimentation may have continued through the late Holocene (including possible sedimentation during the construction of the road) while the well developed A horizon on the fan in which pit 11 is located indicates recent stability. Regardless of the activity level of the surface of the fans throughout the Holocene, I infer that majority of the volume of the fan was deposited during the Pleistocene/Holocene transition as both fans grade to the level of the glacial terrace.

Since it is difficult to differentiate between the two generations of Holocene alluvial fans (Haf2) in the field using stratigraphy and morphology, soil development is useful in identifying the age of those features. Pit 5, which was dug in an Haf2 alluvial fan, contains evidence of buried soils within its profile and has weak horizonation (ABw/Bw/ABb/C). The soil profile's horizons are characterized by uniformly low clay and organic content (Figures 2d and 3d). The location of the pit is near a modern incised stream which flows across an upaved forest service road. It is difficult to determine what human impacts have occurred in the area, specifically during the creation of the road. It is possible that the fan surface received sediment during road construction (as it appears pit 4 did). Nonetheless, an unusually high extractable iron ratio (0.91) implies that the fan consists of relatively unweathered material indicating Late Holocene formation. Pit 10 is from a small Haf2 fan located within a tributary channel that grades above the modern stream level. This pit contains evidence of a buried soil including a significant peak in organic percentage in a buried A horizon and an increase in clay content with depth (Figures 2d and 3d). This soil has been radiocarbon dated to 5384 +/- 65 years. Pit 15 was originally mapped as a Late Holocene fan because it appears to grade to the modern stream elevation (Johnson et al., 2010). Reexamination of the fan reveals that it may actually grade to an older terrace level as the fan occurs along a section of the Conejos River where it is incised less than 1

m into the glacial valley floor (discussion below about the age of the fan). This, along with its size, which is much larger than any other Late Holocene fan, leads us to believe that the fan actually formed during the Pleistocene Holocene transition. Pit 16 is characterized by one of the most poorly developed soils observed in this study with A/Aboxw/Ab/C horizonation and a weathered depth of 29 cm. This is consistent with the interpretation that the fans formed between 1.2 and 2.3 ka BP (Johnson et al., 2010).

Fluvial Terraces

The lone Pleistocene fluvial terrace that was identified in the area is also the only clast supported deposit in the area. The pit is also characterized by generally coarse sediment which is likely to impact soil development. The peak in organic material in the AB and B1 horizons indicates that time and/or high permeability have allowed organic material to illuviate within the profile. The clay content profile is similar to that of a younger feature although this is likely the result of low initial clay content in high energy fluvial deposits. Yet, the soil's extractable iron ratio (0.38) is consistent with the inferred age for the feature (~12.5 k.a. BP) implying that extractable iron may be a good indicator of age across units of vastly different sedimentology.

Late Holocene alluvial terraces have the most varied clay and organic profiles of any of the units examined for soil development. Both clay and organic contents shift rapidly with depth for each pit without any noticeable pattern. Differences in clay content is likely due to changes in initial sediment caused by 1) changes in the river's sediment load through time; and 2) the occurrence of channel switching, as evidenced by boggy deposits in areas where the valley floor remains wide. Varying organic content with depth is likely evidence for weak buried soils that formed as the channel migrated laterally or experienced large flood events. However, extractable iron ratios are as consistent between locations as any other unit (0.66, 0.57, and 0.57) leading me to infer that the variations in clay content and organic percentage are the result of initial sedimentological differences and not of soil forming processes.

Colluvium

Colluvium in the upper Conejos River Valley appears to be stable and has been dated to 9837 +/- 72 and 9567 +/- 67 calibrated years. The extractable iron ratios are similar between exposures (0.35, 0.47, and 0.39) and are consistent with deposit age (Table 6.1, discussion below). The increased amounts of clay in the AB and B horizons of pits 3 and 14 respectively are similar to bulges in pits 2, 8, and 11. In addition, the LGM terminal moraine soil pits outside of the immediate field area also have distinct increases in clay content in their B horizons. The smaller increase in B horizon clay content within the field area can be contrasted with those in terminal moraines to determine that 10,000 years is about the amount of time required to accumulate substantial amounts of illuvial clays in a profile. Furthermore, the fact that not all Pleistocene/Holocene soils examined show evidence of illuvial clays indicates that differences in initial sedimentology prevent illuvial clay content from being a good predictor of age. Lastly, additions to the soil from eolian silts and clays appear to be increasing the amount of fine material near the surface at a faster rate than it can be moved through the profile, thereby leading to a consistent decrease in clay content with depth.

Eolian Input

A horizons in soils throughout the field area are silt-rich and gravel-poor indicating that soils are receiving eolian inputs. The input of dust is supported not only by the presence of dust in A horizons but also by the low gravel content in A horizons. This scarcity of gravel is highlighted by the fact that all of the parent materials are inherently gravel-rich as shown by the dominance of gravel in exposed C horizons (> 70 % in all C horizons). A weak trend does exist between the assigned ages of the landforms and the gravel content in the A horizons (excluding the terminal moraines which are outside the field area). Twelve of the 17 pits in the field area follow the expected trend of low gravel content in the A horizons (<10%, measured in the field) in soils dating to the Early Holocene or Late Pleistocene and high gravel content (20 - 40%) in younger soils. Four of the soils examined had relatively low amounts of silt in their A horizons.

I attribute these anomalously low silt contents to variability in dust accumulation as a function of microclimate and other factors. Wind sheltered areas in the Rocky Mountains appear to accumulate relatively consistent amounts of dust (Painter et al., 2007), however few mountainous areas are shielded from the wind leading to a differential deposition of silt depending on wind patterns (Burns and Tonkin, 1982). These patterns are likely similar to winter patterns of windblown snow whereby ridge tops are bare and lee slopes accumulate more material than valley bottoms.

Extractable Iron

The ratio of Fe_o/Fe_d has been used as a relative indicator of age in soil chronosequences (Alexander, 1974; McFadden and Weldon, 1987; Tsai et al., 2007). Soil age and Fe_o/Fe_d ratio follows an expected trend for soils on the upper Conejos River Valley ($r^2 = 0.62$) although the relationship is stronger when combined with soils from the central Conejos River Valley (Figure 6.4, r2 = 0.70; Layzell, 2010).

Extractable iron data provide insights into the ages of 2 landforms of uncertain age. Pit 15, an alluvial fan originally mapped as Holocene, has an Fe_o/Fe_d ratio (0.45) similar to landforms that formed during the Pleistocene-Holocene transition. From this, I infer that this alluvial fan formed at least 5.5 ka BP and more likely ~10 ka BP. Pit 4, which was dug on an alluvial fan that is similar in size and stratigraphy to Late Pleistocene-Early Holocene alluvial fans but was mantled by a much younger looking soil, has an Fe_o/Fe_d of 0.70. This relatively high Fe_o/Fe_d ratio, combined with evidence of recent accumulations on the soil's surface lead me to infer that while the majority of the fan was deposited during the Late Pleistocene and Early Holocene, the surface is either active today, or was active during recent road construction. Other outliers of lesser magnitude include an extremely high F_{eo}/F_{ed} ratio for pit 5 which was dug on a small fan adjacent to pit 4. This surface may also have received sediment during the construction of the road. The sampled horizon for both of these pits was a Bw implying that a lack of soil development was initially identified in the field. It is also noteworthy that the method of

sampling only the perceived most-developed horizon of each profile presents an additional degree of uncertainty because of the possibility of sampling above or below the most developed horizon.

Soils on the glacial terrace (Pgt) show variability in Fe_o/Fe_d despite indications that the features formed simultaneously. Previous authors have noted that organic content inhibits the crystallization of amorphous Fe (van Breeman and Buurman, 1998) although no correlation exists in the field area between organic content and Fe_o content. Localized pH may influence the rate at which iron bound in silicates is weathered into ferrihydrite. Furthermore, the overall production of Fe_o from parent material is difficult to access for many soils. Over longer time periods, Fe_o content increases as a function of time before it then decreases, indicating an initial accumulation of poorly crystallized iron that eventually transforms into more organized iron forms. In the upper Conejos River Valley, there is no noticeable increase of Fe_o with age of soils, but rather a steady decrease in Fe_o. This indicates that the rate of Fe_o production from parent material is steady and is likely lower than the rate of transformation from Fe_o to Fe_d because a high rate of Fe_o production would lead to an initial increase in Fe_o content. Alternatively, it is possible that the peak in soil horizon development was missed during sampling making the soils appear much younger than they are. The result is that it appears that extractable iron ratios of soils mantling glacial sediments are not as good a predictor of soil age as extractable iron ratios on other types of sediment.

Other Proxies as Soil Age Indicators

Other commonly used indicators of soil age were also examined to determine their usefulness in dating surfaces including soil rubification, profile depth, and soil structure. Observations in the field seemed to indicate that young soils were darker in color, while older soils were lighter, more yellow, or slightly more pink. However, when colors of "most developed" horizons are plotted (value + chroma as all soils have the same hue, Figure 6.4), no pattern can be identified. This may be the result of difficulties in quantifying color, or it may be the result of examining the "most developed" horizon as opposed to sampling at equal depth.

Furthermore, porous parent materials in some deposits may allow for more rapid oxidation of soils, a possibility that is further complicated by the number of buried soils present in some deposits. Regardless, in such young soils, color would likely only be a weak indicator of age under even the most ideal circumstances.

Profile depth was also examined against estimated age as weathering depth has been shown to increase through time. Profile depth is a very poor indicator of soil age in the Conejos Valley (Figure 6.5). This result is not surprising as many young deposits contain buried soils which increase the maximum profile depth despite recent deposition. Furthermore, some glacial deposits were limited in their profile depth by large, buried glacial erratics which served as shallow, unweathered C horizons.

Lastly, soil structure was examined as a possible indicator of relative age since the quality of soil structure generally increases over time. Unfortunately, differences in parent material make structure difficult to compare across sand and gravel rich units (including alluvial fans and fluvial terraces) that tend to exhibit poor structure despite long intervals of soil development.

Conclusions

In the subalpine setting of the San Juan Mountains, typical indicators of soil age such as clay content, soil color, and structure do not provide a reliable record of relative ages for different landforms. However, the linear relationship between Fe_o/Fe_d and age indicates that Fe_o/Fe_d ratio can be used to determine relative ages across multiple parent materials in the upper Conejos River Valley. From this, I infer that Fe_o/Fe_d ratio may be useful for determining relative ages in settings similar to alpine areas in the southern Rocky Mountains. Horizonation also progresses as surfaces age, and older surfaces have noticeably more distinct AB and B horizons although this is muted on landforms which are aggradational (terraces and alluvial fans).

A handful of Fe_o/Fe_d outliers suggest that future authors using extractable iron ratios as indicators of age take numerous samples from each landform, and multiple samples per pit.

Redundant sampling may help identify Fe_o/Fe_d outliers due to differences in initial sedimentology and rates of dust accumulation. Alternatively, researchers may examine iron ratios throughout the entire depth of the profile as has been suggested previously (McFadden and Weldon, 1987).

Peaks in organic content within the depth profiles appear to be indicators of buried soil horizons as they are most common in cummulic profiles. This is not surprising as the relatively young ages of all surfaces within the field area allow for very little time for organic material to have been transferred downward into the profile. Variations in clay content, both across the field area and in relation to depth, seem to be the result of differences in initial sedimentology and not the illuviation of clays in older units. The B horizons of some older surfaces do show evidence of increased clay content but the relationship is not strong enough to be used as a predictor. One source of silt and clay that can be clearly identified is dust. The A horizons of many soil profiles consist of fines which contain little or no gravel content even when the parent material is gravel rich. The accumulation of clay does not appear to be a function of time which suggests that microclimates play a role in the amount of dust carried and deposited by the wind.

In general, soils provide an important window into the evolution of landscapes in the San Juan Mountains. Soil profiles provide evidence that hillslopes in the area have remained relatively stable since they stabilized during the Pleistocene-Holocene transition. However, despite the stability of hillslopes in the area, cummulic soil profiles show that alluvial fans and fluvial terraces have occasionally aggraded. This contrast between the older colluvium and the younger alluvial fans/terraces indicates that the source of the material is not the adjacent hillslopes but is rather the ridgetops. This example shows how important soil examination is to understanding post-glacial landscape evolution in previously glaciated terrain (Chapter 5).

Figures

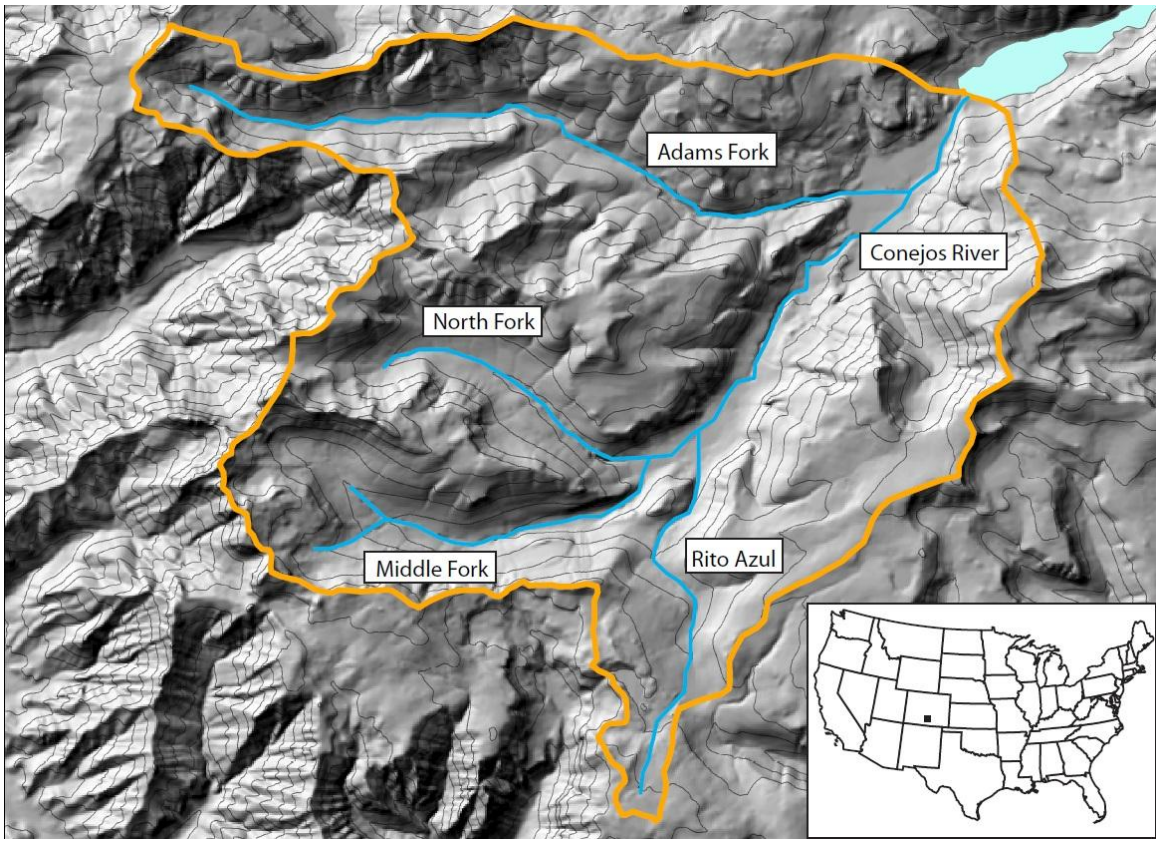

Figure 6.1 Area map of the upper Conejos River Valley indentifying the names of tributaries. Counter interval is 100 m.

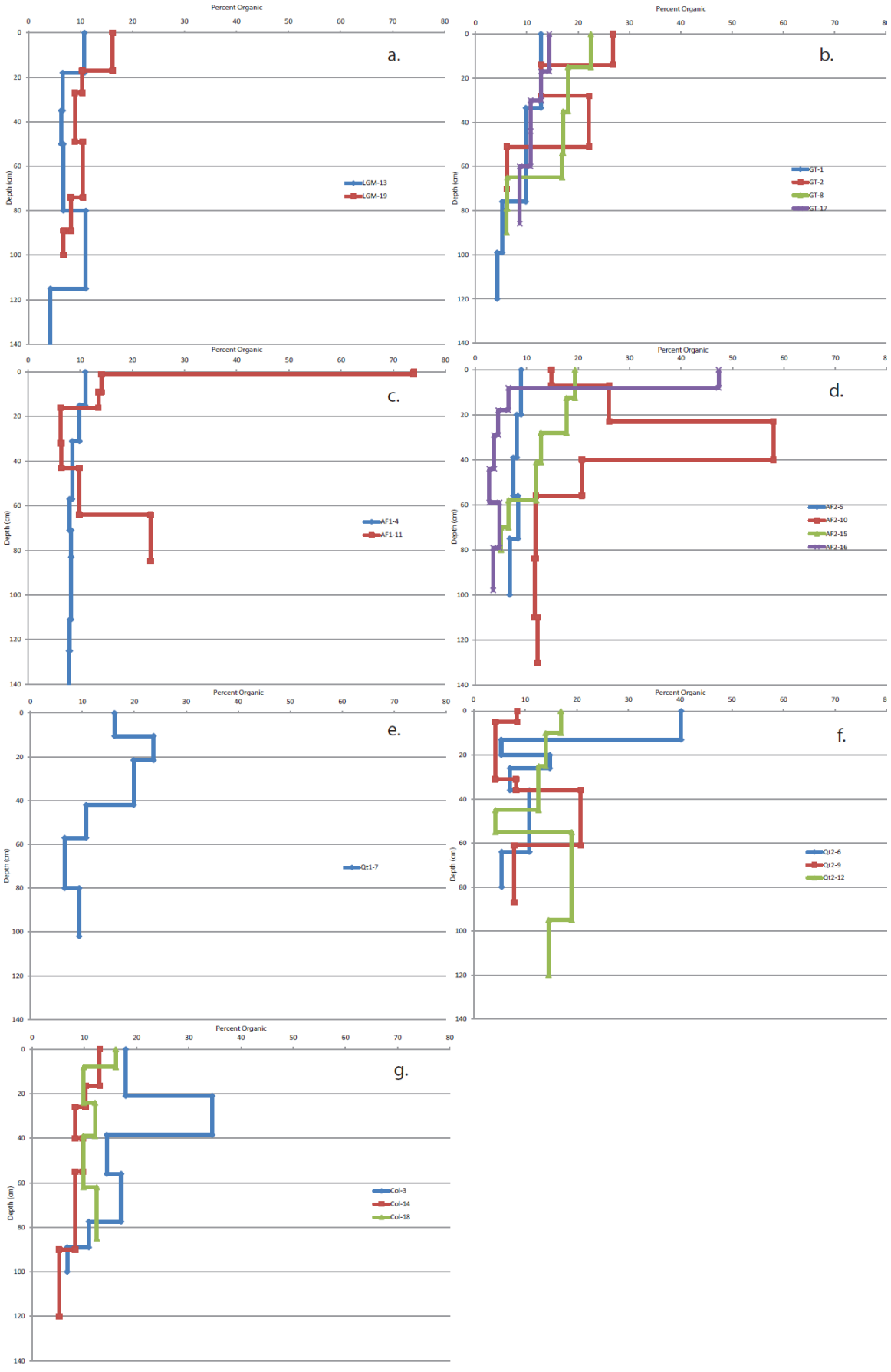
Percent Organic
Depth (cm)
a.
LGM-13
LGM-19
b.
GT-1
GT-2
GT-8
GT-17
c.
AF1-4
AF1-11
d.
AF2-5
AF2-10
AF2-15
AF2-16
e.
Qt1-7
f.
Qt2-6
Qt2-9
Qt2-12
g.
Col-3
Col-14
Col-18

Figure 6.2 Organic content graphed against depth for each of the soils examined in the field area. The soils are grouped on the basis of parent deposit as follows: (A) Last Glacial Maximum moraine, (B) glacial terrace, (C) Pleistocene-Holocene alluvial fan, (D) Holocene alluvial fan, (E) Pleistocene-Holocene fluvial terrace, (F)Holocene fluvial terrace, and (G) colluvium.

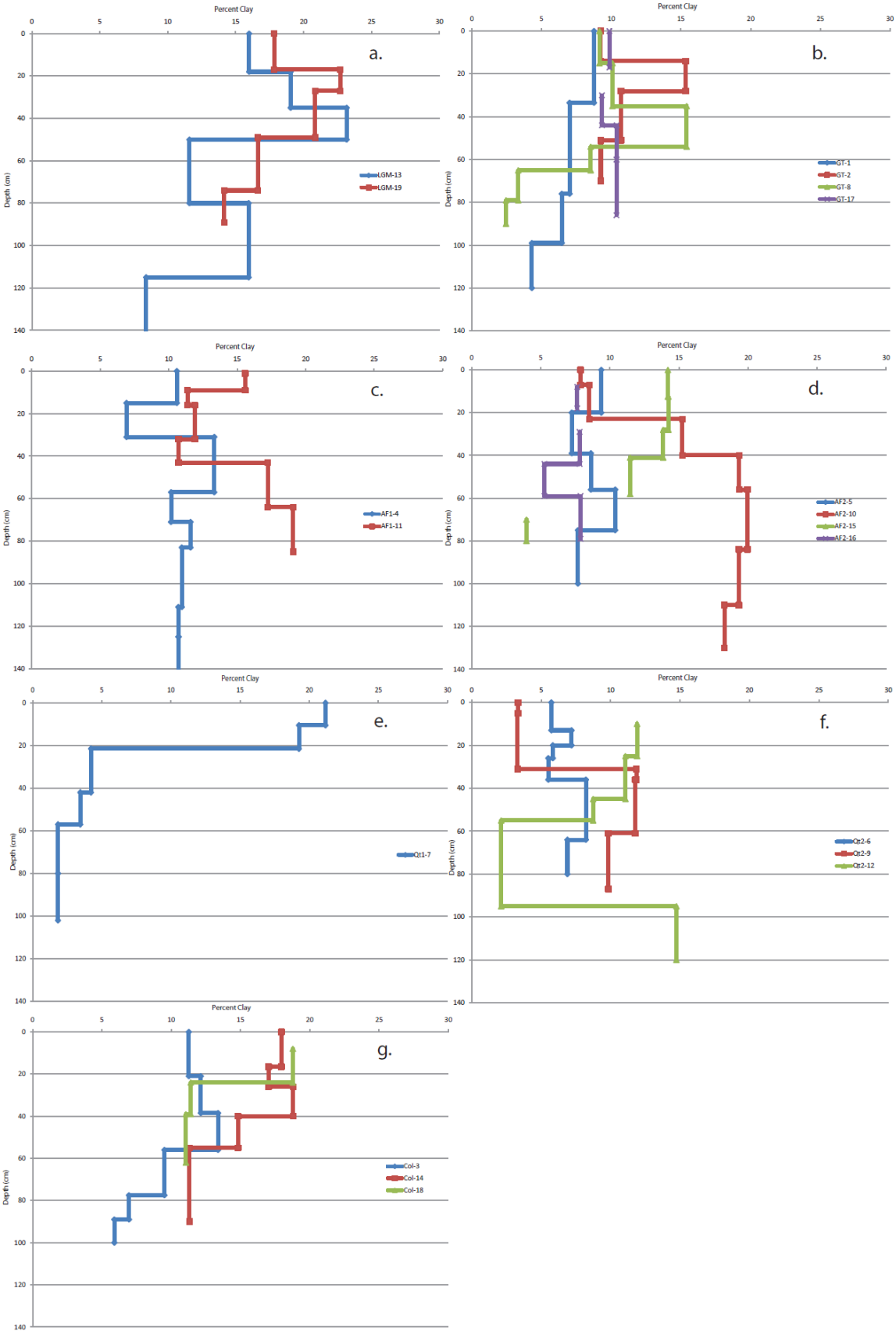
Percent Clay
Depth (cm)
a.
LGM-13
LGM-19
b.
GT-1
GT-2
GT-8
GT-17
c.
AF1-4
AF1-11
d.
AF2-5
AF2-10
AF2-15
AF2-16
e.
Qt1-7
f.
Qt2-6
Qt2-9
Qt2-12
g.
Col-3
Col-14
Col-18

Figure 6.3 Clay content graphed against depth for each of the soils examined in the field area. The soils are divided up based on parent deposit as follows: (A) Last Glacial Maximum moraine, (B) glacial terrace, (C) Pleistocene-Holocene alluvial fan, (D) Holocene alluvial fan, (E) Pleistocene-Holocene fluvial terrace, (F) Holocene fluvial terrace, and (G) colluvium.

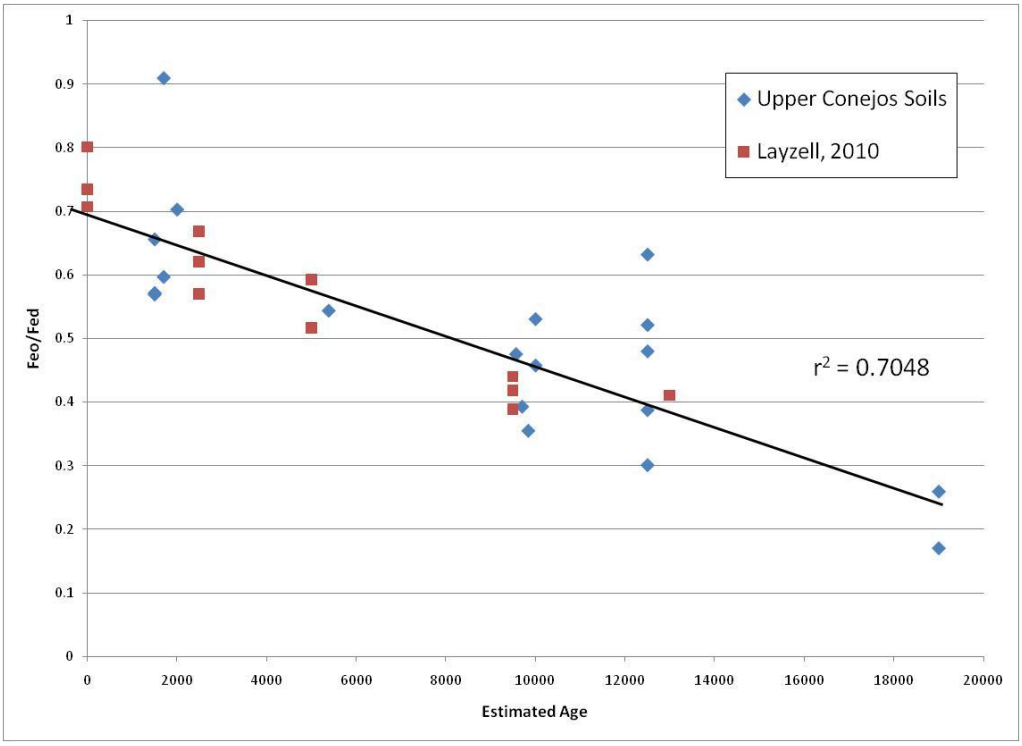

Figure 6.4 The ratio of Feo/Fed graphed against estimated age for deposits in the San Juan Mountains. This figure includes both the data presented here as well as recent data from Layzell (2010).

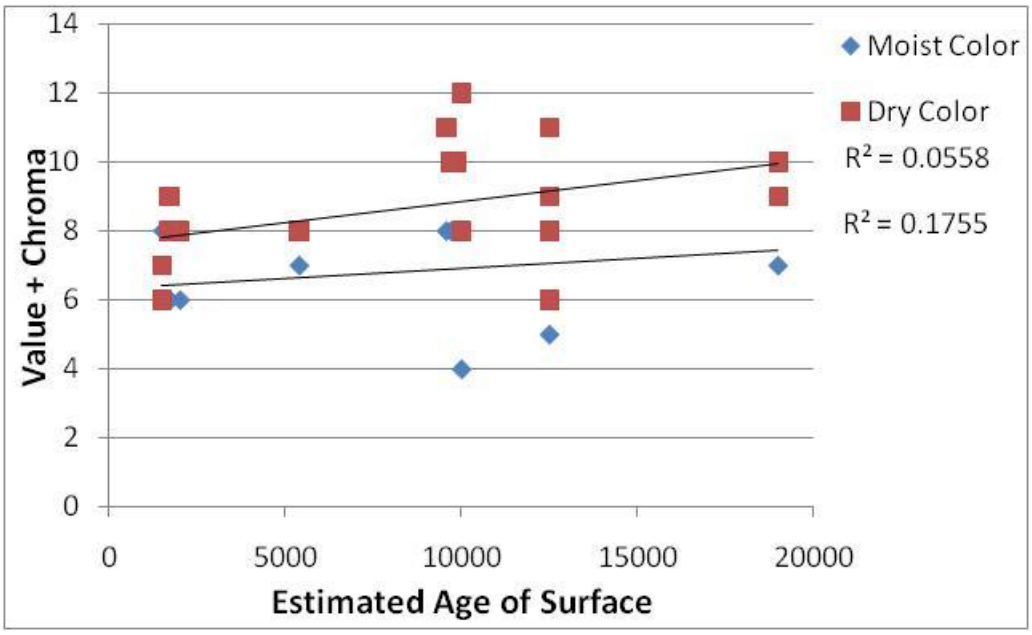

Figure 6.5 As soil hue throughout the field area was generally the same, value was added to chroma and graphed against estimated deposit age for both moist and dry colors. Neither moist or dry color was a good indicator of age.

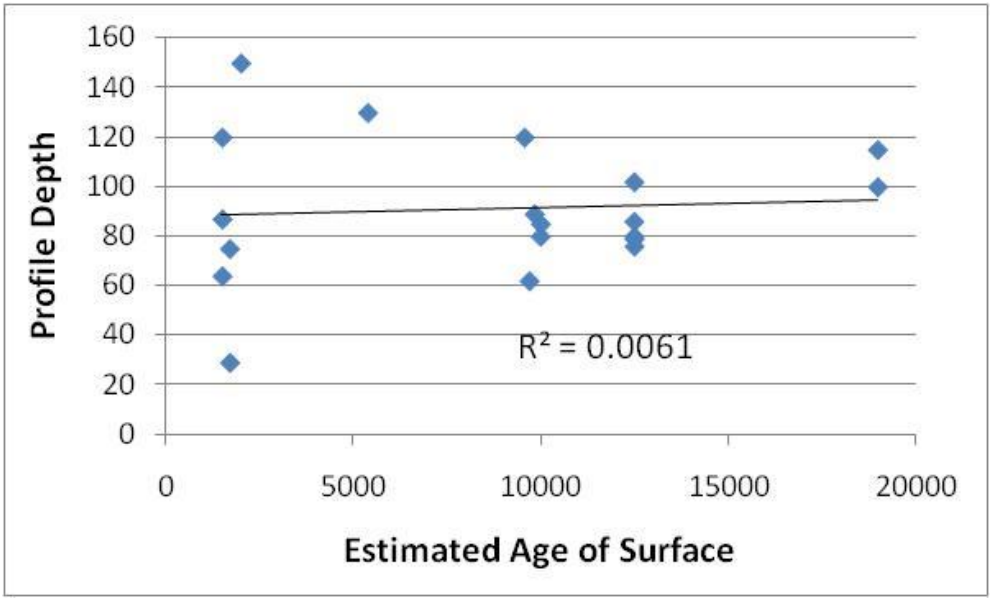

Figure 6.6 Profile depth (cm) graphed against the estimated age of surfaces in the upper Conejos River Valley. Profile depth is not a good indicator of age.

Table 6.1 The sampled horizon for each soil pit along with its extractable iron contents and assumed ages.

Pit Number by Unit	Horizon Sampled	Feo	Fed	Feo/Fed	Est. Age
Hft2					
6	B	0.93131	1.420152	0.655782	1500
9	B3	0.716948	1.254574	0.571467	1500
12	B	1.447248	2.543205	0.569065	1500
Haf2					
10	Bb2	1.007986	1.854255	0.543607	5384
15	B2	0.875154	1.913287	0.457409	10000
16	Abox	0.533784	0.894621	0.596659	1700
5	Bw	0.609351	0.670011	0.909465	1700
Paf1					
4	Bw1	0.611986	0.870864	0.702734	2000
11	Box	1.539177	2.901717	0.530436	10000
Pft1					
7	B2	0.632507	1.633964	0.3871	12500
PHcol					
3	B	0.626406	1.766427	0.354618	9837
14	B2	1.220962	2.569121	0.475245	9567
18	B2	0.346737	0.883103	0.392635	9700
Pgt					
1	A/Box	0.681452	1.420872	0.479601	12500
2	B2	0.646234	1.022764	0.63185	12500
8	B	0.482551	1.605168	0.300623	12500
17	B4	0.742322	1.424472	0.521121	12500
LGM					
13	B3	0.69407	2.681426	0.258844	19000
19	B3	0.161771	0.952214	0.169889	19000

CHAPTER 7 – CONCLUSIONS

Pollen assemblages, diatom assemblages, and sedimentology from Cumbres Bog in the southern San Juan Mountains of Colorado provide a record of climate change since the end of the Last Glacial Maximum. The record provides strong evidence for: cooling during the Younger Dryas (~12.8-11.5 ka), a warm stable climate until 6 ka, and cooler but more variable climate after 6 ka. Pollen ratios and diatoms indicate that cold periods generally match with periods of rapid climate change and occurred at 10.6, 8.7-7.9, 7.0-6.9, 5.4–5.2, 3.3–3.0, 2.3, 2.0 and 1.5 ka. This record also adds resolution to previous regional records and indicates that the periodicity of climate change shortened from 2,000-3,000 years to 700-1,100 years around 6 ka and to <500 years after 3.5 ka. These changes correspond with increased El Niño-Southern Oscillation (ENSO) activity after the mid-Holocene. The mechanism that links ENSO activity to general climate periodicity is not well understood, however, the Cumbres Bog record suggests that both regional and global climate forcings influenced climate in the San Juan Mountains.

Geomorphic mapping in the upper Conejos River Valley of the San Juan Mountains has shown that three distinct periods of aggradation have occurred in valley bottoms since the end of the Last Glacial Maximum (LGM). The first occurred during the Pleistocene-Holocene transition (~12.5 – 9.5 ka) and is interpreted as paraglacial landscape response to deglaciation after the LGM. Evidence of the second period of aggradation is limited but indicates a small pulse of sedimentation at ~ 6 ka. A third, more broadly identifiable period of sedimentation occurred in the Late Holocene (~2.2 – 1 ka). The latest two periods of aggradation are concurrent with ENSO related increases in the frequency of climate change. This suggests that Holocene alpine and subalpine landscapes responded more to rapid changes in climate than to large singular climatic swings. Soil development and radiocarbon dating indicate that hillslopes were largely

stable during the Holocene even while aggradation was occurring in valley bottoms. Thus, we can conclude that erosion does not occur equally throughout the landscape but is focused in stream headwaters, along tributary channels, or on ridgetops.

Nineteen soils were examined in a variety of post-LGM landforms and deposits (glacial, fluvial, alluvial, colluvial), ranging in elevation from ~3600-2600 m, to create a chronosequence across multiple parent materials. Soils developing in deposits ranging in age from ~1-18 ka were examined, described, and sampled in the field for laboratory analyses including particle size, pH, Fe extractions, and total organic carbon. Ratios of oxalate/dithionite Fe extractions exhibit a robust trend with age for all soils. This relationship is in contrast to other properties such as reddening or clay content where qualtifiable trends are not evident. Variation in eolian deposition and parent material sedimentology likely led to the observed variability in soils of similar age.

The combined records clearly indicate that landscapes have been responsive to changes in climate over millennial timescales. It is difficult to determine what the future of the Conejos Valley may be. The location of the Platoro Reservoir isolates the upper river from the lower river and makes the upper Conejos River Valley somewhat of a closed system. Thus, we must look at the area isolated above dam in order to understand how the landscape may continue to evolve. The current global warming trend may be most like the early Holocene in the area which could lead to general stability throughout the field area and minimizing sedimentation in the valley bottom. Alternatively, increased summer temperatures could increase the strength of the summer monsoon (as it did in the summer of 2007) and increase sedimentation above the dam. Either possibility would significantly affect the amount of water delivered to the San Luis Valley influencing the life of people living there. Increased sedimentation could affect the useful life of the dam if the reservoir becomes filled with silt carried by the river during summer storms. Currently, the reservoir is being filled in by larger cobbles and gravel moved during the spring melt but little of this material makes it to the lower reaches of the reservoir because of the low gradient of the river above the constriction of the valley.

Looking at the big picture, the results of this research advance the science of geomorphology in a number of ways. First, the Cumbres Bog core provides a climatic record in a climatically complicated terrestrial region in the western United States. The record increases the spatial resolution of temporally high resolution paleoclimate records in the region. This will help future researchers examining and modeling climate variability regionally and globally. The mapping provides a rare record of landscape response to climate change over millennial time scales. It provides a geologic record of subalpine landscape evolution and provides clues about future landscape response to climate change. For example, the relative stability of colluvium in the area is likely the result of vegetative cover strengthened by monsoon rains in the summer. Thus, future climate change that weakens the strength of the monsoon may increase the amount of sediment generated from hillslopes.

Future research is likely to focus on the creation of new climate records because of their value in understanding and modeling future climate change. However, researchers should focus additionally on high elevation landscapes and their response to climate change. The research on the stability of colluvium presented here displays the poor understanding of hillslope processes that is currently used in landscape evolution models. Furthermore, soils should continue to be integrated into this research as they provide invaluable insight into the original parent material as well as the evolution of the landforms.

More broadly yet, this research progresses society by increasing our understanding of the interactions between climate and landscape systems. Regionally, this is important to farmers in the San Luis Valley who depend on water from the mountains to water crops. It also furthers the field of environmental science by highlighting the feedbacks between ecosystems, climate oscillations, seasonal variability, and global climate forcing. The interdisciplinary nature of geoscience is growing studies like this one will continue to push our understanding of the feedbacks between disciplines.

REFERENCES

Adams, D.K., and Comrie, A.C., 1997, The North American monsoon: Bulletin of the American Meteorological Society, v. 78, p. 2197.

Alexander, E.B., 1974, Extractable iron in relation to soil age on terraces along the Truckee River, Nevada: Soil Science Society of America Procedings, v. 38, p. 121-124.

Anderson, R.S., Betancourt, J.L., Mead, J.I., Hevly, R.H., and Adam, D.P., 2000, Middle- and late-Wisconsin paleobotanic and paleoclimatic records from the southern Colorado Plateau, USA: Palaeogeography, Palaeoclimatology, Palaeoecology, v. 155, p. 31-57.

Ariztegui, D., Bösch, P., and Davaud, E., 2007, Dominant ENSO frequencies during the Little Ice Age in Northern Patagonia: The varved record of proglacial Lago Frías, Argentina: Quaternary International, v. 161, p. 46-55.

Armour, J., Fawcett, P.J., and Geissman, J.W., 2002, 15 k.y. paleoclimatic and glacial record from northern New Mexico: Geology, v. 30, p. 723-727.

Asmerom, Y., Polyak, V., Burns, S., and Rassmussen, J., 2007, Solar forcing of Holocene climate: New insights from a speleothem record, southwestern United States: Geology, v. 35, p. 1-4.

Atwood, W.W., and Mather, K.F., 1932, Physiography and Quaternary Geology of the San Juan Mountains, Colorado: U.S. Geological Survey Professional Paper, v. 166, p. 176.

Bacon, S.N., McDonald, E.V., Caldwell, T.G., and Dalldorf, G.K., 2010, Timing and distribution of alluvial fan sedimentation in response to strengthening of late Holocene ENSO variability in the Sonoran Desert, southwestern Arizona, USA: Quaternary Research, v. 73, p. 425-438.

Ballantyne, C.K., 2002, Paraglacial geomorphology: Quaternary Science Reviews, v. 21, p. 1935-2017.

Benedict, J.B., 1973, Chronology of cirque glaciation, Colorado Front Range: Quaternary Research, v. 3, p. 584-600.

Benson, L., Madole, R., Landis, G., and Gosse, J., 2005, New data for Late Pleistocene Pinedale alpine glaciation from southwestern Colorado: Quaternary Science Reviews, v. 24, p. 49-65.

Berry, M.E., 1987, Morphological and chemical characteristics of soil catenas on pinedale and Bull Lake moraine slopes in the Salmon River Mountains, Idaho: Quaternary Research, v. 28, p. 210-225.

Bierman, P., and Steig, E.J., 1996, Estimating rates of denudation using cosmogenic isotope abundances in sediment: Earth Surface Processes and Landforms, v. 21, p. 125-139.

Birkeland, P.W., 1984, Soils and Geomorphology: New York, Oxford University Press, 372 p.

—, 1999, Soils and Geomorphology: New York, Oxford University Press, 430 p.

Birkeland, P.W., and Burke, R.M., 1988, Soil catena chronosequences on eastern Sierra Nevada moraines, California, U.S.A: Arctic and Alpine Research, v. 20, p. 473-484.

Birkeland, P.W., Shroba, R.R., Burns, S.F., Price, A.B., and Tonkin, P.J., 2003, Integrating soils and geomorphology in mountains - an example from the Front Range of Colorado: Geomorphology, v. 55, p. 329-345.

Blackford, J., 2000, Palaeoclimatic records from peat bogs: Trends in Ecology & Evolution, v. 15, p. 193-198.

Bond, G., Showers, W., Cheseby, M., Lotti, R., Almasi, P., deMenocal, P., Priore, P., Cullen, H., Hajdas, I., and Bonani, G., 1997, A pervasive millennial-scale cycle in North Atlantic Holocene and glacial climates: Science, v. 278, p. 1257-1266.

Brugger, K.A., 2007, Cosmogenic 10Be and 36Cl ages from Late Pleistocene terminal moraine complexes in the Taylor River drainage basin, central Colorado, USA: Quaternary Science Reviews, v. 26, p. 494-499.

Bull, W.B., 1991, Geomorphic responses to climate change: New York, NY, Oxford University Press, 326 p.

Bull, W.B., and Schick, A.P., 1979, Impact of climate change on an arid region watershed: Nahal Yael, southern Israel: Quaternary Research, v. 11, p. 153-171.

Burns, S.F., and Tonkin, P.J., 1982, Soil-geomorphic models and the spatial distribution and development of alpine soils, *in* Thorn, C., ed., Space and Time in Geomorphology: London, Allen and Unwin, p. 25-43.

Carrara, P.E., and Andrews, J.T., 1976, Holocene glacial/periglacial record; Northern San Juan Mountains, Southwestern Colorado: Zeitschrift fur Gletscherkunde and Glazialgeologie, v. 11, p. 155-174.

Carrara, P.E., Mode, W.N., and Rubin, M., 1984, Deglaciation and postglacial timberline in the San Juan Mountains, Colorado: Quaternary Research, v. 21, p. 42-55.

Carrara, P.E., Trimble, D.A., and Rubin, M., 1991, Holocene treeline fluctuations in the northern San Juan Mountains, Colorado, U.S.A., as indicated by radiocarbon-dated conifer wood: Arctic and Alpine Research, v. 23, p. 233-246.

Coulthard, T.J., Macklin, M.G., and Kirkby, M.J., 2002, A cellular model of Holocene upland river basin and alluvial fan evolution: Earth Surface Processes and Landforms, v. 27, p. 269-288.

Crittenden, R.C., and Muhs, D.R., 1986, Cliff height and slope angle relationships in a soil chronosequence of marine terraces, San Clemente, California: Zeitschrift für Geomorphologie, v. 30, p. 291-301.

Curry, A.M., and Morris, C.J., 2004, Lateglacial and Holocene talus slope development and rockwall retreat on Mynydd Du, UK: Geomorphology, v. 58, p. 85-106.

Denton, G.H., and Karlen, W., 1973, Holocene climatic variations: their pattern and possible cause: Quaternary Research, v. 3, p. 155-205.

Dixon, J.L., Heimsath, A.M., Kaste, J., and Amundson, R., 2009, Climate-driven processes of hillslope weathering: Geology, v. 37, p. 975-979.

Douglass, D., and Mickelson, D., 2007, Soil development and glacial history, West Fork of Beaver Creek, Uinta Mountains, Utah: Arctic, Antarctic, and Alpine Research, v. 39, p. 592-602.

Duan, K., and Yao, T., 2003, Monsoon variability in the Himalayas under the condition of global warming: Jounral of the Meteorological Society of Japan, v. 81, p. 251-257.

Engstrom, D.R., and Fritz, S.C., 2006, Coupling between primary terrestrial succession and the trophic development of lakes at Glacier Bay, Alaska: Journal of Paleolimnology, v. 35, p. 873-880.

Enzel, Y., Cayan, D.R., Anderson, R.Y., and Wells, S.G., 1989, Atmospheric circulation during Holocene lake stands in the Mojave Desert: evidence of regional climate change: Nature, v. 341, p. 44-47.

Eppes, M.C., Bierma, R., Vinson, D., and Pazzaglia, F.J., 2008, A soil chronosequence study of the Reno valley, Italy: Insights into the relative role of climate versus anthropogenic forcing on hillslope processes during the mid-Holocene: Geoderma, v. 147, p. 97-108.

Eppes, M.C., and McFadden, L., 2008, The influence of bedrock weathering on the response of drainage basins and associated alluvial fans to Holocene climates, San Bernardino Mountains, California, USA: The Holocene, v. 18, p. 895-905.

Eppes, M.C., McFadden, L.D., Matti, J., and Powell, R., 2002, Influence of soil development on the geomorphic evolution of landscapes: An example from the Transverse Ranges of California: Geology, v. 30, p. 195-198.

Evans, D.J.A., and Benn, D.I., 2004, A practical guide to the study of glacial sediments: London, Arnold, p. 266.

Faegri, K., and Iversen, J., 1989, Textbook of Pollen Analysis: New York, Wiley.

Fall, P.L., 1997, Timberline fluctuations and late Quaternary paleoclimates in the southern Rocky Mountains, Colorado: Geological Society of America Bulletin, v. 109, p. 1306-1320.

Feiler, E.J., Anderson, R.S., and Koehler, P.A., 1997, Late Quaternary paleoenvironments of the White River Plateau, Colorado, U.S.A: Arctic and Alpine Research, v. 29, p. 53-62.

Fortin, D., and Langley, S., 2005, Formation and occurrence of biogenic iron-rich minerals: Earth-Science Reviews, v. 72, p. 1-19.

Franzmeier, D.P., Pedersen, E.J., Longwell, T.J., Byrne, J.G., and Losche, C.K., 1969, Properties of some soils in the Cumberland Plateau as related to slope aspect and position: Soil Science Society of America Journal, v. 33, p. 755-761.

Fritz, S.C., Kreiser, A.M., Appleby, P.G., and Battarbee, R.W., 1990, Recent acidification of upland lakes in north and mid-Wales: paleolimnological evidence, *in* Edwards, R.W., Gee, A.S., and Stoner, J.H., eds., Acid Waters in Wales: Dordrecht, Kluwer Academic Publishers, p. 27-37.

Gergel, S.E., Turner, M.G., Miller, J.R., Melack, J.M., and Stanley, E.H., 2002, Landscape indicators of human impacts to riverine systems: Aquatic Sciences - Research Across Boundaries, v. 64, p. 118-128.

Grissino-Mayer, H.D., Romme, W.H., Lisa Floyd, M., and Hanna, D.D., 2004, Climatic and human influences on fire regimes of the southern San Juan Mountains, Colorado, USA: Ecology, v. 85, p. 1708-1724.

Guido, Z.S., Ward, D.J., and Anderson, R.S., 2007, Pacing the post–Last Glacial Maximum demise of the Animas Valley glacier and the San Juan Mountain ice cap, Colorado: Geology, v. 35, p. 739-742.

Harvey, A.M., Wigand, P.E., and Wells, S.G., 1999, Response of alluvial fan systems to the late Pleistocene to Holocene climatic transition: contrasts between the margins of pluvial Lakes Lahontan and Mojave, Nevada and California, USA: Catena, v. 36, p. 255-281.

Humlum, O., 2000, The geomorphic significance of rock glaciers: Estimates of rock glacier debris volumes and headwall recession rates in west Greenland: Geomorphology, v. 35, p. 41-67.

Hunckler, R.V., and Schaetzl, R.J., 1997, Spodosol development as affected by geomorphic aspect, Baraga County, Michigan: Soil Science Society of America Journal, v. 61, p. 1105-1115.

IPCC, 2007, Summary for policymakers, *in* Solomon, S., D., Q., Manning, M., Chen, Z., Marquis, M., Averyt, K.B., M., T., and Miller, H.L., eds., Climate Change 2007: The Physical Science Basis. Contribution of Working Group 1 to the Fourth Assessment Report to the Intergovernment Panel on Climate Change: Cambridge, United Kingdom and New York, NY, USA, Cambridge University Press.

Jenny, H., 1941, Factors of Soil Formation: New York, McGraw-Hill.

—, 1980, The Soil Resource -- Origin and Behavior: New York, Springer, 377 p.

Jiménez-Moreno, G., Fawcett, P.J., and Scott Anderson, R., 2008, Millennial- and centennial-scale vegetation and climate changes during the late Pleistocene and Holocene from northern New Mexico (USA): Quaternary Science Reviews, v. 27, p. 1442-1452.

Jiménez-Moreno, G., Johnson, B.G., Eppes, M.C., and Diemer, J.A., in prep.

Johnson, B.G., Eppes, M.C., and Diemer, J.A., 2010, Surficial geologic map of the upper Conejos River drainage, southeastern San Juan Mountains, southern Colorado: Journal of Maps, v. v2010, p. 30-39.

Johnson, B.G., Jiménez-Moreno, G., Eppes, M.C., Diemer, J.A., and Stone, J.R., in review, An A 18k high resolution multi-proxy paleoclimate record from a sub-alpine bog in the San Juan Mountains of southern Colorado: Geology.

Johnson, B.G., Thackray, G.D., and Van Kirk, R., 2007, The effect of topography, latitude, and lithology on rock glacier distribution in the Lemhi Range, central Idaho, USA: Geomorphology, v. 91, p. 38-50.

Kelsey, H.M., and Bockheim, J.G., 1994, Coastal landscape evolution as a function of eustasy and surface uplift rate, Cascadia margin, southern Oregon: Geological Society of America Bulletin, v. 106, p. 840-854.

Kilham, S.S., Theriot, E.C., and Fritz, S.C., 1996, Linking planktonic diatoms and climate change in the large lakes of the Yellowstone ecosystem using resource theory: Limnology and Oceanography, v. 41, p. 1052-1062.

Kirchner, J.W., Finkel, R.C., Riebe, C.S., Granger, D.E., Clayton, J.L., King, J.G., and Megahan, W.F., 2001, Mountain erosion over 10 yr, 10 k.y., and 10 m.y. time scales: Geology, v. 29, p. 591-594.

Langbein, W.B., and Schumm, S.A., 1958, Yield of sediment in relation to mean annual precipitation: Transactions, American Geophysical Union, v. 39, p. 1076-1084.

Layzell, T., 2010, Soils and Geomorphology of central Conejos River Valley: Fluvial Response to Post Last Glacial Maximum Climates and Sediment Supply: Charlotte, NC, University of North Caroline - Charlotte.

Lipman, P.W., 1974, Geologic Map of the Platoro Caldera Area, Southeastern San Juan Mountains, Southwestern Colorado, Miscellaneous Investigations Series, Department of the Interior, USGS.

Lipman, P.W., Dungan, M.A., Brown, L.L., and Deino, A., 1996, Recurrent eruption and subsidence at the Platoro caldera complex, southeastern San Juan volcanic field, Colorado: New tales from old tuffs: Geological Society America Bulletin, v. 108, p. 1039-1055.

Lipman, P.W., Steven, T.A., and Mehnert, H.A., 1970, Volcanic history of the San Juan Mountains, Colorado, as indicated by potassium-argon dating: Geological Society of America Bulletin, v. 81, p. 2329-2341.

Liu, Z., Kutzbach, J., and Wu, L., 2000, Modeling climate shift of El Nino variability in the Holocene: Geophysical Research Letters, v. 27.

Lønne, I., and Lysså, A., 2005, Deglaciation dynamics following the Little Ice Age on Svalbard: Implications for shaping of landscapes at high latitudes: Geomorphology, v. 72, p. 300-319.

Lotter, A.F., and Bigler, C., 2000, Do diatoms in the Swiss Alps reflect the length of ice-cover?: Aquatic Sciences - Research Across Boundaries, v. 62, p. 125-141.

Lotter, A.F., Birks, H.J.B., Hofmann, W., and Marchetto, A., 1998, Modern diatom, cladocera, chironomid, and chrysophyte cyst assemblages as quantitative indicators from the reconstruction of past environmental conditions in the Alps. II. Nutrients: Journal of Paleolimnology, v. 19, p. 443-463.

Mann, D.H., and Meltzer, D.J., 2007, Millennial-scale dynamics of valley fills over the past 12,000 14C yr in northeastern New Mexico, USA: Geological Society of America Bulletin, v. 119, p. 1433-1448.

Markgraf, V., and Scott, L., 1981, Lower timberline in central Colorado during the past 15,000 yr: Geology, v. 9, p. 231-243.

Marston, R.A., 2010, Geomorphology and vegetation on hillslopes: Interactions, dependencies, and feedback loops: Geomorphology, v. 116, p. 206-217.

Matsuoka, N., and Sakai, H., 1999, Rockfall activity from an alpine cliff during thawing periods: Geomorphology, v. 28, p. 309-328.

Mayewski, P.A., Rohling, E.E., Curt Stager, J., Karlén, W., Maasch, K.A., David Meeker, L., Meyerson, E.A., Gasse, F., van Kreveld, S., Holmgren, K., Lee-Thorp, J., Rosqvist, G., Rack, F., Staubwasser, M., Schneider, R.R., and Steig, E.J., 2004, Holocene climate variability: Quaternary Research, v. 62, p. 243-255.

McAuliffe, J.R., Scuderi, L.A., and McFadden, L.D., 2006, Tree-ring record of hillslope erosion and valley floor dynamics: Landscape responses to climate variation during the last 400 yr in the Colorado Plateau, northeastern Arizona: Global and Planetary Change, v. 50, p. 184-201.

McDonald, E.V., and Busacca, A.J., 1990, Interaction between aggrading geomorphic surfaces and the formation of a late pleistocene paleosol in the Palouse loess of eastern Washington state: Geomorphology, v. 3, p. 449-469.

McDonald, E.V., McFadden, L.D., and Wells, S.G., 2003, Regional response of alluvial fans to the Pleistocene-Holocene climatic transition, Mojave Desert, California, *in* Enzel, Y., Wells, S.G., and Lancaster, N., eds., Paleoenvironments and paleohydrology of the Mojave and southern Great Basin Deserts, Geological Society of America Speical Paper Volume 368: Boulder, Colorado, Geological Society of America.

McFadden, L.D., and Weldon, R.J., 1987, Rates and processes of soil development on Quaternary terraces in Cajon Pass, California: Geological Society of America Bulletin, v. 98, p. 280-293.

McKeague, J.A., and Day, J.H., 1997, Dithionite and oxalate extractable Fe and Al as aids in differentiating various classes of soils: Canadian Journal of Soil Science, v. 46, p. 13-22.

Mehra, O.P., and Jackson, M.L., 1960, Iron oxide removal from soils and clays by a dithionite citrate system buffered with sodium bicarbonate: Clays Clay Miner, v. 7, p. 313-17.

Menking, K.M., and Anderson, R.Y., 2003, Contributions of La Nina and El Nino to middle Holocene drought and late Holocene moisture in the American Southwest: Geology, v. 31, p. 937-940.

Miller, C.D., 1973, Chronology of Neoglacial deposits in the northern Sawatch Range, Colorado: Arctic and Alpine Research, v. 5, p. 385-399.

Miller, J., Germanoski, D., Waltman, K., Tausch, R., and Chambers, J., 2001, Influence of late Holocene hillslope processes and landforms on modern channel dynamics in upland watersheds of central Nevada: Geomorphology, v. 38, p. 373-391.

Morgan, P., Seager, W., and Golombek, M., 1986, Cenozoic thermal, mechanical and tectonic evolution of hte Rio Grande Rift: Journal of Geophysical Research, v. 91(B6), p. 6263-6276.

Nichols, K.K., Bierman, P.R., Eppes, M.C., Caffee, M., Finkel, R., and Larsen, J., 2007, Timing of surficial process changes down a Mojave Desert piedmont: Quaternary Research, v. 68, p. 151-161.

Painter, T.H., Barrett, A.P., Landry, C.C., Neff, J.C., Cassidy, M.P., Lawrence, C.R., McBride, K.E., and Farmer, G.L., 2007, Impact of disturbed desert soils on duration of mountain snow cover: Geophysical Research Letters, v. 34, p. L12502.

Petit, J.R., Jouzel, J., Raynaud, D., Barkov, N.I., Barnola, J.M., Basile, I., Bender, M., Chappellaz, J., Davis, M., Delaygue, G., Delmotte, M., Kotlyakov, V.M., Legrand, M., Lipenkov, V.Y., Lorius, C., Pepin, L., Ritz, C., Saltzman, E., and Stievenard, M., 1999, Climate and atmospheric history of the past 420,000 years from the Vostok ice core, Antarctica: Nature, v. 399, p. 429-436.

Pierce, J.L., Meyer, G.A., and Timothy Jull, A.J., 2004, Fire-induced erosion and millennial-scale climate change in northern ponderosa pine forests: Nature, v. 432, p. 87-90.

Pierce, K.L., and Scott, W.E., 1982, Pleistocene episodes of alluvial-gravel deposition, southeastern Idaho, *in* Bonnichsen, B., and Breckenridge, R.M., eds., Cenozoic Geology of Idaho: Idaho Bureau of Mines and Geology Bulletin 26, p. 685-702.

Reasoner, M.A., and Jodry, M.A., 2000, Rapid response of alpine timberline vegetation to the Younger Dryas climate oscillation in the Colorado Rocky Mountains, USA: Geology, v. 28, p. 51-54.

Refsnider, K.A., and Brugger, K.A., 2007, Rock glaciers in central Colorado, U.S.A., as indicators of holocene climate change: Arctic, Antarctic, and Alpine Research, v. 39, p. 127-136.

Riebe, C.S., Kirchner, J.W., Granger, D.E., and Finkel, R.C., 2001, Minimal climatic control on erosion rates in the Sierra Nevada, California: Geology, v. 29, p. 447-450.

Riedinger, M.A., Steinitz-Kannan, M., Last, W.M., and Brenner, M., 2002, A ~6100 14C yr record of El Niño activity from the Galápagos Islands: Journal of Paleolimnology, v. 27, p. 1-7.

Ritter, J.B., Miller, J.R., Enzel, Y., Howes, S.D., Nadon, G., Brubb, K.A., Hoover, K.A., Olsen, T., Reneau, S.L., Sack, D., Summa, C.L., Taylor, I., Touysinhthiphonexay, K.C.N., Yodis, E.G., Schneider, N.P., Ritter, D.F., and Wells, S.G., 1993, Quaternary evolution of the Cedar Creek Alluvial Fan, Montana: Geomorphology, v. 8, p. 287-304.

Ritter, J.B., Miller, J.R., Enzel, Y., and Wells, S.G., 1995, Reconciling the roles of tectonism and climate in Quaternary alluvial fan evolution: Geology, v. 23, p. 245-248.

Rodbell, D.T., Seltzer, G.O., Anderson, D.M., Abbott, M.B., Enfield, D.B., and Newman, J.H., 1999, An ~15,000-year record of El Niño-driven alluviation in southwestern Ecuador: Science, v. 283, p. 516-520.

Roering, J.J., Kirchner, J.W., Sklar, L.S., and Dietrich, W.E., 2001, Hillslope evolution by nonlinear creep and landsliding: An experimental study: Geology, v. 29, p. 143-146.

Rubensdotter, L., and Rosqvist, G., 2003, The effect of geomorphological setting on Holocene lake sediment variability, northern Swedish Lapland: Journal of Quaternary Science, v. 18, p. 757-767.

Schoeneberger, P.J., Wysocki, D.A., Benham, E.C., and Broderson, W.D., 2002, Field Book for Describing and Sampling Soils: Version 2.0: Lincoln, NE, Natural Resources Conservation Service, National Soil Survey Center.

Schwertmann, U., Friedl, J., and Stanjek, H., 1999, From Fe(III) ions to ferrihydrite and then to hematite: Journal of Colloid and Interface Science, v. 209, p. 215-223.

Shulmeister, J., and Lees, B.G., 1995, Pollen evidence from tropical Australia for the onset of an ENSO-dominated climate at c. 4000 BP: The Holocene, v. 5, p. 10-18.

Slaymaker, O., Souch, C., Menounos, B., and Filippelli, G., 2003, Advances in Holocene mountain geomorphology inspired by sediment budget methodology: Geomorphology, v. 55, p. 305-316.

Stone, J.R., and Fritz, S.C., 2006, Multidecadal drought and Holocene climate instability in the Rocky Mountains: Geology, v. 34, p. 409-412.

Taylor, A., and Blum, J.D., 1995, Relation between soil age and silicate weathering rates determined from the chemical evolution of a glacial chronosequence: Geology, v. 23, p. 979-982.

Thompson, L.G., Davis, M.E., Mosley-Thompson, E., Sowers, T.A., Henderson, K.A., Zagorodnov, V.S., Lin, P.N., Mikhalenko, V.N., Campen, R.K., Bolzan, J.F., and Cole-Dai, J.A., 1998, 25,000 year tropical climate history from Bolivian ice cores: Science, v. 282, p. 1858-1863.

Toney, J.L., and Anderson, R.S., 2006, A postglacial palaeoecological record from the San Juan Mountains of Colorado USA: fire, climate and vegetation history: The Holocene, v. 16, p. 505-517.

Tsai, H., Hseu, Z.-Y., Huang, W.-S., and Chen, Z.-S., 2007, Pedogenic approach to resolving the geomorphic evolution of the Pakua River terraces in central Taiwan: Geomorphology, v. 83, p. 14-28.

Tudhope, A.W., Chilcott, C.P., McCulloch, M.T., Cook, E.R., Chappell, J., Ellam, R.M., Lea, D.W., Lough, J.M., and Shimmield, G.B., 2001, Variability in the El Nino-Southern Oscillation Through a Glacial-Interglacial Cycle: Science, v. 291, p. 1511-1517.

van Breeman, N., and Buurman, P., 1998, Soil Formation: Boston, Kluwer Academic Publishers, 377 p.

Vierling, L.A., 1998, Palynological evidence for late- and postglacial environmental change in central Colorado: Quaternary Research, v. 49, p. 222-232.

von Blanckenburg, F., 2005, The control mechanisms of erosion and weathering at basin scale from cosmogenic nuclides in river sediment: Earth and Planetary Science Letters, v. 237, p. 462-479.

Weber, W.A., 1976, Rocky Mountain flora, Colorado Associated University Press.

Wells, S.G., McFadden, L.D., and Dohrenwend, J.C., 1987, Influence of late Quaternary climatic change on geomorphic and pedogenic processes on a desert piedmont, eastern Mojave Desert, California: Quaternary Research, v. 27, p. 130-146.

APPENDIX A – LABORATORY PROCEDURES

ORGANIC DIGESTION FOR BOG CORE SAMPLES

Developed by Brad Johnson and Claire Chadwick in 2008

To be completed before any particle size analysis.

Equipment
Balance
250 mL Beakers
250 and 125 mL Erlenmeyer Flask
Hot Plate and Pan for Hot Water Bath
Shaker Table

Reagents
DI H20
Hydrogen Peroxide (H2O2) 30%
10% Sodium Pyrophosphate

Procedure
1. Dry samples in oven at 105°.
2. Use spatula to break up sample (do not use mortar and pestle). Split original samples in half and place half of the material into a 250mL beaker. Material should be between 0.7 g and 2.0 g. The other half of the sample should be reserved for organic content if analysis is to be done. Otherwise, entire sample can be used.
3. Add DI water to the sample and make a mush out of it. Keep in mind that this may be difficult and may take a few hours for dried samples to rehydrate. Shaker table can be used to speed up the process.
4. Add 25 mL of H_20_2 at a rate of 5 mL per minute stirring in between each addition.
5. Place beaker in a hot water bath containing water that is ~ 90°C (194°C) and allow to heat until the majority of fizzing ceases. Add water to beaker as needed to prevent drying.
6. After 1.5-2 hours add an additional 25 mL of H2O2 at a rate of 5 mL per minute stirring between each addition.
7. Heat for roughly 1.5 hours when frothing should be approximately complete.
8. Allow samples to cool while recording the weight of one 250 mL Erlenmeyer flask for each sample that is being processed.
9. Wet sieve samples into 250 mL Erlenmeyer flask.
10. Place flasks in drying oven at 110°C until all moisture is removed.
11. Weigh and record the mass of each flask and the sediment in it.
12. Add 50 mL of 10% Sodium Pyrophosphate to each sample and stir it until sample is suspended in the fluid. Pour the sample into a 125 mL Erlenmeyer flask. Rinse the 250 mL flask with 30 mL of DI water and pour this solution into the 125 mL flask.

Place 125 mL Erlenmeyer flasks on shaker table to break up sediment for particle size analysis.

LASER PARTICLE COUNTER PROCEDURES
Written by Patrick Smyth in 1993
Revised by Claire Chadwick in 2009

1. Turn on the computer, monitor, printer, and LPC. Wait for 30 minutes for the Laser Particle Counter to warm up prior to turning on the scanner.
2. Turn on the scanner.
3. Access the Supercount 8.13 Laser Particle Counter Software from the desktop by clicking the Spectrex LPC icon.
4. Perform the following test counts using the three test standard bottles provided by the manufacturer and settings listed below. Handle these bottles only by the caps and base to avoid getting fingerprints on the bottles.

a. First, leave the sample chamber empty and close the lid. Set the threshold knob to 8. Go to "Utilities" – "Background Calibration". Select "Set/Review Parameters"; change the "Number of Counts" to 10 and "Background Setting" to 8. Click Ok. Select "Take Counts". The LPS will now sample 10 times at a threshold setting of 8. Average counts should be less than 10, indicating that electronic noise has been eliminated.

b. Still in Background Calibration, select "Standard Bottle". Open "Set/Review Parameters" and click "White". Change the "Background Setting" to 41. Click Ok. Set the threshold to 41 and insert the white-capped bottle without shaking it. Line up the bottle in the V groove so that the ellipse of reflected laser light is centered on the laser emitter, not on the back or sides of the chamber (you may want to turn the lights off to do this). Close the lid and select "Take Counts". When all 10 runs are complete, the average count should be < 10.

c. Open "Set/Review Parameters" and click "Red"; change the "Background Setting" to 10 and click OK. Change the setting on the threshold knob to 10. Shake the red-capped bottle well and insert it into the sample chamber. Close the lid and select "Take Counts". When all 10 runs are complete, the average count should be ~ 1000.

d. Repeat step c for the blue bottle, using a threshold of 183 (remember to set the threshold knob and change the value in "Set/Review Parameters"). Average counts should be ~ 1100.

e. The results of each test count should be compared to the standard test counts provided by the laboratory. If any abnormal counts result from the test, clean the bottle, check the threshold setting, and run the count again. If the count is still abnormal, obtain technical assistance.

5. For the remainder of the particle counts, set the threshold setting to 12. Failure to do this will invalidate subsequent analyses.
6. Rinse and fill the beaker labeled "LPC" with approximately 100 mL of filtered water diluent. This beaker should be used for all particle counts to ensure that comparisons are valid. Make sure the outside of the beaker is clean and dry. Do NOT touch the sides of the beaker – hold the beaker by the top and bottom.
7. Rinse the stir bar and place it in the beaker.
8. Place the LPC beaker in the sample chamber so that it fits in the V groove with the lip of the beaker at the 11 o'clock position.
9. Rinse and fill a second 100mL beaker (the "sample beaker", labeled Dil. 1) with 100mL of filtered water.
10. Shake the sediment sample bottle vigorously until all of the sediment is released from the bottom of the bottle and is able to float about freely.
11. Pipette 1mL of sample from the bottom of the sample bottle to ensure that large particles are well represented and deposit it into the sample beaker. Draw 1 mL of water back into the pipette and discharge it back into the sample beaker to rinse particles from the pipette.
12. Run a background count on the diluent in the LPC beaker by clicking the Σ (Integrated Sample) button. Counts should not exceed 100; below 50 is preferable.
13. Using a clean pipette, remove ½ ml of water from the bottom of the sample beaker and

deposit it in the LPC beaker; rinse the pipette as in step 9. Although ½ ml is the desired amount of sample solution to be placed in the diluent, in practice only 0.2 to 0.35 ml of solution can normally be transferred from the sample beaker to the diluent before maximum acceptable count limit is exceeded. The importance of caution in this step cannot be overemphasized, as it is easy to add sediment to the diluent if the count is too low but impossible to remove it if the count is too high.

14. Run a test count with the stirrer off to make sure that the particle count is between 500 and 1000 counts. If the counts are below 500, add another aliquot of sample from the sample beaker and recount. If counts are above 1000, rinse out the LPC beaker and start again, adding less than ½ ml to the beaker from the sample beaker. After working enough with a particular batch of samples, the operator may become familiar enough with the characteristics of the sediment solution that this step may be bypassed except as an occasional safeguard.
15. Once you have achieved the appropriate number of counts, turn the stirrer on to setting 4 (about 11 o'clock position).
16. Press Σ to begin the count. Note: It is important that the LPC beaker has remained in exactly the same position from the background count up to this point.
17. When the count is complete, save the results by going to File – Save Histogram As. You may want to go to Output – Cumulative Graph and print a copy of the histogram. Label the printout with the following information:
    a. Date
    b. Full ID number of the sample
    c. File name under which the data is stored
    d. Average total count obtained by the computer for this sample, and whether or not the stir bar was used during the count.
18. Rinse out both beakers with deionized water; be sure to rinse the LPC beaker 3 times.
19. Fill and discharge the pipettes three times to remove all residue of the previous sample (or get clean pipette tips).
20. Place a check mark on the top of the sample bottle to indicate that it has been run.
21. To return to the main screen, click Stop. To begin a new analysis, click "File – New (Clear) Histogram". Repeat from step 6 for all samples, including duplicates of samples already run.
22. Analysis results can be brought into Excel by opening the desired histogram file and clicking on Output – Review Report, then selecting Output- Save report to file. Type the file name and put ".txt" at the end to save the file as a text file (the default is a ".prn" file). These files can then be opened in Excel as comma delimited files.
23. To shut down, close the Supercount program. Turn off the scanner on the LPC. Right click on the desktop or go to File – Shut down and select yes to shutdown the computer. When the message "It is now safe to turn off your computer" appears, turn the computer power off. Turn off the LPC power switch.

Troubleshooting

The problem most often encountered during the LPC process is unacceptably high particle counts from the filtered water diluent. When the filtered water is first put into storage jugs, some of the remaining unfiltered particles will float to the top and some will sink to the bottom. Consequently, the top few cm of water may give abnormally high counts, and the bottom few cm may do likewise. The jugs should be handled carefully to avoid agitating the water, and should be stored in a dark place to avoid algae growth in the water. A gallon of newly filtered water must typically settle for four days before being usable as a diluent.

For those wanting to conserve filtered water: just because a quantity of filtered water is not clean

enough to use as a diluent does not mean that it can't be used as a rinse. Using substandard filtered water solely as a rinse saves the cleanest filtered warer to actually fill the beakers with. This practice can stretch usable water a long way when large quantities of samples are being done, and the quality of the diluent is not compromised (unless the filtered rinse water is unusually filthy, of course).

Other potential difficulties are as follows:

Problem: High diluent counts

Possible causes:
- Incorrect positioning of the LPC beaker in the scanner.
- Fingerprints or smudges on the beaker.
- Insufficiently settled dilute. If the diluent has been sitting for less than a minute, allow it to settle for another minute or two and do a recount.
- Insufficiently rinsed beaker. Empty the diluent and pour another 100 ml of filtered water, either from the same jug or a new jug if diluent counts have been increasing dramatically for this particular jug.
- Dirty beaker walls. The beaker's inner walls occasionally need to be scrubbed off, after which thorough rinsing is necessary.

Problem: High sample counts without the stirbar.

Possible causes:
- Settling sediment. If the counter is activated only a few seconds after sediment is introduced into the diluent, then particles settling downwards through the laser beam will result in abnormally high counts. Wait thirty seconds and do a recount.
- Too much sediment. There is unfortunately nothing whatsoever to be done about this problem other than empty the diluent, rinse the LPC beaker three times, and go back to the background check stage with a new diluent. Put in less solution from the sample beaker the second time around.

Problem: Very strange particle analysis results while using the stir bar.

Possible causes:
- Incorrect bar setting. A low setting of the stir bar will not agitate the diluent adequately and will result in lower that expected counts. If the stir bar knob is set much higher than 4, an extremely odd sediment distribution curve will be produced as a result of the cone of depression entering the path of the laser beam.

Other notes of interest

It is not necessary to keep the scanner motor running except when there is actually a sample being analyzed, and it may prolong the life of the scanner machinery for it to be left off except when in use.

EXTRACTION OF FE OXYHYDROXIDES USING THE CITRATE-DITHIONITE BICARBONATE METHOD

(Hendricks, written communication, McKeague and Day, 1966, Mehra and Jackson, 1960)

Dithionite-citrate treatment is thought to remove the total free iron that is not included in silicate minerals; these are the crystalline oxides (geothite and hematite), amorphous hydrous oxides, and organic-bound iron.

EQUIPMENT

Centrifuge
Hot plate
30 ml pipette
190 x 100 mm pyrex dish
Centrifuge tube rack to fit pyrex dish
Thermometer
Stir rods
Spatula
50 ml centrifuge tubes with rack
100 ml or 150 ml volumetric flasks (250 ml flasks necessary for samples with >2% iron)
Semi-logarithmic paper (1 cycle x 70 Divisions)

REAGENTS

Sodium Citrate - Bicarbonate buffer

For 100mL, add 90 ml 0.3 M Na Citrate (88.23 g/l) to 10 ml 1M $NaHCO_3$ (84.01 g/l).
For 2250 mL, add 178.67 g of Na Citrate to 2025 ml DI water. In a separate beaker, add 18.9 g of $NaHCO_3$ to 225 ml of DI water. Mix the two solutions together.

Sodium dithionite ($Na_2S_2O_4$) Fe-standard

PROCEDURE

1.Weigh 0.5 g ground (100-mesh) soil into 50 ml centrifuge tubes (2 samples for each horizon).
2.Label 7 empty centrifuge tubes for blanks used to make standards.
3.Add 30 ml citrate-bicarbonate buffer to each centrifuge tube.
4.Place tubes in H_20 bath and bring temperature to about 80°C.
5.Add about 0.2 g $Na_2S_20_4$ (sodium dithionate). Stir for 1 minute, and then occasionally for 15 minutes.
6.Remove from bath. Cool solution by adding ≈15 ml cool distilled H_20 to tube.
7.Centrifuge at 1500-2000 RPM for 10 minutes (Blanks do not need to be centrifuged).
8.Transfer supernatant to 100 ml volumetric flask.
9.Repeat steps 3-8, with original sample.
10. Set blanks aside for preparation of standards.
11. Dilute to 100 ml.
12. Make 100 ml of each Fe standard in the following concentrations by adding to a 100mL volumetric flask:

Standard Concentration ppm (µg/ml)	mL of 1000ppm Fe Stock Solution
0 (Blank)	0
10	1
20	2

50	5
100	10
200	20

Add the contents of one blank centrifuge tube to the flask, and bring up to the 100mL mark with DI water.

13. Run the standards on the AA to determine how absorbance corresponds to concentration (see page ## for instructions on operating the AA). Plot the absorbance vs. concentration on a graph. There should be a linear relationship between absorbance and concentration. Usually, concentrations above 20 µg/mL show a non-linear relationship between absorbance and concentration.

14. Run a few samples to estimate the range of iron content. If the range of the samples is outside the linear range of the standards, the samples will need to be diluted. *If using this option then the calculations in the spreadsheet must be changed to allow for this.

15. Dilution: Since both the samples and standards must be in the same matrix (DI water, buffer, etc), standards and samples should be diluted in the same way. Adding 5mL of sample or standard to a 100mL volumetric flask and bringing to 100mL with DI will result in a 20X dilution (concentration is now $1/20^{th}$ of what it was prior to dilution). Make an extra solution of your most highly concentrated standard to use as a setup solution for the AA.

16. Run standards, run samples, and then rerun standards. Rerun standards in middle of samples if more than 20 samples.

CALCULATIONS

1.Plot standards on semi-logarithmic paper (1 cycle x 70 divisions) (Turn paper upside-down, on bottom have µg/ml, on side have absolute value as read off of graph (Fig. 8.3)).

2.Use graph to determine µg/ml of Fe in each sample.

3.To calculate weight percent Fe2O3: **µg/ml Fe** * 100mL solution = **µg Fe** * 10^-6 = **g Fe** * (1 mol / 55.85 g Fe) = **mol Fe** * ½ = **mol Fe2O3** * (159.7g Fe2O3 / 1 mol) = **g Fe2O3** / sample weight = **weight fraction Fe2O3** * 100 = **weight % Fe2O3**. OR **Wt % Fe2O3 = ((µg/ml Fe * 1.4297)/Sample Weight)* 100mL* 10^-4**. If samples and standards were diluted, you must multiply this result by the dilution factor (for a dilution factor of 20X, multiply by 20).

REMOVAL OF THE MAGNETIC FRACTION

Magnetite must be removed from all samples are prior to extraction of iron by ammonium oxalate. This procedure is performed because magnetite is soluble in ammonium oxalate, and extraction of Fe^{3+} from magnetite is not desired.

EQUIPMENT

Analytical balance
Magnetic stirrer
Magnetic stirring rod (long rod with magnetic tip)
Glass plate, approximately 30 x 20 cm
Tongs or tweezers, stainless steel
Crucible, porcelain or glass, 4 cm tall, 4.5 cm diameter
Small artist's paint brush, camel's hair, round tip, size 3-5
Weighing tin

PROCEDURE

1. Weigh 2-5 grams of soil sample ground to pass a 100-mesh sieve.
2. Transfer the sample quantitatively into a crucible.
3. Stir sample with long magnetic stirring rod. Magnetic particles will attach themselves to the tip of the rod. As they also carry along some soil particles, knock the bar against the inner walls of the crucible a few times to remove excess soil from the magnetic material.
4. Position a clean glass plate over a magnetic stirrer such that its right half will be located over the stirrer center.
5. Gently rub the stirring bar with the tongs until it appears clean.
6. Tap the material adhering to the tongs on the glass plate near its right edge.
7. Repeat steps 3-6 until no more visible accumulation of particles occurs on the stirring bar.
8. Turn on the magnetic stirrer. Slowly increase the stirrer to a medium setting. The magnetic particles on the plate will separate from the soil and migrate toward a spot above the center of the stirrer.
9. Gently stir the remaining soil with a camel hair brush while slowly moving the glass plate to the right.
10. Let particles collect to a whirl. Carefully stir it with the brush and move the plate farther to the right while brushing together any visible "outsiders" circling on more distant courses. By now the material should be free of any adhering soil.
11. When the whirl has come within approximately 5 cm of the left edge of the glass plate, turn off the stirrer and remove the plate (vertically away from the stirrer at first).
12. Brush material carefully into pre-weighed tin.
13. Record the weight of magnetic material and tin.
14. The sample in the crucible is saved for Fe-oxalate analysis.

CALCULATIONS

% Magnetics =

EXTRACTION OF FE OXYHYDROXIDE WITH OXALATE

(From Hendricks, written communication, and McKeague and Day, 1966)

Oxalate treatment removes the amorphous hydrous oxides (much of which probably is ferrihydrite) and some of the organic-bound Fe.

EQUIPMENT

Scale
50 ml centrifuge tubes
20 ml pipette
Shaking table (in dark place)
Centrifuge

REAGENTS

Ammonium oxalate extracting solution

Dissolve 56.8g NH_4 Oxalate in 1L of DI water. Dissolve 36.016g oxalic acid in 1L of DI water. To make 0.4M NH_4 Oxalate, mix 350 ml of NH_4 Oxalate solution with 218 ml of Oxalic acid solution. To make 0.2M NH_4 Oxalate extracting solution, dilute 0.4M NH_4 Oxalate solution 2X (1 part 0.4M NH_4 Oxalate, 1 part DI water).

STANDARDS

Standards must be made to duplicate the solution in the centrifuge tubes. This method makes a 0.4M solution which is then diluted by half before adding it to the centrifuge tubes. This allows for greater accuracy and less chance for contamination. The problem with this method is that to create a 0.4 M solution the solutions must be heated slightly to attain total solubility. Therefore, after the extracting solution is mixed and added to the volumetrics, add enough water to bring the solution to below the 100 ml line. Let the solution cool to room temperature then top off to 100 ml.

To make 100 ml of Fe standards, add the following to a 100mL volumetric flask:

Standard Concentration ppm	mL of 1000ppm Fe Stock Solution	mL of 0.4M extracting solution	mL Deionized water
0 (Blank)	0	50	Up to the 100mL mark
10	1	50	Up to the 100mL mark
50	5	50	Up to the 100mL mark
100	10	50	Up to the 100mL mark
200	20	50	Up to the 100mL mark
300	30	50	Up to the 100mL mark

Shake the solution well.

PROCEDURE

1. Sample must be demagnetized. See Procedure for Removal of the Magnetic Fraction.

2. Weigh out 0.500 grams of 80-100 mesh crushed and de-magnetized sample and place in a 50 ml centrifuge tube.
3. Add 20 m1 of 0.2 M NH_4 oxalate extracting solution.
4. Shake samples for 4 hours on a covered shaking table. The extracting solution is light sensitive and therefore should be covered and stored in a dark cabinet.
5. Centrifuge samples for 10 minutes at 1300-2000 rpm.
6. Run the standards on the AA to determine how absorbance corresponds to concentration (see page 34 for instructions on operating the AA). Plot the absorbance vs. concentration on a graph. There should be a linear relationship between absorbance and concentration. Usually, concentrations above 20 µg/mL show a non-linear relationship between absorbance and concentration.
7. Run a few samples directly from centrifuge tube to estimate the range of iron content. If the range of the samples is outside the linear range of the standards, the samples will need to be diluted. *If using this option then the calculations in the spreadsheet must be changed to allow for this.
8. Dilution: Since both the samples and standards must be in the same matrix (DI water, buffer, etc), standards and samples should be diluted in the same way. Adding 5mL of sample or standard to a 100mL volumetric flask and bringing to 100mL with DI will result in a 20X dilution (concentration is now $1/20^{th}$ of what it was prior to dilution). Make an extra solution of your most highly concentrated standard to use as a setup solution for the AA.
9. Run standards, run samples, and then rerun standards. Rerun standards in middle of samples if more than 20 samples.
10. Plot standards on semi-log paper, absorbance on log scale. Read values for samples off of graph.

CALCULATIONS

To calculate weight percent Fe2O3: **µg/ml Fe** * 20mL solution = **µg Fe** * 10^-6 = **g Fe** * (1 mol / 55.85 g Fe) = **mol Fe** * ½ = **mol Fe2O3** * (159.7g Fe2O3 / 1 mol) = **g Fe2O3** / sample weight = **weight fraction Fe2O3** * 100 = **weight % Fe2O3**. OR Wt % Fe2O3 = ((µg/ml Fe * 1.4297)/Sample Weight)* 20mL* 10^-4. If samples and standards were diluted, you must multiply this result by the dilution factor (for a dilution factor of 20X, multiply by 20).

PARTICLE SIZE ON THE SEDIGRAPH 5100 WITH A MASTERTECH 52
Written by Brad Johnson, 2010

1. Start by turning the computer on. While it is booting, go ahead and turn on the Mastertech, the SediGraph, and the controller (on top of the SediGraph). The switches for these 3 are on the back right of each of them. Make sure you turn the X-RAY key on the SediGraph to the ON position.

2. Open the program on the desktop of the computer called SEDIGRAPH 5100, this will take a couple of minutes.

3. While this is occurring, organize the samples on the counter. These samples should already be sieved and material >2mm should be removed.

4. Once the program boots, pull down the "Unit 1" menu and select "Rinse Both." It will ask where the rinsing solution is being placed in the autosampler. Typically the rinse solution is placed in position "1." Fill a beaker with superwater and put it wherever you told the computer you planned to put it.

5. Before starting the rise, make sure there is water in the rinse bucket on the floor and that the hoses go all the way into the waste and rinse buckets.

6. In order to run samples, files must be created for the information to be deposited into. To do this, pull down the "File" menu and choose "Open sample information." Type a file name into the box, and it will prompt you to create a new file (go ahead). This is the opportunity to change settings including, stir time, ultrasonic probe time, and charts output. Choosing to create specific charts at this point will not affect what charts can be created later. The program will enable you to create whatever you want later. Make all files for the samples to be run that today. Create file numbers that will instantly identify what sample is being run. Save all files in the default "data" folder.

7. When preparing and weighing samples, it is important to remember how the machine works. The machine passes X-Rays through a column of water to a sensor. In order for it to get correct results, between 50 and 70 % of the X-rays must make it through to the sensor. The average baseline for the machine is 160 KCnts meaning that between 80 and 112 KCnts need to make it through when analyzing samples. However, different sediments will be absorbed at different rates meaning that different amounts of the sediment need to be tested to see what works for your materials. Different horizons within a soil pit will have very different mineralogy and may require different amounts. Keep in mind that the amount of liquid, as well as the amount of sediment, can be altered. Thus, it is often better to have concentrations too high initially and then dilute them later.

8. Pull down the "Unit 1" menu and select "MasterTech Schedule." Here the autosampler (MasterTech 52) can be set up so that it can run multiple samples.

9. Pull down the menu on the scheduler and select "Operation." Click insert and highlight "Baseline" and select the next beaker (probably 2 if you used 1 for rinse).

10. Click "Insert" again and click sample analysis. Browse for the file for the first sample and select it. Click OK and continue to do this for all files. Only one baseline per session is necessary. Record the beaker location of each sample in the lab notebook.

11. Next, weigh out sediment on the scale and record this weight. Recording to 1/100 of a gram is sufficiently accurate. Ten grams is probably a good place to start.

12. Sieve the weighed sediment through a 500 um sieve making sure that any flocculated clays and silts are crushed with fingers.

13. Using a brush, sweep the <500 um material back onto a weighing dish and record.

14. Now place the sediment in one of the autosampler's plastic beakers and add the deflocculant. We use 0.05% Sodium Pyrophosphate which we make from 10% Sodium Pyrophosphate. Sixty ml of deflocculant added to 5-7 grams of fine sediment will typically provide satisfactory x-ray attenuation.

15. Place the plastic beaker in its proper spot as stated in the lab notebook. Make sure that you have put a beaker of pure 0.05% Sodium pyrophosphate in the beaker location that you entered when you created the MasterTech schedule.

16. You can now press start on the MasterTech Schedule Mode window.

17. The Sedigraph should first run a baseline. The manual says that the baseline should be close to 140 KCnts but ours have always been closer to 160 KCnts. You can view the creation of the baseline (and samples being run) by pulling down the "view" menu in the MasterTech Schedule Mode window and selecting "Analysis Results."

18. After the baseline is done, the sedigraph will run the first sample. Before analyzing the sample, it will run a "full scan" to determine overall attenuation. Once again, the immediate results can be viewed in "Analysis Results." The line created here should be relatively flat with 1-3 KCnts of variation. A line with high variability is a sign of problems with clogging. Do not use the results of samples run with highly varied initial lines.

19. It will take the sedigraph ~ 25 min to run a sample and then an addition 10-15 minutes between samples to run the default number of rinses (3).

20. While the Sedigraph is running, it is advisable to manually rinse the highest points of the mixing chamber (since rinse water doesn't get that high) and the shaft of the probes in the plastic beaker.

21. Once analyses are complete, you will need to create reports for export into Excel (hopefully on another computer). Do this by pulling down the Reports menu and selecting "start report."

22. Change the destination to "File" and select a name and location for the new report.

23. This file can be imported into Excel via typical procedures for importing foreign data into the program.

LOSS ON IGNITION

Note: Wearing close-toed shoes is important during this procedure.

1. Label crucibles with permanent marker (side) and pencil (bottom). These are likely to burn off in the furnace so always keep them arranged in a way whereby they can be identified.
2. Heat crucibles in an ordinary drying oven at 110 degrees for longer than 1 hour.
3. Place the crucibles in a desiccator to cool. Leave them in the desiccator until needed to prevent them from absorbing moisture.
4. Weigh dry, cool crucibles and record the weight to the nearest 0.000 g.
5. Grind ~ 2 – 5 g of dry sample with mortar and pestle. Mortar and pestle can be washed between samples using acetone and Kimwipes which will dry quickly and keep samples dry.
6. Place sample in crucible and weigh, recording the weight to 0.000 g. Make sure that you note which sample is in each specific crucible.
7. Using heat resistant gloves and appropriate (extra long) tongs, place crucibles in the furnace at 550 C. Remember, the labels are going to burn off so place them in a known and consistent order.
8. Heat for 1 hour or until all dark, organic material is gone (shouldn't be more than 1.5 hours). Note: Flames will die down when you close the door.
9. Take crucibles out and place them in a heat resistant desiccator in a known and consistent order.
10. Weigh and record weight to 0.000 g when cool.
11. Note: If many samples are being run, the dry crucibles do not need to be reweighed after each batch as long as the numbers are always kept the same. Thus, it is critical to always keep the crucibles in a known order and relabel them after each use. Reweigh crucibles after every 4 uses to ensure that they have not chipped.

APPENDIX B – PARTICLE SIZE AND ORGANIC CONTENT FROM CUMBRES BOG

Particle size analysis for the Cumbres Bog core was completed using a laser particle counter while organic content was measured using loss on ignition (see Appendix A). In the raw data contained here, Core ID refers to the location, hole number, and drive. For instance, CB2-6 is the Cumbres Bog location, hole 2, and drive number 6. For Cumbres Bog, the first 5 drives were taken but not recovered. Increment depth refers to the depth within the specific drive while the Real Depth column is the cumulative depth. The age is based on the age model (Chapter 4) and is calculated in calibrated radiocarbon years before present with "present" being defined as 1950. Thus, -32 years is actually 1982.

APPENDIX B - RAW DATA FROM CUMBRES BOG

Core ID	Increment Depth	Real Depth	Cal. Years Age	Weight % Clay	Weight % Silt	Organic %
CB2-6	1	1	-32.1	2.473471	97.52648	
CB2-6	3	3	17.7			
CB2-6	5	5	67.5	0.161952	99.83795	
CB2-6	7	7	117.3			
CB2-6	9	9	167.1	1.344727	98.65526	
CB2-6	11	11	216.9			
CB2-6	13	13	266.7	1.383904	98.61607	
CB2-6	15	15	316.5	0.385285	99.61469	
CB2-6	17	17	366.3	1.123109	98.87694	
CB2-6	19	19	416.1	0.791894	99.20813	
CB2-6	21	21	465.9	13.87337	86.12672	
CB2-6	23	23	515.7	1.780113	98.21984	
CB2-6	25	25	565.5	1.180611	98.81939	
CB2-6	27	27	615.3	1.117026	98.88301	
CB2-6	29	29	665.1	1.453093	98.5469	
CB2-6	31	31	714.9	0.187756	99.81221	
CB2-6	33	33	764.7	0.197763	99.80217	
CB2-6	35	35	814.5	2.812471	97.1875	
CB2-6	37	37	864.3	2.6185	97.38145	
CB2-6	39	39	914.1	4.144016	95.85595	
CB2-6	41	41	963.9	0.17542	99.82462	
CB2-6	43	43	1014	4.595743	95.40424	
CB2-6	45	45	1064			52.50917993
CB2-6	47	47	1113	0.235863	99.76412	
CB2-6	49	49	1163			
CB2-6	51	51	1213	0.534945	99.46503	
CB2-6	53	53	1263	1.688558	98.31138	
CB2-6	55	55	1313	1.505966	98.49406	
CB2-6	57	57	1362	8.377421	91.62261	47.38149847
CB2-6	59	59	1412	2.377621	97.62231	53.80765105
CB2-6	61	61	1446	5.233307	94.7666	50.69499082
CB2-6	63	63	1463	7.205394	92.7946	62.04081633
CB2-6	65	65	1480	3.907336	96.09267	63.52171882
CB2-6	67	67	1497	0.214452	99.78563	61.99513382
CB2-6	69	69	1514	8.811192	91.18877	60.20730059
CB2-6	71	71	1531	2.397962	97.60204	59.80537339
CB2-6	73	73	1549	3.364246	96.6358	59.89926385
CB2-6	75	75	1566	0.719881	99.28006	58.60892388
CB2-6	77	77	1583	1.591071	98.40893	59.6097081
CB2-6	79	79	1600	12.04013	87.95997	61.09576427
CB2-6	81	81	1617	10.41921	89.58089	59.01024744

Core ID	Increment Depth	Real Depth	Age	% Clay	% Silt	Organic %
CB2-6	83	83	1634	1.743975	98.25601	57.85732419
CB2-6	85	85	1652	1.412687	98.58738	60.2561997
CB2-6	87	87	1669	1.582774	98.41719	57.69736056
CB2-6	89	89	1686	7.606905	92.39312	54.50657895
CB2-6	91	91	1703	4.258513	95.74152	55.2672148
CB2-6	93	93	1720	2.051946	97.94807	56.64893617
CB2-7	1	94	1737	2.560815	97.43917	40.37793223
CB2-7	3	96	1754	2.136069	97.86394	39.90249974
CB2-7	5	98	1763	8.267862	91.73217	41.73948887
CB2-7	7	100	1780	7.282702	92.71735	39.66900279
CB2-7	9	102	1797	0.409857	99.59017	39.19970699
CB2-7	11	104	1815	0.945759	99.05418	43.75081796
CB2-7	13	106	1832	1.184095	98.8159	40.77467722
CB2-7	15	108	1849	4.563812	95.4362	34.17440452
CB2-7	17	110	1866	2.514028	97.48596	34.63697967
CB2-7	19	112	1883	8.49903	91.5009	33.15255836
CB2-7	21	114	1900	13.50963	86.4903	34.76079347
CB2-7	23	116	1917	10.71197	89.28807	35.11056972
CB2-7	25	118	1935	0.387861	99.61216	36.00862999
CB2-7	27	120	1952	8.453173	91.54683	35.86660617
CB2-7	29	122	1969	13.44523	86.55463	35.91455274
CB2-7	31	124	1986	3.16664	96.83333	37.37352445
CB2-7	33	126	2003	4.10592	95.8941	36.56030287
CB2-7	35	128	2020	7.539685	92.46034	41.81163767
CB2-7	37	130	2038	0.606381	99.3937	43.57879758
CB2-7	39	132	2055	12.15278	87.84711	41.09608955
CB2-7	41	134	2072	8.077136	91.92278	30.57154894
CB2-7	43	136	2089	1.613278	98.38679	44.91141327
CB2-7	45	138	2106	1.843418	98.15662	38.70511233
CB2-7	47	140	2123	5.661168	94.33881	
CB2-7	49	142	2141	3.9654	96.03457	41.36178862
CB2-7	51	144	2158	8.072369	91.92758	30.47660691
CB2-7	53	146	2175	2.657786	97.3422	62.32245681
CB2-7	55	148	2192	7.304853	92.6951	66.81425725
CB2-7	57	150	2209	10.0232	89.97682	66.53311336
CB2-7	59	152	2226	2.024531	97.9755	61.96385804
CB2-7	61	154	2244	1.993939	98.00606	62.84894339
CB2-7	63	156	2261	4.076054	95.92399	58.8070394
CB2-7	65	158	2305	1.928758	98.07124	56.05693519
CB2-7	67	160	2349	1.64934	98.35068	52.68355517
CB2-7	69	162	2393	5.104754	94.89517	48.89821616
CB2-7	71	164	2437	8.329801	91.67023	47.42576373

Core ID	Increment Depth	Real Depth	Age	% Clay	% Silt	Organic %
CB2-7	73	166	2481	8.471328	91.52871	30.03412969
CB2-7	75	168	2525	2.359905	97.64001	35.68257492
CB2-7	77	170	2569	0.503938	99.49604	30.3330773
CB2-7	79	172	2613	0.901348	99.09865	32.25195595
CB2-7	81	174	2657	10.41921	89.58089	32.93379455
CB2-7	83	176	2701	2.746482	97.25359	35.93869732
CB2-7	85	178	2745	0.03928	37.95477	40.85702843
CB2-7	87	180	2789	2.171242	97.8288	34.38008839
CB2-7	89	182	2833	0.303601	99.69637	35.16202546
CB2-7	91	184	2877	0	0	
CB2-7	93	186	2921	0.041486	14.73941	38.26667823
CB2-7	95	188	2965	4.627091	95.37289	39.24221922
CB2-8	1	189	2987	4.969392	95.03054	46.12188366
CB2-8	3	191	3031	4.039662	95.96033	41.01260675
CB2-8	5	193	3075	3.043687	96.95636	43.40469171
CB2-8	7	195	3119	3.831982	96.16794	48.43610366
CB2-8	9	197	3163	3.975454	96.02453	49.42985266
CB2-8	11	199	3207	2.12763	97.87229	44.10367617
CB2-8	13	201	3251	0.549005	99.45102	49.76027397
CB2-8	15	203	3295	0.526406	99.47354	47.97097885
CB2-8	17	205	3339	3.931308	96.0687	52.76276001
CB2-8	19	207	3384	0.879441	99.1206	45.74958329
CB2-8	21	209	3428	0.309913	99.69009	61.70596728
CB2-8	23	211	3472	6.370718	93.62935	68.28865222
CB2-8	25	213	3516	7.079403	92.9206	53.15712188
CB2-8	27	215	3560	5.854884	94.1451	61.64484331
CB2-8	29	217	3604	1.595208	98.40483	59.16144434
CB2-8	31	219	3648	0.97773	99.02228	42.54400909
CB2-8	33	221	3692	0.510724	99.4893	31.88347158
CB2-8	35	223	3736	1.024737	98.97523	29.99179431
CB2-8	37	225	3780	0.767348	99.23266	37.68256118
CB2-8	39	227	3824	0.612242	99.3878	35.30632694
CB2-8	41	229	3868	2.277003	97.72293	33.53600608
CB2-8	43	231	3912	2.286584	97.71348	62.31594709
CB2-8	45	233	3956	4.621394	95.37853	62.32704403
CB2-8	47	235	4000	2.021435	97.97859	60.39593479
CB2-8	49	237	4044	8.210784	91.78923	59.19321836
CB2-8	51	239	4088	0	0	53.02146668
CB2-8	53	241	4132	1.565258	98.43467	46.33527532
CB2-8	55	243	4176	0	0	33.31011909
CB2-8	57	245	4220	8.377421	91.62261	34.16580549
CB2-8	59	247	4264	5.300394	94.69955	34.85204015

Core ID	Increment Depth	Real Depth	Age	% Clay	% Silt	Organic %
CB2-8	61	249	4308	0.742271	99.25773	38.73134328
CB2-8	63	251	4352	11.61117	88.3888	40.96667667
CB2-8	65	253	4396	4.769376	95.23064	39.91510769
CB2-8	67	255	4440	6.182515	93.81745	35.16500786
CB2-8	69	257	4484	4.863808	95.13613	43.12616037
CB2-8	71	259	4528	7.085586	92.91441	81.40606992
CB2-8	73	261	4572	0.431999	99.568	87.49722407
CB2-8	75	263	4616	0	21.69289	83.02634647
CB2-8	77	265	4660	4.176578	95.8234	65.59649763
CB2-8	79	267	4704	3.210236	96.78975	49.39956332
CB2-8	81	269	4748	0.564328	99.43572	53.9756398
CB2-8	83	271	4792	1.564342	98.43558	48.44015882
CB2-8	85	273	4836	7.633699	92.3663	43.07183885
CB2-8	87	275	4907	2.486861	97.51311	30.08406938
CB2-8	89	277	5003	9.061897	90.93801	35.57285873
CB2-8	91	279	5098	0.152814	99.84722	36.0402119
CB2-8	93	281	5194	9.470357	90.52973	37.54724906
CB2-8	95	283	5290	0	0	
CB2-8	97	285	5385	11.5841	88.4159	
CB2-8	99	287	5481	2.808676	97.19133	40.83363021
CB2-8	101	289	5577	0.356534	99.64346	59.68237255
CB2-8	103	291	5672	11.97527	88.02469	73.05125872
CB2-8	105	293	5768	0.021123	99.97882	69.90022173
CB2-9	1	294	5816	2.064648	97.93532	41.21555718
CB2-9	3	296	5911	1.524926	98.4751	37.6819593
CB2-9	5	298	6007	0.3556	99.64431	26.54281444
CB2-9	7	300	6103	2.696366	97.30368	32.36306729
CB2-9	9	302	6198	7.688045	92.31197	32.33898675
CB2-9	11	304	6294	2.65049	97.34943	42.04553994
CB2-9	13	306	6390	4.258601	95.74141	45.79998699
CB2-9	15	308	6485	9.121425	90.87869	47.98441045
CB2-9	17	310	6581	0	0	45.66708792
CB2-9	19	312	6677	9.547216	90.45283	43.75246132
CB2-9	21	314	6772	1.162039	98.83799	43.89095079
CB2-9	23	316	6868	0.065282	99.93467	41.51123596
CB2-9	25	318	6964	6.582755	93.4172	43.21192053
CB2-9	27	320	7059	2.937754	97.06224	43.74896047
CB2-9	29	322	7155	0	0	38.70452529
CB2-9	31	324	7251	0.206952	99.79297	42.57185371
CB2-9	33	326	7346	14.134	85.86606	40.89442895
CB2-9	35	328	7442	1.196336	98.80367	45.50679852
CB2-9	37	330	7538	2.114598	97.8854	47.64171671

Core ID	Increment Depth	Real Depth	Age	% Clay	% Silt	Organic %
CB2-9	39	332	7633	3.779246	96.22081	44.91807559
CB2-9	41	334	7729	0.047835	0.734617	43.27038761
CB2-9	43	336	7825	7.598124	92.40176	45.67150211
CB2-9	45	338	7920	13.98643	86.01359	42.739851
CB2-9	47	340	8016	2.029418	97.9706	42.18645612
CB2-9	49	342	8112	0.221945	99.77803	43.05117896
CB2-9	51	344	8207	0	0	48.91075721
CB2-9	53	346	8303	0.042155	18.84237	45.70561457
CB2-9	55	348	8379	5.765679	94.23434	45.87868234
CB2-9	57	350	8454	0.320431	99.67959	49.49020233
CB2-9	59	352	8530	4.192198	95.80785	47.01865626
CB2-9	61	354	8605	10.52777	89.47216	46.42281253
CB2-9	63	356	8681	0.590953	99.40901	
CB2-9	65	358	8757	0.691365	99.30861	43.81078224
CB2-9	67	360	8832	0.051134	99.94883	46.09993217
CB2-9	69	362	8908	7.966671	92.03334	46.06346177
CB2-9	71	364	8984	2.19518	97.80482	45.72915161
CB2-9	73	366	9059	0.649221	99.35083	46.42857143
CB2-9	75	368	9135	0.41477	99.58516	45.80338061
CB2-9	77	370	9210	0	100	45.15988118
CB2-9	79	372	9286	1.204707	98.79533	45.24179352
CB2-9	81	374	9362	6.505916	93.49409	46.08205507
CB2-9	83	376	9437	1.569241	98.43074	44.79054005
CB2-9	85	378	9513	0.232271	99.76769	41.84786034
CB2-9	87	380	9589	1.980347	98.01962	39.97123879
CB2-9	89	382	9664	6.053514	93.94654	45.1446281
CB2-9	91	384	9740	0.320975	99.67902	45.96904441
CB2-9	93	386	9815	0.279755	99.72022	45.81177965
CB2-9	95	388	9891	8.424577	91.57542	44.97231649
CB2-9	97	390	9967	4.556508	95.44347	45.88345571
CB2-9	99	392	10042	1.393609	98.60636	44.53854131
CB2-9	101	394	10118	2.106534	97.89349	44.87460433
CB2-9	103	396	10193	1.078575	98.92135	
CB2-10	1	397	10231	0.512654	99.48734	46.17990215
CB2-10	3	399	10307	9.067133	90.93286	46.92611393
CB2-10	5	401	10382	0.059254	14.2757	47.61828645
CB2-10	7	403	10458	2.768438	97.2316	43.13065432
CB2-10	9	405	10534	0.335948	99.66409	44.65231204
CB2-10	11	407	10609	1.001604	98.9984	46.33637054
CB2-10	13	409	10685	0.080277	99.91972	46.32900911
CB2-10	15	411	10761	2.516301	97.48362	45.17097967
CB2-10	17	413	10836	3.105926	96.89413	45.21814819

Core ID	Increment Depth	Real Depth	Age	% Clay	% Silt	Organic %
CB2-10	19	415	10912	6.730778	93.2693	44.99121265
CB2-10	21	417	10987	5.405071	94.59492	45.97619722
CB2-10	23	419	11063	4.476796	95.52319	47.23625343
CB2-10	25	421	11139	0.848734	99.15136	46.60576247
CB2-10	27	423	11214	8.046333	91.95378	46.8359054
CB2-10	29	425	11290	7.639012	92.36109	48.01762115
CB2-10	31	427	11366	0.182265	99.81773	51.41132611
CB2-10	33	429	11441	10.91198	89.08803	50.39201711
CB2-10	35	431	11517	9.080221	90.91973	45.32643596
CB2-10	37	433	11592	4.085069	95.91495	44.40269951
CB2-10	39	435	11668	0.85619	99.14379	41.24759068
CB2-10	41	437	11718	10.72165	89.27835	28.99942496
CB2-10	43	439	11767	5.411651	94.58829	20.55848467
CB2-10	45	441	11817	17.44403	173.3879	28.3749333
CB2-10	47	443	11867	0.318186	99.6818	27.78423622
CB2-10	49	445	11917	1.497208	98.50277	25.98504943
CB2-10	51	447	11966	9.592687	90.40732	25.58428642
CB2-10	53	449	12016	14.61422	85.38573	25.21878808
CB2-10	55	451	12066	1.59665	98.40328	24.73519565
CB2-10	57	453	12116	2.088782	97.91118	24.12091898
CB2-10	59	455	12165	1.271738	98.72828	23.881484
CB2-10	61	457	12215	2.214653	97.78528	23.03622129
CB2-10	63	459	12265	5.459727	94.54024	21.96670135
CB2-10	65	461	12314	8.134085	91.86593	23.69207458
CB2-10	67	463	12364	0.549864	99.45015	26.61227227
CB2-10	69	465	12414	0.20554	99.79449	24.12247946
CB2-10	71	467	12464	2.725817	97.27421	27.14536757
CB2-10	73	469	12513	8.811918	91.18808	23.43460827
CB2-10	75	471	12563	3.158487	96.84145	23.710308
CB2-10	77	473	12613	4.519407	95.4806	23.59410431
CB2-10	79	475	12663	27.60468	72.39534	23.91292055
CB2-10	81	477	12712	0.054919	99.94508	26.52535776
CB2-10	83	479	12762	4.326965	95.67307	26.88048324
CB2-10	85	481	12812	1.042745	98.95727	27.34970364
CB2-10	87	483	12862	10.57405	89.4259	22.98047048
CB2-10	89	485	12911	13.84608	86.1539	22.51594614
CB2-10	91	487	12961	5.011701	94.98821	21.51628796
CB2-10	93	489	13011	1.122583	98.87738	20.12383901
CB2-10	95	491	13060	8.992706	91.00724	36.8641532
CB2-11	1	492	13085	0.333651	99.66636	23.0638659
CB2-11	5	496	13135	1.582597	98.41745	
CB2-11	7	498	13185	11.74434	88.25575	39.54819986

Core ID	Increment Depth	Real Depth	Age	% Clay	% Silt	Organic %
CB2-11	9	500	13234	0.148943	99.85104	43.77939793
CB2-11	13	504	13284	18.10778	81.89219	
CB2-11	15	506	13334	0.257092	11.44336	
CB2-11	17	508	13384	4.469786	95.53013	23.34998335
CB2-11	19	510	13433	6.528481	93.47158	23.7593104
CB2-11	21	512	13483	0.340392	99.65965	26.44954128
CB2-11	23	514	13533	41.70147	58.29853	26.26218663
CB2-11	25	516	13583	6.998249	93.00173	30.52114638
CB2-11	27	518	13632	12.44389	87.55619	30.88479416
CB2-11	29	520	13682	2.868464	97.13157	25.63550194
CB2-11	31	522	13732	50.15468	49.84538	21.5212528
CB2-11	33	524	13782	1.603384	98.39666	19.69410479
CB2-11	35	526	13831	0	0	18.40961266
CB2-11	37	528	13881	0	0	18.57315599
CB2-11	39	530	13931	0	0	17.03422812
CB2-11	41	532	13980	12.3891	87.61089	
CB2-11	43	534	14030	3.383854	96.61614	
CB2-11	45	536	14080	2.02193	97.9781	
CB2-11	47	538	14130	21.10709	78.89294	16.15487828
CB2-11	49	540	14179	18.01628	81.98382	16.44002127
CB2-11	51	542	14229	0.181877	99.81815	17.50189318
CB2-11	53	544	14279	3.460466	96.53951	16.84096496
CB2-11	55	546	14329	2.302343	97.69767	14.98727886
CB2-11	57	548	14378	10.15175	89.84824	14.27340299
CB2-11	59	550	14428	33.46027	66.53973	14.27978291
CB2-11	61	552	14504	0.018313	5.595174	12.98988926
CB2-11	63	554	14580	29.881	70.11889	13.19810414
CB2-11	65	556	14656	8.917518	91.08246	12.78494951
CB2-11	67	558	14732	5.04686	94.95314	12.47709646
CB2-11	69	560	14808	0	0	13.72498416
CB2-11	71	562	14884	0.206363	99.79364	13.00644041
CB2-11	73	564	14960	0	0	13.650591
CB2-11	75	566	15036	76.14605	23.85397	13.23353453
CB2-11	77	568	15112	0.151751	99.84828	13.21493686
CB2-11	79	570	15188	55.83547	44.16451	0
CB2-11	81	572	15264	1.270287	98.72964	12.05003134
CB2-11	83	574	15340	0.060428	99.93962	12.79436366
CB2-11	85	576	15416	0	0	13.001072
CB2-11	87	578	15492	2.429004	97.57102	13.05436522
CB2-11	89	580	15568	0.000125	20.24186	12.64533918
CB2-11	91	582	15644	49.47431	50.52566	0
CB2-11	93	584	15720	18.89762	81.10245	12.91986247

Core ID	Increment Depth	Real Depth	Age	% Clay	% Silt	Organic %
CB2-11	95	586	15796	46.33519	53.66478	13.27267136
CB2-11	97	588	15872	20.18835	79.81172	13.14571014
CB2-11	99	590	15948	0.054217	99.94582	13.179982
CB2-11	101	592	16024	38.1456	61.85429	12.7387354
CB2-11	103	594	16100	69.57144	30.42864	12.81833616
CB2-11	105	596	16176			12.70331667
CB2-11	107	598	16252			12.57765842
CB2-12	1	599	16328	0	100	15.75446705
CB2-12	3	601	16403	0	99.99999	16.04244694
CB2-12	5	603	16593	15.07048	84.92949	19.41135249
CB2-12	7	605	16669	8.25672	91.7433	18.02263713
CB2-12	9	607	16745	21.99228	78.00761	13.53287286
CB2-12	11	609	16821	35.02863	64.97137	12.53517062
CB2-12	13	611	16897	6.180744	93.81931	
CB2-12	15	613	16973	85.74311	14.25688	13.88545137
CB2-12	17	615	17049	27.74921	72.25077	12.35560589
CB2-12	19	617	17125	14.39121	85.60875	12.17487258
CB2-12	21	619	17201	42.14288	57.8571	11.30485836
CB2-12	23	621	17277	1.865094	98.13489	12.63817687
CB2-12	25	623	17353	16.49794	83.50209	11.56900829
CB2-12	27	625	17429	55.1126	44.88746	12.91992751
CB2-12	29	627	17505	0	100	12.61411417
CB2-12	31	629	17581	37.00658	62.99348	11.85007227
CB2-12	33	631	17657	0	0	12.83063339
CB2-12	35	633	17733	0.434797	99.56526	13.14124456
CB2-12	37	635	17809	66.12457	33.8755	13.57569272
CB2-12	39	637	17885	15.20048	84.79949	12.20316163
CB2-12	41	639	17961	39.82179	60.17821	12.37284176
CB2-12	43	641	18037	0.014269	99.98573	12.22279731
CB2-12	45	643	18113	30.8063	69.1937	14.34186821
CB2-12	47	645	18189	12.2963	87.70371	8.93647938
CB2-12	49	647	18265	19.34591	80.65403	13.90475103
CB2-12	51	649	18341	0.002628	32.75273	13.54452229
CB2-12	53	651	18417	37.78961	62.21036	13.09048444
CB2-12	55	653	18493	50.93026	49.06975	13.89446313
CB2-12	57	655	18569	29.41469	70.58532	14.64973655
CB2-12	59	657	18645	37.032	62.968	15.59142707
CB2-12	61	659	18721	18.0357	81.96425	15.88020776
CB2-12	63	661	18797	13.58368	86.41626	15.10310236
CB2-12	65	663	18873	69.67233	30.3276	15.58919582
CB2-12	67	665	18949	0.020613	24.91828	16.70459945
CB2-12	69	667	19025	0.020792	17.06655	11.24163606

Core ID	Increment Depth	Real Depth	Age	% Clay	% Silt	Organic %
CB2-12	71	669	19101	51.18403	48.81604	10.31643786
CB2-12	73	671	19177	0.120683	99.87933	15.86318738
CB2-12	75	673	19253	4.326493	95.67338	14.40254193
CB2-12	77	675	19329	0	0	14.13425621
CB2-12	79	677	19405	0	99.99989	16.76017954
CB2-12	81	679	19481	92.13773	7.86229	18.81138168
CB2-12	83	681	19557	63.39222	36.60779	16.50538142
CB2-12	85	683	19633	71.74193	28.25803	15.75115975
CB2-12	87	685	19709	0	99.99995	14.55619118
CB2-12	89	687	19785	71.20275	28.79724	15.37962362
CB2-12	92	690	19899			13.28455182

APPENDIX C – POLLEN DATA FROM CUMBRES BOG

Pollen was extracted from sediment and examined by Gonzalo-Jimenez Moreno. Here I present the values for pollen ratios presented in Chapter 4. As in Appendix B, increment depth refers to the depth within a specific drive whereas actual depth is cumulative depth. The ages are interpolated from calibrated radiocarbon ages meaning that they should be interpreted as years before 1950. The sampling interval is calculated from the age model and varies because the age model varies with depth (Appendix D).

Drive	Increment Depth-cm	Actual Depth-cm	Age	spruce pine	spruce Artemisia	Pinus Artemisia	Sample Interval
6	15	15	316.5	-0.05882	-0.16667	-0.15464	249
	25	25	565.5	-0.41053	-0.38462	-0.03279	249
	35	35	814.5	-0.49315	-0.09756	0.343066	298.8
	47	47	1113.3	-0.70423	-0.3913	0.421687	199.2
	55	55	1312.5	-0.36842	0.116279	0.401575	167.4
	65	65	1479.9	-0.41667	-0.31707	0.06087	85.8
	75	75	1565.7	-0.5641	-0.54054	0.017241	85.8
	85	85	1651.5	-0.25373	0.010101	0.24031	68.64
	93	93	1720.14	-0.40146	-0.01205	0.363636	42.9
7	5	98	1763.04	-0.53247	-0.5	0.035714	85.8
	15	108	1848.84	-0.47917	-0.38272	0.089431	85.8
	25	118	1934.64	-0.57303	-0.56818	-0.02222	85.8
	35	128	2020.44	-0.68421	-0.74286	-0.12963	77.22
	44	137	2097.66	-0.42149	-0.06667	0.327731	94.38
	55	148	2192.04	-0.48515	-0.35802	0.140625	112.98
	65	158	2305.02	-0.74468	-0.65714	0.147059	220.1
	75	168	2525.12	-0.60976	-0.33333	0.29927	110.05
	80	173	2635.17	-0.39241	-0.52941	-0.2093	110.05
	85	178	2745.22	-0.62353	-0.52239	0.113043	220.1
	95	188	2965.32	-0.375	-0.42857	-0.06383	110.05
8	5	193	3075.37	-0.66667	-0.80488	-0.29825	220.1
	15	203	3295.47	-0.44118	-0.57778	-0.18333	220.1
	25	213	3515.57	-0.45455	-0.49474	-0.0597	220.1
	35	223	3735.67	-0.64444	-0.11111	0.558824	220.1
	45	233	3955.77	-0.53846	-0.33333	0.25	220.1
	55	243	4175.87	-0.5	-0.29825	0.221053	220.1
	65	253	4395.97	-0.65957	-0.41818	0.327586	220.1
	75	263	4616.07	-0.65854	0.217391	0.766234	220.1
	85	273	4836.17	-0.53488	-0.10448	0.451852	453.33
	95	283	5289.5	-0.78378	-0.67347	0.233645	430.5
	104	292	5720	-0.61667	-0.23333	0.447761	287
9	5	298	6007	-0.59036	-0.33333	0.306122	478.3333
	15	308	6485.333	-0.4433	-0.21739	0.25	478.3334
	25	318	6963.667	-0.45455	-0.45455	0	478.3333
	35	328	7442	-0.34286	-0.2459	0.105882	478.3333
	45	338	7920.333	-0.66667	-0.52	0.22449	458.2847
	55	348	8378.618	-0.56863	-0.56	0.012658	378.0899
	65	358	8756.708	-0.575	-0.41379	0.211538	378.0899
	75	368	9134.798	-0.29032	0.208791	0.470588	378.0898
	85	378	9512.888	-0.57962	-0.09589	0.512195	302.472
	93	386	9815.36	-0.57838	-0.03704	0.553191	340.2804
	102	395	10155.64	-0.71613	-0.44304	0.4	226.854

Drive	Increment Depth-cm	Actual Depth-cm	Age	spruce pine	spruce Artemisia	Pinus Artemisia	Sample Interval
10	5	401	10382.49	-0.67407	-0.32308	0.448718	378.09
	15	411	10760.58	-0.58242	-0.54217	0.058824	378.09
	25	421	11138.67	-0.67939	-0.41667	0.36646	189.045
	30	426	11327.72	-0.76796	-0.28814	0.614213	189.045
	35	431	11516.76	-0.70513	-0.44578	0.378238	300.425
	45	441	11817.19	-0.62745	-0.66372	-0.06215	248.649
	55	451	12065.84	-0.71429	-0.82482	-0.26904	248.648
	65	461	12314.49	-0.29091	-0.47297	-0.21111	248.649
	75	471	12563.14	-0.30864	-0.54098	-0.27891	248.649
	85	481	12811.78	-0.23077	-0.38462	-0.16883	248.648
	95	491	13060.43	-0.33333	-0.53968	-0.25161	124.325
11	5	496	13184.76	-0.5122	-0.3617	0.184713	124.324
	10	501	13309.08	-0.32039	-0.0411	0.254902	124.324
	15	506	13433.41	-0.30612	-0.67925	-0.47107	248.649
	25	516	13682.05	-0.53659	-0.58696	-0.07353	248.649
	35	526	13930.7	-0.57143	-0.88991	-0.648	248.648
	45	536	14179.35	-0.36508	-0.66667	-0.3986	124.325
	50	541	14303.68	-0.53125	-0.71429	-0.29496	124.324
	55	546	14428	-0.32143	-0.77647	-0.61497	379.902
	65	556	14807.9	-0.59322	-0.82857	-0.47977	379.902
	75	566	15187.8	-0.68627	-0.9	-0.57513	379.902
	85	576	15567.71	-0.44444	-0.46903	-0.04403	303.921
	93	584	15871.63	-0.67568	-0.78947	-0.2439	455.883
	105	596	16327.51	-0.73333	-0.92208	-0.58289	265.931
12	5	603	16593.44	-0.4	-0.68421	-0.41176	379.902
	15	613	16973.34	-0.71875	-0.8875	-0.48039	341.912
	24	622	17315.26	-0.53846	-0.7541	-0.37179	417.892
	35	633	17733.15	-0.55	-0.88387	-0.66857	379.902
	45	643	18113.05	-0.41935	-0.9	-0.77202	379.902
	55	653	18492.95	-0.64444	-0.90062	-0.62766	493.873
	68	666	18986.82	-0.65517	-0.81481	-0.34247	265.931
	75	673	19252.76	-0.51852	-0.69412	-0.27434	493.872
	88	686	19746.63	-0.46429	-0.80519	-0.54444	

APPENDIX D – CUMBRES BOG AGE MODEL AND MAGNETIC SUSEPTIBILITY

The age model was developed from 7 radiocarbon dates (see Chapter 4) and ages between the fixed points were interpolated to create this annual age model. The magnetic susceptibility record was measured at LacCore laboratory at the University of Minnesota.

cm Depth	Modeled Age (yrs)	MS (SI)
0.1	-57	0.9
1	-32.1	0.4
2	-7.2	-0.2
3	17.7	-0.3
4	42.6	-0.7
5	67.5	-0.6
6	92.4	-0.8
7	117.3	-0.7
8	142.2	-0.3
9	167.1	0.1
10	192	-1
11	216.9	-0.9
12	241.8	-0.8
13	266.7	-0.6
14	291.6	-0.8
15	316.5	-0.8
16	341.4	-0.7
17	366.3	-0.7
18	391.2	-0.7
19	416.1	-0.7
20	441	-0.6
21	465.9	-0.6
22	490.8	-0.3
23	515.7	0
24	540.6	-0.2
25	565.5	-0.3
26	590.4	
27	615.3	-0.5
28	640.2	-0.6
29	665.1	0.3
30	690	0.9
31	714.9	0.3
32	739.8	
33	764.7	
34	789.6	-0.4
35	814.5	-0.6
36	839.4	-0.5
37	864.3	-0.4
38	889.2	-0.7
39	914.1	-0.7
40	939	-0.9
41	963.9	-1

cm Depth	Modeled Age (yrs)	MS (SI)
345	8255.167	1.1
346	8303	0.2
347	8340.809	0.9
348	8378.618	0.4
349	8416.427	0.2
350	8454.236	0.4
351	8492.045	0.1
352	8529.854	0.1
353	8567.663	0.1
354	8605.472	0.2
355	8643.281	-0.2
356	8681.09	0.3
357	8718.899	0.4
358	8756.708	0.2
359	8794.517	0.5
360	8832.326	0.3
361	8870.135	0.5
362	8907.944	0.6
363	8945.753	0.2
364	8983.562	0.4
365	9021.371	0.5
366	9059.18	0.5
367	9096.989	0.3
368	9134.798	0.1
369	9172.607	0.5
370	9210.416	0.5
371	9248.225	0.3
372	9286.034	0.8
373	9323.843	0.4
374	9361.652	0.5
375	9399.461	0.2
376	9437.27	0.3
377	9475.079	
378	9512.888	0.1
379	9550.697	0.6
380	9588.506	0.7
381	9626.315	0.2
382	9664.124	0.1
383	9701.933	0.1
384	9739.742	0.7
385	9777.551	0.7
386	9815.36	0.2

cm Depth	Modeled Age (yrs)	MS (SI)
42	988.8	-0.6
43	1013.7	-0.9
44	1038.6	-0.8
45	1063.5	-1.1
46	1088.4	-1
47	1113.3	-1
48	1138.2	-1
49	1163.1	-0.6
50	1188	-0.8
51	1212.9	
52	1237.8	-0.9
53	1262.7	
54	1287.6	-0.7
55	1312.5	-1
56	1337.4	-0.9
57	1362.3	-0.2
58	1387.2	
59	1412.1	-0.2
60	1437	-0.6
61	1445.58	-0.9
62	1454.16	-1
63	1462.74	-1
64	1471.32	-1
65	1479.9	-0.8
66	1488.48	-1
67	1497.06	-1
68	1505.64	-1
69	1514.22	-1
70	1522.8	-0.6
71	1531.38	-0.7
72	1539.96	-0.8
73	1548.54	-0.7
74	1557.12	-0.5
75	1565.7	-0.5
76	1574.28	-0.7
77	1582.86	-0.5
78	1591.44	-0.7
79	1600.02	-0.6
80	1608.6	-0.7
81	1617.18	-0.6
82	1625.76	-0.5
83	1634.34	-0.7

cm Depth	Modeled Age (yrs)	MS (SI)
387	9853.169	0.2
388	9890.978	0.4
389	9928.787	0.4
390	9966.596	0.5
391	10004.4	0.4
392	10042.21	0.3
393	10080.02	0
394	10117.83	0.1
395	10155.64	
396	10193.45	
396.1	10193.45	0.7
397	10231.26	0.2
398	10269.07	0.1
399	10306.88	0
400	10344.69	0
401	10382.49	0.7
402	10420.3	0.8
403	10458.11	0.2
404	10495.92	0.3
405	10533.73	0.3
406	10571.54	0.1
407	10609.35	0.3
408	10647.16	0.5
409	10684.97	0.3
410	10722.78	0
411	10760.58	0.2
412	10798.39	0.3
413	10836.2	0.6
414	10874.01	1
415	10911.82	0.7
416	10949.63	0.1
417	10987.44	0.3
418	11025.25	0.5
419	11063.06	0.5
420	11100.87	0.2
421	11138.67	
422	11176.48	0.3
423	11214.29	0.3
424	11252.1	1.7
425	11289.91	0.5
426	11327.72	0.2
427	11365.53	1

cm Depth	Modeled Age (yrs)	MS (SI)
84	1642.92	-0.7
85	1651.5	-0.8
86	1660.08	-0.8
87	1668.66	-0.7
88	1677.24	
89	1685.82	
90	1694.4	-0.5
91	1702.98	-0.3
92	1711.56	0.3
93	1720.14	
93.1	1720.14	1.1
94	1728.72	0.7
95	1737.3	0.2
96	1745.88	0.3
97	1754.46	-0.5
98	1763.04	-0.2
99	1771.62	-0.1
100	1780.2	-0.1
101	1788.78	-0.1
102	1797.36	-0.4
103	1805.94	0.1
104	1814.52	0.2
105	1823.1	0.3
106	1831.68	0.3
107	1840.26	0
108	1848.84	-0.1
109	1857.42	-0.1
110	1866	-0.3
111	1874.58	-0.4
112	1883.16	-0.5
113	1891.74	-0.4
114	1900.32	-0.5
115	1908.9	-0.3
116	1917.48	-0.5
117	1926.06	-0.5
118	1934.64	0
119	1943.22	0.4
120	1951.8	0.3
121	1960.38	0.2
122	1968.96	0.3
123	1977.54	0.4
124	1986.12	0.4

cm Depth	Modeled Age (yrs)	MS (SI)
428	11403.34	0.2
429	11441.15	0.5
430	11478.96	1.3
431	11516.76	1.1
432	11554.57	2.2
433	11592.38	0.7
434	11630.19	0.9
435	11668	1.3
436	11692.86	2.8
437	11717.73	12.3
438	11742.59	27.8
439	11767.46	20.9
440	11792.32	7.7
441	11817.19	5.3
442	11842.05	3.6
443	11866.92	2.7
444	11891.78	4.6
445	11916.65	4.3
446	11941.51	5.5
447	11966.38	5
448	11991.24	4.6
449	12016.11	4.4
450	12040.97	4
451	12065.84	3
452	12090.7	5.9
453	12115.57	9.7
454	12140.43	7
455	12165.3	6
456	12190.16	5.3
457	12215.03	6.6
458	12239.89	7.1
459	12264.76	5.9
460	12289.62	7.5
461	12314.49	9.1
462	12339.35	6.2
463	12364.22	5.6
464	12389.08	6.2
465	12413.95	7
466	12438.81	9.6
467	12463.68	7.9
468	12488.54	9.6
469	12513.41	9.6

cm Depth	Modeled Age (yrs)	MS (SI)
125	1994.7	0.3
126	2003.28	-0.1
127	2011.86	-0.4
128	2020.44	0.1
129	2029.02	-0.1
130	2037.6	0.2
131	2046.18	0.3
132	2054.76	0.4
133	2063.34	0.1
134	2071.92	0.1
135	2080.5	-0.2
136	2089.08	-0.2
137	2097.66	-0.3
138	2106.24	-0.5
139	2114.82	0.1
140	2123.4	0
141	2131.98	-0.1
142	2140.56	-0.1
143	2149.14	-0.8
144	2157.72	-0.8
145	2166.3	-0.6
146	2174.88	-0.7
147	2183.46	-0.6
148	2192.04	-0.8
149	2200.62	-0.7
150	2209.2	-0.9
151	2217.78	-0.9
152	2226.36	-1
153	2234.94	-0.9
154	2243.52	-1
155	2252.1	-0.9
156	2261	-1
157	2283.01	-1.2
158	2305.02	-1
159	2327.03	-0.9
160	2349.04	-0.9
161	2371.05	-1
162	2393.06	-0.8
163	2415.07	-1
164	2437.08	-1.2
165	2459.09	-0.8
166	2481.1	-0.9

cm Depth	Modeled Age (yrs)	MS (SI)
470	12538.27	8.2
471	12563.14	7.1
472	12588	5.8
473	12612.86	7.1
474	12637.73	7.3
475	12662.59	6.2
476	12687.46	4.4
477	12712.32	4.7
478	12737.19	4.3
479	12762.05	1.3
480	12786.92	2
481	12811.78	2.9
482	12836.65	1.8
483	12861.51	4
484	12886.38	3.5
485	12911.24	3.2
486	12936.11	3.8
487	12960.97	5
488	12985.84	13.5
489	13010.7	13.6
490	13035.57	0.3
491	13060.43	
491.1	13060.43	4.3
492	13085.3	4.5
493	13110.16	8
494	13135.03	7.3
495	13159.89	2.7
496	13184.76	1
497	13209.62	0.8
498	13234.49	0.8
499	13259.35	2.9
500	13284.22	1.6
501	13309.08	1.7
502	13333.95	5.2
503	13358.81	6.5
504	13383.68	4.9
505	13408.54	4.3
506	13433.41	6.3
507	13458.27	6.8
508	13483.14	5.2
509	13508	5
510	13532.86	4.9

cm Depth	Modeled Age (yrs)	MS (SI)
167	2503.11	-0.8
168	2525.12	-1
169	2547.13	-0.6
170	2569.14	0.5
171	2591.15	1.5
172	2613.16	0.8
173	2635.17	0.6
174	2657.18	0.6
175	2679.19	0.5
176	2701.2	0.2
177	2723.21	0.1
178	2745.22	-0.5
179	2767.23	0
180	2789.24	0.7
181	2811.25	0.2
182	2833.26	0.1
183	2855.27	0.5
184	2877.28	0.2
185	2899.29	-0.1
186	2921.3	-0.1
187	2943.31	0.1
188	2965.32	0.4
188.1	2965.32	0.6
189	2987.33	0.4
190	3009.34	-0.1
191	3031.35	-0.8
192	3053.36	-0.9
193	3075.37	-0.4
194	3097.38	-0.5
195	3119.39	-1
196	3141.4	-1
197	3163.41	-0.9
198	3185.42	-0.7
199	3207.43	-0.6
200	3229.44	-0.8
201	3251.45	-0.7
202	3273.46	-0.5
203	3295.47	-0.2
204	3317.48	-0.6
205	3339.49	-1.1
206	3361.5	-1
207	3383.51	-1

cm Depth	Modeled Age (yrs)	MS (SI)
511	13557.73	3.3
512	13582.59	2.5
513	13607.46	1.1
514	13632.32	0.4
515	13657.19	0.2
516	13682.05	1.1
517	13706.92	5.3
518	13731.78	8.7
519	13756.65	10.9
520	13781.51	11.3
521	13806.38	13.3
522	13831.24	15.5
523	13856.11	17.1
524	13880.97	16.3
525	13905.84	15.2
526	13930.7	12.3
527	13955.57	14.2
528	13980.43	17.9
529	14005.3	17.7
530	14030.16	14.7
531	14055.03	19.2
532	14079.89	18.3
533	14104.76	18.4
534	14129.62	15.8
535	14154.49	14.9
536	14179.35	14.8
537	14204.22	12.2
538	14229.08	12.7
539	14253.95	14.7
540	14278.81	16
541	14303.68	19.4
542	14328.54	17.1
543	14353.41	22.3
544	14378.27	28.2
545	14403.14	37.3
546	14428	31.2
547	14465.99	34.8
548	14503.98	47.5
549	14541.97	54.2
550	14579.96	48.8
551	14617.95	53.6
552	14655.94	54.3

cm Depth	Modeled Age (yrs)	MS (SI)
208	3405.52	-1.2
209	3427.53	-0.8
210	3449.54	-1.3
211	3471.55	-1.2
212	3493.56	-0.7
213	3515.57	-1
214	3537.58	-1.1
215	3559.59	-1.2
216	3581.6	-1.1
217	3603.61	-1.2
218	3625.62	-1.2
219	3647.63	-1
220	3669.64	-1.3
221	3691.65	-1.5
222	3713.66	-1.2
223	3735.67	-0.9
224	3757.68	-0.7
225	3779.69	-0.7
226	3801.7	-0.4
227	3823.71	0.3
228	3845.72	0.4
229	3867.73	-0.7
230	3889.74	0
231	3911.75	-0.7
232	3933.76	-1.3
233	3955.77	-1
234	3977.78	-0.5
235	3999.79	-1
236	4021.8	-1
237	4043.81	-1
238	4065.82	-0.3
239	4087.83	-0.6
240	4109.84	-1.1
241	4131.85	-1
242	4153.86	-0.7
243	4175.87	0.3
244	4197.88	0.4
245	4219.89	0.6
246	4241.9	-0.1
247	4263.91	-0.6
248	4285.92	0.2
249	4307.93	-0.1

cm Depth	Modeled Age (yrs)	MS (SI)
553	14693.93	52.9
554	14731.92	63.1
555	14769.91	54.5
556	14807.9	55.1
557	14845.89	68.4
558	14883.88	61.1
559	14921.87	50.3
560	14959.86	42.8
561	14997.85	32.6
562	15035.84	38.6
563	15073.83	59.3
564	15111.82	59.2
565	15149.81	58.4
566	15187.8	60.8
567	15225.79	79.1
568	15263.78	64.9
569	15301.77	32.3
570	15339.76	55.2
571	15377.75	48.7
572	15415.75	58.6
573	15453.74	64.6
574	15491.73	121.7
575	15529.72	89.3
576	15567.71	65
577	15605.7	60.8
578	15643.69	45.9
579	15681.68	51.9
580	15719.67	24.2
581	15757.66	33.2
582	15795.65	52.3
583	15833.64	61.7
584	15871.63	90.1
585	15909.62	88.6
586	15947.61	85.1
587	15985.6	54.5
588	16023.59	86.8
589	16061.58	91.8
590	16099.57	108.3
591	16137.56	125.2
592	16175.55	107.2
593	16213.54	104.4
594	16251.53	84

cm Depth	Modeled Age (yrs)	MS (SI)
250	4329.94	0.1
251	4351.95	0.1
252	4373.96	0.5
253	4395.97	0.2
254	4417.98	0.5
255	4439.99	-0.3
256	4462	-0.6
257	4484.01	-0.4
258	4506.02	-1.3
259	4528.03	-1.2
260	4550.04	-0.3
261	4572.05	-0.1
262	4594.06	-0.1
263	4616.07	
264	4638.08	
265	4660.09	-0.4
266	4682.1	-0.9
267	4704.11	-1.1
268	4726.12	-0.4
269	4748.13	0.1
270	4770.14	0.2
271	4792.15	-0.2
272	4814.16	-0.5
273	4836.17	-0.6
274	4859	-0.7
275	4906.833	-0.7
276	4954.667	0.1
277	5002.5	0.2
278	5050.333	0.4
279	5098.167	0.5
280	5146	0.4
281	5193.833	0.4
282	5241.667	0.4
283	5289.5	0.5
284	5337.333	0.7
285	5385.167	0.3
286	5433	0.4
287	5480.833	0.1
288	5528.667	0.4
289	5576.5	0.6
290	5624.333	0.2
291	5672.167	0.3

cm Depth	Modeled Age (yrs)	MS (SI)
595	16289.52	63.4
596	16327.51	46
597	16365.5	2.1
598	16403.49	
598.1	16403.49	7.5
599	16441.48	3.5
600	16479.47	4.4
601	16517.46	7.3
602	16555.45	11.9
603	16593.44	22.7
604	16631.43	35.7
605	16669.42	40.3
606	16707.41	35.8
607	16745.4	49.2
608	16783.39	30.4
609	16821.38	28.9
610	16859.37	36.8
611	16897.36	55.6
612	16935.35	38.8
613	16973.34	112.5
614	17011.33	64.7
615	17049.32	74.5
616	17087.31	113.6
617	17125.3	142.2
618	17163.29	130
619	17201.28	125
620	17239.27	132.6
621	17277.26	177.9
622	17315.25	153.6
623	17353.25	160.6
624	17391.24	131.7
625	17429.23	191.4
626	17467.22	145.1
627	17505.21	128.4
628	17543.2	188.4
629	17581.19	115.9
630	17619.18	128
631	17657.17	204.1
632	17695.16	165.2
633	17733.15	157.2
634	17771.14	110.9
635	17809.13	124.2

cm Depth	Modeled Age (yrs)	MS (SI)
292	5720	0
293	5767.833	0.1
293.1	5767.833	1
294	5815.667	0.2
295	5863.5	-0.2
296	5911.333	-0.3
297	5959.167	0.2
298	6007	1.3
299	6054.833	0.3
300	6102.667	1
301	6150.5	1.5
302	6198.333	0.2
303	6246.167	0
304	6294	0.1
305	6341.833	0.4
306	6389.667	0.2
307	6437.5	0.5
308	6485.333	-0.3
309	6533.167	-0.4
310	6581	0.1
311	6628.833	-0.2
312	6676.667	0
313	6724.5	0.6
314	6772.333	0.4
315	6820.167	0.3
316	6868	0.5
317	6915.833	0.3
318	6963.667	0.5
319	7011.5	0.5
320	7059.333	0
321	7107.167	0.9
322	7155	0.7
323	7202.833	0.5
324	7250.667	0.2
325	7298.5	0.4
326	7346.333	1.3
327	7394.167	0.7
328	7442	0.7
329	7489.833	0.8
330	7537.667	0.3
331	7585.5	0.7
332	7633.333	0.5

cm Depth	Modeled Age (yrs)	MS (SI)
636	17847.12	94.7
637	17885.11	140.5
638	17923.1	150.4
639	17961.09	133.4
640	17999.08	168.5
641	18037.07	146.8
642	18075.06	108.7
643	18113.05	125
644	18151.04	129.5
645	18189.03	150.5
646	18227.02	125.3
647	18265.01	105.1
648	18303	124.5
649	18340.99	156.7
650	18378.98	135.5
651	18416.97	102
652	18454.96	102.1
653	18492.95	142.3
654	18530.94	77.5
655	18568.93	133.9
656	18606.92	121.5
657	18644.91	97.5
658	18682.9	99.1
659	18720.89	101.9
660	18758.88	126.1
661	18796.87	112.5
662	18834.86	113.2
663	18872.85	108.6
664	18910.84	111.6
665	18948.83	36.5
666	18986.82	117
667	19024.81	266.1
668	19062.8	291.1
669	19100.79	176.4
670	19138.78	107.4
671	19176.77	100.7
672	19214.76	128.2
673	19252.75	124
674	19290.75	118.6
675	19328.74	123.6
676	19366.73	93.6
677	19404.72	111.7

cm Depth	Modeled Age (yrs)	MS (SI)
333	7681.167	0.6
334	7729	0.7
335	7776.833	0.7
336	7824.667	0.6
337	7872.5	0.6
338	7920.333	0.9
339	7968.167	1.8
340	8016	0.9
341	8063.833	1.1
342	8111.667	1
343	8159.5	0.8
344	8207.333	0.9

cm Depth	Modeled Age (yrs)	MS (SI)
678	19442.71	79.5
679	19480.7	46.5
680	19518.69	81.9
681	19556.68	116.4
682	19594.67	109.2
683	19632.66	116
684	19670.65	116.5
685	19708.64	164.6
686	19746.63	135.7
687	19784.62	126.1
688	19822.61	69
689	19860.6	41.6
690	19898.59	1.3

APPENDIX E – SOIL FIELD DATA

Soils were described in the field in accordance with the Field Book for Describing and Sampling Soils and Birkeland (1999). Some dry colors were measured in the lab when samples would not dry in the field. UTM coordinates are provided when available but all pit locations are mapped in Johnson et al. (2010).

Surface	Pit	Horizon	Depth (cm)	Color Moist	Color Dry	Gravel (%)	Texture	Structure	Clay Films	Consistence Dry	Consistence Moist	Consistence Wet	Boundary	Roots	Pores	
GT	SJ08-1	A	0-33.5	10 YR 3/2	10 YR 4/3	10	SL	1&2 m&c sbk	None	---	vfr-fr	ss-po	g s	2m 3f 3vf	1f 1vf	Double sampled - structure better on bottom half
		A/Box	33.5-76	10YR 3/3	10 YR 3/3	50	SL	1 m-c sbk	None	---	vfr	ss-po	c s	1m 2f 2vf	1f 1vf	A is dominant, B described seperately below.
		Box		10 YR 3/3	10YR 5/4	50	SL	1-2 m-c abk	None	---	vfr	ss-po	a b	2f 1vf	1f 2vf	Inclusions in above horizon
		C	76-120	10 YR 3/3	10 YR 7/4	75	SL	sg	None	---	lo	ss po	---	1f 1vf	---	No pores due to granular nature
		GT	SJ08-1													

Location: Adams Fork
Date: 5-30-08
Time: 4:00pm
Described: Johnson, Eppes, and Link
UTM: 13S 0357909 / 4231068

Parent Materials: Lowever Gravents clast supported, moderately sorted, sub rounded clasts, largest clast 30cm, gravels exclusive to bottom of pit, top horizons may be dust
Terrace May be fluvial not glacial

Surface	Pit	Horizon	Depth (cm)	Color Moist	Color Dry	Gravel (%)	Texture	Structure	Clay Films	Consistence Dry	Consistence Moist	Consistence Wet	Boundary	Roots	Pores	
		GT	SJ08-2													
GT	SJ08-2	A	0-14	10 YR 3/1	10 YR 3/2	<1	L	2 m-c sbk	None	---	fr	s p	c s	1m 3f 3vf	2m 3f 3vf	
		AB	14-28	10 YR 3/2	10 YR 4/2	<5	L	2 m-c sbk	None	---	vfr	s ps	a s	1m 3f 3vf	2m 3f 3vf	More structure and reddening than B
		B	28-51	10 YR 3/2	10 YR 5/3	60	SLC-L	1 f0m0c abk	None	---	fr	s ps	c s	1m 2f 3vf	1m 3f 3vf	
		Box	51-Water	10 YR 3/4	10 YR 5/4	40	SCL	1 m-f sbk	None	---	vfr-fr	s p	a s	1m 2f 2vf	underwater	

Location: Main Fork
Date: 5-31-08
Time: 12:30 pm
Described: Johnson, Eppes, and Link
No UTM Available

Parent Materials: Gravel - sub-angular to sub rounded, matrix supported in places, moderately sorted
Glacial material including boulders, some fluvial gravels, dust (?) on top

---

Col	SJ08-3	A	0-21	10YR 3/2	10YR 3/3	<5	L	2 m-f-vf abk	None		fr	ss ps	c s	'vc 2c 3m 3f 3'1c 2m 1f 2vf		larger peds are friable, smaller are firm
		AB1	21-38.5	10YR 3/2	10YR 4/3	<5	L	2 c-m-f-vf abk	None		fr	ss ps	g s	2c 3c 3m 3f 3v1c 3m 1f 3vf		larger peds are friable, smaller are firm. Siltier than A
		AB2	38.5-56	10YR 3/4	10YR 5/4	<5	L	2 c abk	None		fr	s p	c s	2c 2m 3f 3vf	1f 3vf	
		Box	56-77.5	10YR 4/6	10YR 6/4	<1	L	2 c-m-f-vf abk	None		fr	ss ps	c s	2m 1f	3f 3vf	
		B	77.5-89	10YR 4/6	10YR 7/3	<5	L	2 c-m-f-vf abk	None		fr	ss ps	a s	1m 1f	1m 3f 3vf	
		C	89-bottor	10YR 3/3	10YR 5/3	70	LS	1 m-f gr	None		vfr	so po		1f 2vf	1f 1vf	
		Col	SJ08-3													

Location: Road cut near mouth of Adam
Date: 5-31-08
Time: 4:45 pm
Described: Johnson, Eppes, and Link
No UTM Available

Parent Materials: Glacial material including a fine grained matrix, rounded to sub-rounded clasts up to 40 cm in size
General Comments: Road Cut

AF1	SJ08-4	AC	0-15	10YR 3/2	10YR 4/3	25	L	1&2 c-m-f gr	None	---	vfr	ss ps	c s	1m 3f 3vf	1f 2vf	small peds are granular and larger ones are..
		AB1	15-31	10YR 3/2	10YR 4/2	15	L	1&2 c-m-f sbk	None	---	vfr	ss ps	c s	1m 3f3vf	3m 3f 3vf	same as above. Increased porosity due to granuals
		AB2	31-57	10YR 3/2	10YR 4/2	10	L	2 vc-c-m sbk	None	---	vfr	ss p	c s	3f 3vf	1m 2f 2vf	
		AB3	57-71	10YR 4/2	10YR 5/4	35	L	2 c-m sbk	None	---	fr-vfr	s p	g s	1f 1vf	1c 1m 1f 3vf	
		AB4(ABb'	71-83	10YR 3/3	10YR 5/3	<10	L	2 c-m abk	None	---	fr-vfr	s p	c s	1f 1vf	1m 1f 3vf	
		AB5	83-111	10YR 4/2	10YR 4/3	10	L	2 c-m abk	None	---	fr-vfr	s p	c s	1f 1vf	3f 3vf	charcoal sampled @ 104cm
		Bw1	111-125	10YR 4/2	10YR 5/3	25	L	2 c-m abk	None	---	fr-vfr	s ps	a s	1f 1vf	1f 3vf	
		Bw2	125-150	10YR 4/4	10YR 5/3	?	SL	c-m abk	None	---	vfr	ss ps	---	---	3f 3vf	

Location: AF1 between car camp spot ar
Date: 6-1-08 **AF1** SJ08-4
Time: 11:30am
Described: Johnson, Eppes, and Link
No UTM Available

Parent Materials: Alluvial fan materials including silt, sand, and coarse gravel. Gravel is angular to sub rounded and ranges from <1 cm to 10 cm
Gravel appears in lenses throughout pit. Pit is in middle of fan surface on a slight local high. 1.5 m deep pit. Sparse bushes on surface pit dug between bushes

AC (cont)... subangular. Structure 2 for granular, 1 sbk

		AF2	SJ08-5													
AF2	SJ08-5	ABw	0-39	10YR 4/2	10YR 4/3	40	SL	1&2 f&c gr&sbk	None	---	fr	s po-ps	c s	1m 3f 3vf	1f 3vf	Granular peds are fine and 2. Sbk peds are c and 1...
		Bw	39-56	10YR 4/2	10YR 5/3	25	SL	2 f-m sbk	None	---	vfr	ss po	c s	2m 1f 1vf	1f 3vf	
		ABb	56-75	10YR 4/2	10YR 4/4	25	L		None		fr	s p	a w	3m 2f 2vf	1f 3vf	slight burn lense in middle @ 56-58 cm...
		C	75-100	10YR 4/3	10YR 5/3	75	SL	3 c abk	None	---	vfr	ss ps		2f 2vf	granuals	larges clasts (30cm), gravels, high porosity

Location: AF2 inset into pit 4 surface
Date: 6-1-08
Time: 4:00pm
Described: Johnson, Eppes, and Link
No UTM Available

Parent Materials: Alluvial fan materials including silt, sand, and coarse gravel.
Gravel is angular to sub rounded and ranges from <1 cm to 10 cm. Gravel more uniform throughout than AF1
Pit on right side of culvert channel in the middle of the surface. Grasses more sparse than AF1.

Abw (cont)... Worms are abundant in this layer.
ABb (cont)... Two samples: A charcoal better than B

		Qt2	SJ08-6													
Qt2	SJ08-6	Aw	0-13	10YR 3/3	3 5/4 and 10Y	<10	L	1.5 f-m sbk	None	---	vfr	ss-ps	c s	3m 3f 3vf	1f 1vf	
Distal		AB	13-20	10YR 3/4	10YR 4/3	<5	SL-L	.5 c-m-f pl&ab	None	---	vfr&fi-vfi	ss ps	aw	3m 1f 1vf	1vf	Highly variable horizon- Platey and firm stuff...
		Ab	20-26	10YR 3/3	10YR 4/2	25	L	2 f-m-c abk	None		fr	ss ps	c s	1m 2f 2vf	2f 1vf	
		ABb	26-36	10YR 4/3	10YR 5/3	10	SL-L	2 c-m-f abk	None	---	vfr	ss ps	a s	1m 1f 1 vf	3f 3vf	
		B	36-64	10YR 3/3	10YR 3/3	<10	SL-L	2 c-m-f abk	None		fr	ss p	a s	1f 1vf	3f 3vf	Water in bottom
		C	64-80													

Location: Field at 3 Forks
Date: 6-4-08
1:30
Described: Johnson and Link
UTM: 13S 0356056 / 4126623

Parent Materials: A and AB are fine and dusty (silt), others are gravely and clast supported with high sand content. Clasts up to 50 cm. In AB, spots may be aprolit. They are v. firm, platey and con not be split with a knife.

AB (cont)...may be saprolite that's been transported? Two main groups firm-pl-2 and vfr-abk-1.

		OT/Qt1	SJ08-7													
OT/Qt1	SJ08-7	A	0-10.5	10YR 4/2	10YR 4/4	<10	L	1.5 c-m-f sbk	None	---	fr	ss ps	c s	m3 f3 vf3	None?	Roots Dom?
		AB	10.5-21.5	10YR 4/2	10YR 5/4	15	L	1.5 f-m-c sbk	None	---	fr-vfr	ss ps	g s	m3 f3 vf3	f1	
		B1	21.5-42	10YR 3/3	10YR 5/6	65	LS	1 m-c abk	None		vfr	ss po	c w	vf3 f2 m1	f1 vf1	
		B2	42-57	10YR 3/3	10YR 5/3	70	LS	1-sg f g-sbk	None	---	fr-vfr	ss po	s a	f1 vf2	vf2 f1	
		BC	57-102	10YR 3/4	10YR 5/4	70	S	sg g	None		lo	so po		vf1	vf1	Double Sampled; 57-80 and 80-102

Location: Adams fork
Date: 6-6-08

Described: Johnson and Link
UTM: 13 S 0355551 / 4131730

Parent Materials: Mixture of materials which are very hummocky sandy areas border clay/silt laterally and vertically.
General Comments: V. little porosity, not sure why, too granular? Soil Overlies ~ 6 m of sediment. Overlies numerous springs, high porosity. Stream Cut

		GT	SJ08-8													
GT	SJ08-8	AB	0-15	10YR 4/3	10YR 5/4	<10	L	1.5 f-m-c sbk	None	---	fr-vfr	ss ps	c s	2m 3f 3vf	1vf	
		AB	15-54	10YR 3/3	10YR 5/4	<10	L	2 c-m-f sbk	None	---	vfr	ss ps	a s	1m 2f 2vf	1m 2f 3vf	
		B	54-65	10YR 4/4	10YR 7/4	40	L	2 m-f abk	None		fr-vfr	s ps	a w	1f 1vf	1f 3vf	
		Bw	65-79	10YR 3/6	10YR 6/4	35	LS	1 m-f-sbk	None	---	vfr	so po	a w	1f 1vf	1f 3vf	Could be Sapprolite
		C (R?)	79-90	10YR 4/4	10YR 6/3	>75	S	sg gr	None		lo	so po		---	---	Double Sampled; 57-80 and 80-102

Location: North Fork
Date: 6-7-08
1:50
Described: Johnson and Link
UTM: 13 S 0354179 / 4127837

Parent Materials: Large clasts up to 30cm in diameter; sand and gravel in te bottom. No boulders until B horizon. Silty/typical A. Matrix supported in A-Bw. C may be clast supported
General Comments: 80% of area still covered in snow. Pit just beyond stream cut

		Qt2	SJ08-9													
Qt2	SJ08-9	A	0-5	10YR 3/3	10YR 6/2	40	SL	1c-m sbk	None	---	vfr-fr	so po	c s	1m 3f 3vf	Too Granular/ Sandy	
		Aw	5-31	10YR 3/2	10YR6/1	50	S	sg-1f-m gr-sbk	None	---	vf-lo	so po	g s	2f 3vf	Too Granular	
		B1	31-36	10YR 3/4	10YR 5/3	0	L	2 f-m-c abk	None		fr	ss p	a s	2f 2vf	1f 3vf	
		B2	36-61	10YR 3/4	10YR 4/4	30	L	2 f-m-c abk	None	---	fr	s p	c s	2c 1m 1f 1vf	1f 3vf	Could be Sapprolite
		B3	61-87	10YR 3/3	10YR 4/3	40	L	2 m-c abk	None		fr	ss ps	---	3m 1f 1vf	1 vf	Double Sampled; 57-80 and 80-102
				(Wouldn't dry in field)												

Location: Three Forks
Date: 6-8-08
12:00
Described: Johnson and Link
UTM: 13 S 0355865 / 4126576

Parent Materials: Fluvial; rounded and sub-rounded gravels and small clasts (15-20cm). Very sandy
General Comments: On cut bank; distinct charcaol lense @ 35cm where date came from (Diemer; 1200 BP) Cumulic over stable B?
Sream Cut

AF2	SJ08-10	Aw	0-7	10YR 3/3	10YR 4/4	50	SL-L	1f-m gr-sbk	None	---	lo-vfr	ss po	c s	3f 3vf	Too Loose	
		Bw	7-23	10YR 3/2	10YR 6/5	25/75?	SL-L	sg gr	None	---	lo	ss po	c s	1m 3f 3vf	Too Loose	
		Ab	23-40	10YR 3/2	10YR 4/3	35	L	2 f-m-c abk	None		vfr	s p	a s	1m 3f 3vf	2f 2vf	
		Bb1	40-56	10YR 3/3	10YR 5/2	30	L	2 f-m-c abk	None	---	fr	s p	c w	2f 2vf	3m 3f 3vf	
		Bb2(Ab2?	56-85	10YR 4/3	10YR 5/3	25	L	2 f-m-c abk-sb	None		fr	s ps	c s	1m 1f 1vf	3f 3vf	
		Bb3	85-110	10YR 2/3	10YR 6/3	25	L	2 f-m abk	None		fr-vfr	s p	c s	2m 1f 1vf	1m 3f 3vf	Velvey, only sligh grit
		Bb4	110-130	10YR 4/3	10YR 6/3	45	L	2 f-m sbk	None		vfr	s p		1f 2vf	1m 3f 3vf	Velvey, only sligh grit
		AF2	SJ08-10													

Location: Main Fork
Date: 6-8-08
2:30
Described: Johnson and Link
UTM: 13 S 0357241 / 4128313

Parent Materials: Fluvial rounded and sub-rounded gravels; largest clasts above buried soil ~15-20cm
General Comments: Cut bank; soils still frozen, buried soil dips more steeply than the modern surface to depthes vary across the pit.
This is the location of Eppes' 4500ky date came from
Stream Cut

AF1	SJ08-11	O	0-1		10YR 2/2	---	-	---	None	---	---	---	a s	1m 3f 3vf		Looks like a peat layer
		A	1-9	10YR 3/2	10YR 5/4	<5	SIL	1c-m-f sbk	None	---	vfr-fr	ss ps	c s	1c 3m 3f 3vf	1vf	
		AB	9-16	10YR 3/3	10YR 4/3	<10	SIL	1m-f abk-sbk	None		vfr-fr	ss ps	c s	2c 3m 3f 3vf	1f	
		Box	16-32	10YR 4/4	10YR 6/6	70	L	1 vf-f sbk	None	---	vfr-fr	s ps	c s	1c 1m 3f 3vf	1m 1f 2vf	
		B1(Ab?)	32-43	10YR 4/3	10YR 4/3	50	L	1f-m sbk	None		vfr-fr	s ps	c s	1m 3f 3vf	2m 2vf	Not sure about buried soil
		B2 (Bb?)	43-85	10YR 4/3	10YR 3/4	10	SICL	2 f-m-c abk	None		vfr-fr	s p		2m 1f 1vf	2m 3f 3vf	double sample - siltans present
		AF1	SJ08-11													

Location: Main Fork
Date: 6-10-08
4:00
Described: Johnson and Link
UTM: 13 S 0359240 / 4130688

Parent Materials: Angular clasts from gravel to 20 cm in size. Most are 3cm in siz3. Gravel/clast lense @ 9cm-43cm.
43 and below is very clean with little gravel
General Comments: Everything below Box appears to be former cummulic soil. Located across the reservoir from Adams Fork

LA/Qt2	SJ08-12	A	0-10	10YR 3/3	10YR 5/4	25	L	1 m-f sbk	None	---	fr	ss ps	c s	1m 3f 3vf	---	
		AB	10-25	10YR 3/3	10Yr 6/3	10	L	1 f-m-c sbk	None	---	fr vfr	ss ps	c s	3f 3vf	1f 1vf	
		B	25-45	10YR 4/4	10YR 4/3	10	L	2 f-m-c sbk	None		fr-vfr	ss ps	c w	2f 3vf	1f 3vf	
		Ab	45-55	10YR 3/3	10YR 6/3	<10	L	2 f-m-c abk	None	---	fr	s ps	c s	1f 2vf	2f 3vf	Charcoal found @ 52 cm Darker color and...
		Bb1	55-95	10YR 3/4	10YR 5/6	>75	S	sg-1 f gr-sbk	None		vfr-fr	so po	a s	2vf	Too Coarse	
		Bb2	95-120	10YR 5/4	10YR 5/4	<10	SIL	2.5 m-c abk	None		fr-fi	s ps		---	1.5f 3vf	
		LA/Qt2	SJ08-12													

Location: Middle Fork
Date: 6-11-08
3:00
Described: Johnson and Link
UTM: 13 S 0354965 / 4125591

Parent Materials: The top is mostly dusty. Coarse gravel (10 cm) in middle (55-95cm) clay @ bottom
General Comments: Out in the middle of flat surface thought it was LA but might actually be QT2 with a layer of dust on top

Ab (cont)...better strucure than above horizons

LGM	SJ08-13	A	0-18	10YR 3/2	10YR 4/2	35	L	2 c-m-f sbk	None	sh	---	ss ps	c w	3m 2f 2vf	3vf	Roots are laterally variable
		B1	18-35	10YR 4/2	10YR 4/3	25	SCL	2 v-m abk	None	h	---	s-vs p	c w	3m 2f 2vf	1vf	
		B2	35-50	10YR 5/3	10YR 4/4	30	SCL	2 f-m abk	None	sh	---	s-vs p	c s	2m 2f 2vf	2f 3vf	
		B3	50-80	10YR 5/2	10YR 5/4	75	SIL	1 f-m abk	None	sh	---	s ps	c s	2m 1f 1vf	too gravely,	Partially loose/sg due to amount of cobles
		BC	80-115	10YR 5/3	10YR 4/3	90	SCL	sg-1 f- fr-sbk	None	lo-so	---	s p	c w	1m 1f 1vf	too gravely	
		C	115-160	10YR 5/4	10YR 6/3	>75	LS	sg gr	None	lo	---	so po		1m 1f 1vf	too loose	
		LGM	SJ08-13													

Location: Terrace Res
Date: 6-12-08
11:30
Described: Johnson and Link
UTM: 13 S 0386676 / 4134880

Parent Materials: Glaical till. Fine matrix - coarase gravel up to 3m in diameter
General Comments: Very dry and dusty. Climate different from rest of field area, dry and hot.
Parent bedrock upstream may be naturally more red due to higher Iron and acidity
Stream Cut

Col	SJ08-14	A	0-16.5	10YR 4/2	10YR 5/3	25	L	1.5 f-m-c sbk	None	---	fr	ss ps	c s	2m 3f 3vf	1f 1vf	
		AB	16.5-26	10YR 4/3	10YR 5/3	25	L	1.5 f-m-c sbk	None	---	vfr-fr	ss ps	g s	1m 2f 3vf	3f 3vf	
		B1	26-40	10YR 4/3	10YR 5/4	25	L	1.5 f-m-c abk	None	---	vfr-fr	ss ps	c s	1m 2f 2vf	2f 3vf	
		B2	40-55	10YR 4/4	10YR 5/6	50	CL	2 f-m-c abk	None	---	vfr	s p	c s	1c 1m 1f 3vf	3f 3vf	
		BC1	55-90	10YR 4/4	10YR 4/6	60	CL	2 f-m-c abk	None	---	vfr	s p	c s	2m 1f 1vf	3f 3vf	
		BC2	90-120	10YR 4/4	10YR 6/3	65	SCL	1.5 f-m sbk	None	---	vfr	s p		----	3f 3vf	Bottom of layer is wet but no standing water
		Col	SJ08-14													

Location: Adams Fork, near wilderness b
Date: 6-13-08
1:00
Described: Johnson and Link
No UTM available

Parent Materials: Well mixed gravels and small boulders (<40cm), mostly angular but but few sub-angular and sub rounded. Matrix supported
General Comments: Bottomis damp; side of hillslope along trail. Steep section below but not immediately. Location of Char date @ ~8ky
Trail Cut

AF2	SJ08-15	A	0-12.5	10YR 3/2	10YR 4/4	10	L	1f-m sbk	None	---	vfr-fr	ss ps	c s	2m 3f 3vf	1vf	
		AB	12.5-28	10YR 3/2	10YR 5/3	25	L	vc-c-m-f abk-	None	---	fr	ss ps	c s	2f 3vf	2f 1vf	
		B1	28-41	10YR 3/3	10YR 5/2	10	L	2 vc-c-m-f sbk	None	---	fr	ss ps	c s	1vf	1f 3vf	
		B2	41-58	10YR 2/2	10YR 5/3	40	L	2 f-m-c abk	None	---	fr	ss ps	c s	1vf	2f 3vf	
		BC1	58-70	10YR 3/3	10YR 5/4	50	SL	1f sbk	None	---	lo	ss po	c s	---	---	Very rocky, can hardly get sediment out. Too gran for pores
		BC2	70-80	10YR 3/3	10YR 6/4	45	LS-SL	1f-m sbk	None	---	lo	so po		----	---	water is flowing on top of this layer. Too gran for pores
		AF2	SJ08-15													

Location: Main fork near ship bend
Date: 6-14-08
11:30
Described: Johnson and Link
UTM: 13S 0357292 / 4127820

Parent Materials: Dust on top with rocks underneath. Bottom is very rock and wet.
General Comments: Water in bottom, couldn't go any deeper

AF2	SJ08-16	A	0-8	10YR 2/2	10YR 3/2	<5	L	sg-1f-m sbk	None	---	vfr	ss ps	c s	3m 2f 3vf	too rooty	
		Aboxw	8-18	10YR 3/3	10YR 5/4	50	SL	sg-1f sbk	None	---	vfr	so po	c s	2m 2f 3vf		
		Abw	18-29	10YR 3/2	10YR 6/3	50	LS	1f-m sbk	None	---	lo-vfr	so po	c s	1c 1m 2f 2vf		
		C1	29-59	10YR 3/2	10YR 5/3	>75	LS	sg-1f gr-sbk	None	---	lo-vfr	so po	g s	1m 3f 3vf	oo granula Double sampled (29-44 and 44-59)	
		C2	59-98	10YR 2/2	10YR 5/3	75	LS	g-1f-m abk-sb	None	---	lo-vfr	so po		1m 1f 1vf	oo granula Double sampled - Clay rich peds mixed in...	
		AF2	SJ08-16													

..Top half matrix is much less loose,

Location: Middle fork below Conejos Fall
Date: 6-19-08
1:45
Described: Johnson and Link
UTM: 13S 0353005 / 4125221

Parent Materials: Matrix supported coarse gravels and large clasts boulders up to 40cm
General Comments: Strange lighting on pit wal. Least developed soil yet.
Stream Cut

GT	SJ08-17	AB	0-17	10YR 3/3	10YR 3/3	35	L	1.5 m-c sbk	None	---	vfr-fr	ss ps	c s	3m 3f 3vf	too roory	
		B1	17-30	10YR 3/3	10YR 5/3	25	L	1.5 c-m-f sbk	None	---	vfr-fr	ss ps	c s	3m 3 f 2vf	2f 3vf	
		B2	30-44	10YR 3/4	10YR 5/4	15	L	m-c-vc abk-st	None	---	vfr-fr	ss ps	g s	2m 3f 1vf	1m 2f 3vf	
		B3	44-60	10YR 4/3	10YR 5/4	35	L	2 f-m-c abk-sb	None	---	vfr-fr	ss ps	g s	3m 1f 1vf	1m 1f 3vf	
		B4	60-86	10YR 3/3	10YR 5/4	35	L	2 m-c pl-abk	None	---	fr	ss ps		2m 1f 1vf	1m 2f 3vf	
		GT	SJ08-17													

Location: Middle Fork Below Conejos Fal
Date: 6-19-08
3:30
Described: Johnson and Link
UTM: 13S 0353957 / 4125340

Parent Materials: Sub-angular to sub-rounded gravel up to 3 cm in size. Rare boulders up to 20 cm in size.
General Comments: Cloudy while describing pit. Water in bottom of pit.

Col	SJ08-18	A	0-8	2.5Y 3/2	2.5Y 4/2	<10	SIL	2 f abk	None	---	?	ss ps	c s	3f 3vf	1f 2vf	Many worm poops
		AB	8-24	10YR 3/2	10YR 4/3	10	SCL	1.5 f-m-c abk	None	---	vfr-fr	s ps	c l	1m 1f 3vf	1vf	many worm poops
		B1	24-39	2.5Y 4/3	2.5Y 6/3	0	SIL	2 f-m abk	None	---	vfr-fr	s ps	c s	1f 2vf	1f 2vf	
		B2	39-62	2.5Y 5/3	2.5Y 6/4	15	SIL	2 f-m abk	None	---	vfr-fr	ss ps	c w	1f 1vf	1f 1vf	
		Cr	62-85	2.5Y 4/3	2.5Y 6/3	<10	L	2 m-c abk	None	---	fi-vfi	ss ps		1m 1f 1vf	-	Sapprolite
		Col	SJ08-18													

Location: Mainfork, north of trailhead
Date: 6-20-08
11:00
Described: Johnson and Link
UTM: 13S 0358109 / 4139778

Parent Materials: Bedrock underneath, very few colluvial boulders. Majority of B and deeper is weathered from the bedrock
General Comments: Just north of trailhead along road, sampled charcoal from here last year but did not sample.
Road Cut

LGM	SJ08-19	A	0-17	10YR 3/2	10YR 4/2	50	L	1f sbk	None	---	vfr	ss ps	c s	1m 3f 3vf	---	Too Rooty and granular for pores
		AB	17-27	10YR 3/3	10YR 5/3	40	SL	2 f-m abk	None	---	vfr	ss ps	c s	2m 1f 3vf	2f 3vf	
		B1	27-49	7.5YR 4/4	10YR 5/4	40	SCL	2 m-c abk	None	---	fr	s ps	g s	2m 1f 3vf	2f 1vf	Clasts are weathering heavily, can be broken
		B2	49-74	7.5YR 4/3	10YR 7/4	35	SCL	2 f-m-c abk	None	---	fr	s ps	g s	2m 1f 1vf	3f 3vf	with bare hand
		B3	74-89	7.5YR 5/4	10YR 6/4	50	SCL	2 f-m-c abk	None	---	fr	s ps	c s	1f 1vf	3f 3vf	
		BC	89-100	7.5YR 5/4	10YR 5/4	50	SCL	sg-1 f-m sbk	None	---	lo-vfr	s ps		---	---	
		LGM	SJ08-19													

Location: Cumbres Bog
Date: 6-22-08
11:30
Described: Johnson and Link
UTM: 13S 0370944 / 4097961

Parent Materials: Glacial till including porrly sorted gravels and boulders up to 40 cm in size
General Comments: charcoal sampled @ 32 cm more info in field book
Pit Left Open

Texture	**Structure**	**Structure2**	**Structure3**		**Clayfilr**	**Clayfilms**	**Clayfilms**
C - Clay	1-few	f-fine	abk - angular blocks		1- few	f - faint	co - coats grains
CL - Clay Loam	2-comm	m-medium	sbk - subangular blo		2- comn	d - distinct	pf - ped faces
SiCL - Silty Clay L	3-many	c-coarse	pl - plates		3 - many	p - prominent	br - bridges between grains
SiC - Silty Clay	m-massive						po - pores
L - Loam	sg - sing	**moist consi**	**wet consis**	**Boundaries**		**Roots & Pores**	
SiL - Silty Loam		lo - loose	so - non stick	a - abrupt		1 - few	
SL - Sandy Loam		fr - friable	po - non plas	c - clear		2 - common	--- Data not available
LS - Loamy Sand		fi - firm	ss - slightly st	g - gradual		3 - many	
S - Sand		vfi - very firm	ps - slightly p	d - diffuse		vf - very fine	
		efi - extremel	s - sticky	s - smooth		f - fine	
			p - plastic	w - wavy		m - medium	

APPENDIX F – SOIL SAMPLE PARTICLE SIZE AND ORGANIC CONTENT

Soil samples were examined for particle size using a Sedigraph and for organic content using loss on ignition (Appendix A). The totals for sand, silt, and clay do not always equal 100% when using a Sedigraph so size distributions were recalculated to equal 100% after analyses were complete. Also, since sand >300 microns is removed and weighed before samples are run through the Sedigraph, this sand weight is added back in after analyses were complete to calculate total sand percentage.

Sample ID	Depth (Mid)	LOI	Total Sand % Percentages with >300 um sand added back in	Total Silt %	Total Clay %
Pit 1	GT-1				
A1	10	12.75046	47.59535405	43.63967572	8.764970229
A2	20	12.29918			
ABox	45	9.810334	51.776	41.2096	7.0144
Box	60	5.040742	62.42818121	32.59976786	4.972050926
C1	90	5.209562	64.0911877	29.45679522	6.452017081
C2	105	4.210477	72.89847419	22.79672544	4.304800371
Box_rr			60.13823805	32.41096532	7.450796626
Pit 2	GT-2				
A	7	26.77081	56.53613767	34.22179732	9.24206501
AB	21	12.76511	50.81224852	33.84573416	15.34201732
B	39	22.10984	56.62315264	32.66456023	10.71228712
Box	65	6.115157	51.54804973	39.20539488	9.246555395
AB_rr			34.3179374	44.50778155	21.17428105
AB_rr			24.88262911	0	0
Pit 3	Col-3				
A	10	17.91548	65.49278248	23.23730712	11.2699104
AB1	30	34.48622	62.69337901	25.1731054	12.13351559
AB2	47	14.27644	57.44556182	29.17368435	13.38075382
Box	67	17.04374	51.84266478	38.64280652	9.514528703
B	83	10.84246	47.68452171	45.36059706	6.954881232
C	95	6.707808	63.17573109	30.92809776	5.89617115
Box_rr			17.72986633	63.25617944	19.01395423
Pit 4	AF1-4				
AC	7	10.94538	56.03836071	33.36060398	10.6010353
AB1	22	9.836206	61.52179878	31.5511761	6.927025128
AB2	45	8.4246	59.31506305	27.35193864	13.3329983
AB3	64	7.918005	53.27181022	36.55032895	10.17786083
AB4(ABb?)	77	8.271128	54.79752755	33.6051794	11.59729305
AB5	97	8.241758	51.79294889	37.2455456	10.96150551
Bw1	118	7.998484	47.01553187	42.27484159	10.70962654
Bw2	137	7.808094	49.55317802	39.70914502	10.73767697
AB5_rr			23.00857019	55.6828678	21.30856201

Sample ID	Total %	Sand <300 Silt Clay Percentages recalculated to equal 100%			Sand<300um Silt Sedigraph raw percentages	
Pit 1						
A1	100	8.6	76.1	15.3	8	70.7
A2					0	0
ABox	100	12.0	75.2	12.8	12	75.2
Box	100	20.0	69.4	10.6	20	69.5
C1	100	18.1	67.2	14.7	17.8	66.2
C2	100	22.2	65.4	12.4	20.7	60.9
Box_rr	100	11.8	71.8	16.5	11.4	69.6
					0	0
Pit 2					0	0
A	100	4.7	75.0	20.3	4.9	78.5
AB	100	4.1	66.0	29.9	4.1	65.3
B	100	15.0	64.0	21.0	14.5	61.9
Box	100	18.8	65.7	15.5	18.2	63.6
AB_rr	100	3.6	65.3	31.1	3.5	63.9
AB_rr	24.88263					
Pit 3					0	0
A	100	4.1	64.6	31.3	4	63.3
AB1	100	3.2	65.3	31.5	3.1	63.9
AB2	100	3.8	65.9	30.2	3.7	64.1
Box	100	9.0	73.0	18.0	9	72.7
B	100	14.1	74.4	11.4	14	73.7
C	100	24.3	63.5	12.1	22.1	57.7
Box_rr	100	5.2	72.9	21.9	4.9	68.2
					0	0
Pit 4					0	0
AC	100	15.9	63.8	20.3	16.6	66.4
AB1	100	14.6	70.0	15.4	13.9	66.5
AB2	100	10.4	60.2	29.4	11	63.8
AB3	100	16.6	65.2	18.2	16.6	65
AB4(ABb?)	100	12.3	65.2	22.5	11.8	62.3
AB5	100	14.5	66.0	19.4	13.9	63.2
Bw1	100	16.4	66.7	16.9	14.7	60
Bw2	100	20.3	62.8	17.0	19	58.8
AB5_rr	100	8.6	66.1	25.3	8.3	63.5
					0	0

Sample ID	Clay	Total	300 250 Medium	250 200 Medium to	200 150 to	150 100 to	100 80 Fine
Pit 1							
A1	14.2	92.9	0.2	0.3	0.5	1.6	1.9
A2	0	0					
ABox	12.8	100	0.2	0.2	0.6	2.4	2.9
Box	10.6	100.1	0.3	0.5	1.2	4.2	4.8
C1	14.5	98.5	0.2	0.4	0.8	3.6	4.4
C2	11.5	93.1	0.3	0.4	1	4.3	5.2
Box_rr	16	97	0.2	0.3	0.6	2	2.6
	0	0					
Pit 2	0	0					
A	21.2	104.6	0	0	0	0.6	1.1
AB	29.6	99	0.1	0.1	0.1	0.6	0.9
B	20.3	96.7	0.2	0.2	0.4	2.3	3.7
Box	15	96.8	0.3	0.3	0.8	3.4	4.6
AB_rr	30.4	97.8	0	0	0.1	0.5	0.8
AB_rr							
Pit 3	0	0					
A	30.7	98	0	0.1	0.2	0.8	0.9
AB1	30.8	97.8	0	0	0.1	0.4	0.7
AB2	29.4	97.2	0.1	0.1	0.2	0.6	0.8
Box	17.9	99.6	0.1	0.2	0.3	1.5	2.1
B	11.3	99	0.2	0.2	0.4	1.8	3.4
C	11	90.8	0.4	0.4	0.7	3.6	5.6
Box_rr	20.5	93.6	0.1	0.1	0.2	0.7	1.1
	0	0					
Pit 4	0	0					
AC	21.1	104.1	0.2	0.4	0.7	3	4.1
AB1	14.6	95	0.2	0.3	0.8	2.9	3.3
AB2	31.1	105.9	0.2	0.3	0.6	2.1	2.6
AB3	18.1	99.7	0.2	0.3	0.7	3.2	4.1
AB4(ABb?)	21.5	95.6	0.2	0.3	0.6	2.2	2.8
AB5	18.6	95.7	0.2	0.3	0.7	2.8	3.4
Bw1	15.2	89.9	0.2	0.3	0.7	2.6	3.4
Bw2	15.9	93.7	0.3	0.4	0.8	3.8	4.9
AB5_rr	24.3	96.1	0.1	0.1	0.4	1.6	2
	0	0					

Sample ID	80	60	50	40	30	25	20
	60	50	40	30	25	20	15
	Sand	Silt	Silt	Silt	Silt	Silt	Silt
Pit 1							
A1	3.5	3.1	5.5	10	7.2	8.5	9.5
A2							
ABox	5.7	4.9	7.6	11.7	7.4	8.4	9.6
Box	9	6.7	8.7	11.7	7.2	8.1	8.7
C1	8.4	6.3	8.1	10.3	6.2	7.1	8
C2	9.5	6.5	7.9	9.7	5.6	6.2	6.7
Box_rr	5.7	4.9	6.9	9.8	6.4	7.6	8.7
Pit 2							
A	3.2	3.7	6.5	11	7.8	9.4	10.8
AB	2.3	2.3	3.9	7	5.3	7.2	9.4
B	7.7	5.6	6.9	8.4	4.9	5.8	7.2
Box	8.8	6.3	7.8	9.7	5.7	6.3	7
AB_rr	2.1	2.2	3.8	6.9	5.4	7.2	9
AB_rr							
Pit 3							
A	2	1.9	3.6	7	5.3	6.6	8.4
AB1	1.9	2	3.5	6.4	5	6.8	8.7
AB2	1.9	1.8	3.2	6.2	5	6.7	8.8
Box	4.8	4.2	6.3	9.6	6.4	7.6	9.1
B	8	6.4	8.6	11.2	6.6	7.6	8.9
C	11.4	8.1	9.3	10.1	5.3	5.4	5.5
Box_rr	2.7	2.8	4.6	7.5	5.6	7.3	9.2
Pit 4							
AC	8.2	6.4	8.6	10.5	5.5	6	7
AB1	6.4	5	6.8	9.2	5.9	7	8.2
AB2	5.2	4	5.6	8.1	5.3	6.4	7.9
AB3	8.1	5.9	7.1	9	5.7	6.9	8.1
AB4(ABb?)	5.7	4.3	5.8	8.5	5.7	6.7	7.9
AB5	6.5	4.9	6.6	9.2	5.7	6.6	7.7
Bw1	7.5	5.9	7.4	8.9	5.2	6.1	7.2
Bw2	8.8	6.2	7.5	9	5.2	5.9	6.4
AB5_rr	4.1	3.6	5.3	8	5.4	6.6	7.8

Sample ID	**15**	**10**	**8**	**6**	**5**	**4**	**3**
	10	**8**	**6**	**5**	**4**	**3**	**2**
	Silt	**Silt**	**Silt**	**Silt**	**Silt**	**Clay**	**Clay**
Pit 1							
A1	10.7	5.1	5.2	2.7	3.2	3.5	3.3
A2							
ABox	10.8	4.7	4.9	2.5	2.7	2.9	3
Box	8.8	3.3	3	1.5	1.8	2.2	1.8
C1	8.7	3.7	3.7	1.9	2.2	2.3	2.7
C2	7.4	3.4	3.7	1.8	2	2.5	2.4
Box_rr	10.7	4.9	4.7	2.4	2.6	3	3.1
Pit 2							
A	12.3	5.2	5.4	3	3.4	3.9	3.9
AB	11.3	5.4	6.1	3.5	3.9	4.6	5.6
B	9.3	4.1	4.2	2.5	3	3.5	3.9
Box	8.2	3.8	4.1	2.2	2.5	3.1	3.2
AB_rr	11	5.3	5.8	3.3	4	4.8	5.4
AB_rr							
Pit 3							
A	10.8	5.4	6.3	3.7	4.3	5.1	6.3
AB1	11.1	5.7	6.6	3.7	4.4	5.3	7
AB2	11.5	5.6	6.6	4	4.7	5.3	6.4
Box	11.1	5.3	6.1	3.4	3.6	3.8	4.5
B	10.5	4.6	4.6	2.3	2.4	2.3	2.4
C	6.3	2.7	2.7	1.2	1.1	1.3	2.2
Box_rr	11.1	5.6	6.6	3.7	4.2	5	5.5
Pit 4							
AC	8	3.7	4.7	2.9	3.1	3.3	3.9
AB1	9.8	4.4	4.8	2.6	2.8	3.1	3.3
AB2	10	4.7	5.4	3	3.4	4	4.8
AB3	8.9	3.9	4.4	2.4	2.7	3.1	3.7
AB4(ABb?)	8.9	4	4.7	2.7	3.1	3.6	4.2
AB5	8.7	3.8	4.5	2.6	2.9	3.4	4
Bw1	7.6	3.4	3.9	2.1	2.3	2.7	3.1
Bw2	7.4	3.5	3.7	1.9	2.1	2.6	3
AB5_rr	9.4	4.7	5.5	3.3	3.9	4.5	5

Sample ID	**2 1.5 Clay**	**1.5 1 Clay**	**1 0.8 Clay**	**0.8 0.6 Clay**	**0.6 0.5 Clay**	**0.5 0.4 Clay**	**0.4 0.3 Clay**
Pit 1							
A1	1.9	2.2	0.8	0.7	0.4	0.5	0.9
A2							
ABox	1.7	1.8	0.3	0.1	0.1	0.3	0.9
Box	0.9	1	0.1	0.2	0.5	0.9	1.3
C1	1.7	1.6	0.4	0.4	0.5	0.9	1.5
C2	1.8	2	0.3	0.4	0.5	0.8	0.8
Box_rr	1.3	1.8	0.8	0.7	0.6	0.8	0.8
Pit 2							
A	2.1	2.6	1.3	1.7	1.1	1.4	1.6
AB	3.3	4.1	2.2	2.6	1.5	1.8	2
B	2.2	2.9	1.6	1.7	1	1.5	1.6
Box	1.5	1.9	1.1	1.2	0.7	1	1.2
AB_rr	3.6	5	2.5	2.8	1.5	1.5	1.5
AB_rr							
Pit 3							
A	4.3	5.4	2.3	2.4	1.2	1.3	1.3
AB1	4.3	5	2.4	2.4	1.2	1.4	1.5
AB2	4	4.5	2.1	2.2	1.1	1.2	1.2
Box	2.4	2.2	0.9	0.9	0.4	0.4	0.6
B	1.4	1.3	0.3	0.2	0.1	0.3	0.6
C	1.3	1.4	0.7	0.6	0.2	0.2	0.8
Box_rr	2.8	3	1.3	1.2	0.6	0.6	0.5
Pit 4							
AC	2.4	2.5	1.3	1.6	0.8	0.6	0.9
AB1	2	2	1.1	1.6	0.7	0.4	0.4
AB2	3.4	5.6	3.1	3.4	1.6	1.3	1.4
AB3	2	2.3	1.4	1.7	0.7	0.5	0.7
AB4(ABb?)	2.5	2.6	1.5	2	1	0.8	0.9
AB5	2.2	2.4	1.3	1.6	0.8	0.6	0.7
Bw1	1.9	2.2	1.2	1.4	0.7	0.5	0.6
Bw2	1.5	1.8	1.1	1.4	0.6	0.5	0.9
AB5_rr	2.8	3.5	1.7	1.9	1.1	1.2	1.3

Sample ID	0.3 0.2 Clay	Total	Measured Original Wt.	Measured < 300um Wt.	>300um
Pit 1					
A1	0	92.9	10.01	5.74	4.27
A2		0	10.01	5.7	4.31
ABox	1.7	100	10	5.48	4.52
Box	1.7	100.1	10.01	4.7	5.31
C1	2.5	98.5	14.99	6.57	8.42
C2	0	93.1	18.02	6.28	11.74
Box_rr	3.1	97	10.56	4.77	5.79
		0			0
					0
Pit 2		0			0
A	1.6	104.6	10	4.56	5.44
AB	1.9	99	13.33	6.84	6.49
B	0.4	96.7	12.64	6.45	6.19
Box	0.1	96.8	12.77	7.62	5.15
AB_rr	1.8	97.8	11.01	7.5	3.51
AB_rr		0	10.65	8	2.65
					0
					0
Pit 3		0			0
A	1.1	98	16.4	5.9	10.5
AB1	0.3	97.8	15.08	5.81	9.27
AB2	1.4	97.2	15.1	6.68	8.42
Box	1.8	99.6	14.62	7.74	6.88
B	2.4	99	14.59	8.89	5.7
C	2.3	90.8	15.04	7.32	7.72
Box_rr	0	93.6	12.59	10.93	1.66
					0
		0			0
Pit 4		0			0
AC	3.8	104.1	15.64	8.18	7.46
AB1	0	95	15.73	7.09	8.64
AB2	2.5	105.9	15.22	6.91	8.31
AB3	2	99.7	15.34	8.6	6.74
AB4(ABb?)	2.4	95.6	15.63	8.06	7.57
AB5	1.6	95.7	15.55	8.77	6.78
Bw1	0.9	89.9	15.74	9.97	5.77
Bw2	2.5	93.7	14.46	9.15	5.31
AB5_rr	1.3	96.1	11.57	9.75	1.82
					0
		0			0

Sample ID	Depth (Mid)	LOI	Total Sand % Percentages with >300 um sand added back in	Total Silt %	Total Clay %
Pit 5	AF2-5				
ABw1	13	8.928711	56.90553946	33.71873256	9.37572798
ABw2	26	8.051011	65.07270873	27.69269458	7.234596682
Bw	47	7.394991	48.24291242	43.13090631	8.626181263
ABb	65	8.305648	40.59398406	49.02203754	10.3839784
C	87	6.682169	55.6805254	36.63401658	7.685458024
Bw_rr					0
Pit 6	Qt2-6				
Aw	6	40.18493	41.02839374	53.23825565	5.733350609
AB	17	5.342261	42.5656387	50.24354239	7.190818911
Ab	23	14.75396	38.49402711	55.66462351	5.84134938
ABb	31	7.023294	51.92231006	42.56057798	5.517111961
B	51	10.79575	30.23976801	61.54163523	8.218596756
C	72	5.424852	62.20249967	30.90970283	6.8877975
Pit 7	Qt1-7				
A	5	16.19695	15.67046958	63.15548528	21.17404514
AB	15	23.70816	17.18838402	63.5570633	19.25455269
B1	31	19.86622	49.09196738	46.69357	4.214462621
B2	49	10.7214	66.22367381	30.33286265	3.443463539
BC1	72	6.578947	67.84125802	30.32725583	1.831486143
BC2	87	9.384224			
AB-rr			17.88024303	61.88983772	20.22991925
Pit 8	GT-8				
A	7	22.47539	19.25258004	71.58958825	9.157831707
AB1	28	18.01522	17.51571129	72.39361815	10.09067056
AB2	41	17.06008	13.40241423	71.18533469	15.41225108
B	60	16.87359	35.82278481	55.65017261	8.527042578
Bw	72	6.191184	61.65442561	35.01765537	3.327919021
C (R?)	85	6.072383	71.87052126	25.68010917	2.449369578
AB1_rr			13.99566229	69.97868472	16.02565299
Pit 9	Qt2-9				
A	2.5	8.417213	60.72713091	35.93838021	3.334488885
Aw	18	4.160918	64.21474867	32.48763432	3.297617017

Sample ID	Total %	Sand <300 Silt Clay Percentages recalculated to equal 100%			Sand<300um Silt Sedigraph raw percentages	
Pit 5					0	0
ABw1	100	19.3	63.1	17.5	18.3	59.7
ABw2	100	20.0	63.4	16.6	18.2	57.8
Bw	100	28.4	59.7	11.9	27.6	58
ABb	100	19.8	66.2	14.0	18.2	60.9
C	100	29.0	58.7	12.3	28.2	57.2
Bw_rr					0	0
					0	0
					0	0
Pit 6					0	0
Aw	100	28.6	64.4	6.9	26	58.5
AB	100	33.1	58.5	8.4	30.8	54.5
Ab	100	17.5	74.7	7.8	15.2	64.8
ABb	100	23.6	67.6	8.8	22.6	64.8
B	100	26.0	65.2	8.7	25.1	62.9
C	100	27.8	59.0	13.2	25.6	54.3
					0	0
					0	0
Pit 7					0	0
A	100	2.6	72.9	24.4	2.5	68.9
AB	100	3.8	73.9	22.4	3.8	74.6
B1	100	16.9	76.2	6.9	15.5	69.8
B2	100	24.8	67.5	7.7	22	59.9
BC1	100	33.5	62.7	3.8	30.1	56.3
BC2					0	0
AB-rr	100	3.7	72.6	23.7	3.7	72.2
					0	0
Pit 8					0	0
A	100	6.3	83.0	10.6	6.2	81.3
AB1	100	5.6	82.8	11.5	5.3	78.2
AB2	100	2.5	80.2	17.4	2.3	73.9
B	100	13.3	75.2	11.5	13.2	74.4
Bw	100	18.2	74.7	7.1	17.2	70.5
C (R?)	100	22.3	70.9	6.8	21.1	67.1
AB1_rr	100	2.8	79.1	18.1	2.8	78.6
					0	0
Pit 9					0	0
A	100	38.5	56.3	5.2	39.8	58.2
Aw	100	41.5	53.1	5.4	41.5	53.2

Sample ID	Clay	Total	300 250 Medium	250 200 Medium to	200 150 to	150 100 to	100 80 Fine
Pit 5	0	0					
ABw1	16.6	94.6	0.2	0.4	0.8	3.5	4.6
ABw2	15.1	91.1	0.3	0.4	0.9	3.5	4.5
Bw	11.6	97.2	0.5	0.7	1.5	5.9	7
ABb	12.9	92	0.3	0.4	0.9	3.4	4.5
C	12	97.4	0.5	0.7	1.6	6.1	7.1
Bw_rr	0	0					
	0	0					
	0	0					
Pit 6	0	0					
Aw	6.3	90.8	0.3	1.2	4.2	5.1	9
AB	7.8	93.1	0.5	0.7	1.6	6.8	8
Ab	6.8	86.8	0.3	0.3	0.7	2.6	3.7
ABb	8.4	95.8	0.3	0.4	0.9	4.3	5.8
B	8.4	96.4	0.4	0.6	1.4	5.1	6
C	12.1	92	0.4	0.6	1.4	6.1	6.7
	0	0					
	0	0					
Pit 7	0	0					
A	23.1	94.5	0.1	0.1	0.2	0.5	0.5
AB	22.6	101	0	0	0.1	0.6	0.9
B1	6.3	91.6	0.2	0.3	0.8	3.6	4.1
B2	6.8	88.7	0.3	0.5	1.2	5.1	5.6
BC1	3.4	89.8	0.5	0.8	2	6.9	7.3
BC2	0	0	Missing?				
AB-rr	23.6	99.5	0	0	0.1	0.6	0.9
	0	0					
Pit 8	0	0					
A	10.4	97.9	0.1	0.1	0.3	1.1	1.5
AB1	10.9	94.4	0	0.2	0.6	0.8	1.9
AB2	16	92.2	0	0.1	0.2	0.5	0.4
B	11.4	99	0.3	0.4	0.7	2.5	3.1
Bw	6.7	94.4	0.3	0.4	0.8	3.2	4.2
C (R?)	6.4	94.6	0.3	0.4	0.6	3.3	5.5
AB1_rr	18	99.4	0	0	0.1	0.4	0.6
	0	0					
Pit 9	0	0					
A	5.4	103.4	0.7	4.5	6	11.4	7.8
Aw	5.4	100.1	1	1.4	3.2	10.6	10.3

Sample ID	80	60	50	40	30	25	20
	60	50	40	30	25	20	15
	Sand	Silt	Silt	Silt	Silt	Silt	Silt
Pit 5							
ABw1	8.8	6.2	7.1	8.5	5.4	6.5	7
ABw2	8.6	6.2	7.8	9.6	5.3	5.7	6.3
Bw	12	7.6	8.4	9.5	5.3	5.8	6.3
ABb	8.7	6.1	7.5	9.3	5.4	6	7
C	12.2	7.9	8.5	8.8	4.7	5.5	6.3
Bw_rr							
Pit 6							
Aw	6.2	8	10.9	6.6	7.3	7.7	7.5
AB	13.2	8	8.5	9.2	4.9	5.2	5.7
Ab	7.6	5.6	7	9.4	5.9	6.9	8.3
ABb	10.9	7.5	8.8	10	5.5	6.2	7.4
B	11.6	8	9.1	10.2	5.5	5.8	6.4
C	10.4	6.4	7.3	8.9	5.2	5.4	5.9
Pit 7							
A	1.1	1.4	3.4	7.9	6.6	8.7	10.6
AB	2.2	2.3	4.1	7.7	6.3	8.6	10.9
B1	6.5	4.5	6.4	9.9	6.7	8.3	10.2
B2	9.3	6.4	7.9	9.3	5.4	6.4	7.3
BC1	12.6	8.6	9.8	10.5	5.5	5.7	5.5
BC2							
AB-rr	2.1	2	3.6	7.1	5.8	8	10.5
Pit 8							
A	3.1	2.5	3.9	8.5	8.7	13.3	16.4
AB1	1.8	3.4	7.5	6.6	9.3	11.8	14.2
AB2	1.1	1.4	3.2	7.5	6.1	8.2	11.3
B	6.2	4.7	6.5	9.4	6.2	7.8	10.1
Bw	8.3	6.2	7.8	10.3	6.5	7.5	8.6
C (R?)	11	7.6	8.7	10.2	5.8	6.6	7.8
AB1_rr	1.7	1.9	3.8	7.7	6.3	8.8	11.9
Pit 9							
A	9.4	11.7	6.7	7.1	7.1	7.6	3.9
Aw	15	8.4	8.5	8.9	4.8	5.2	5.4

Sample ID	**15**	**10**	**8**	**6**	**5**	**4**	**3**
	10	**8**	**6**	**5**	**4**	**3**	**2**
	Silt	**Silt**	**Silt**	**Silt**	**Silt**	**Clay**	**Clay**
Pit 5							
ABw1	6.8	3.2	4	2.4	2.6	3	3.3
ABw2	6.8	2.8	3.3	1.9	2.1	2.4	3.1
Bw	6.4	2.7	2.9	1.5	1.6	1.6	2.2
ABb	8.1	3.6	3.8	2	2.1	2.3	2.8
C	6.4	2.7	3.1	1.6	1.7	1.8	2
Bw_rr							
Pit 6							
Aw	2.8	2.9	1.6	1.6	1.6	1.9	1
AB	5.9	2.3	2.4	1.2	1.2	1.2	1.5
Ab	9.5	4	4.1	2.1	2	1.7	1.6
ABb	8.5	3.5	3.7	1.9	1.8	1.8	2
B	7.7	3.3	3.4	1.7	1.8	1.9	1.8
C	6.7	2.5	2.8	1.6	1.6	1.8	2
Pit 7							
A	12.2	5.2	5.7	3.3	3.9	4.6	5.3
AB	13.6	6.4	6.9	3.7	4.1	4.7	5.4
B1	11.3	4.3	4.2	2	2	2.1	1.7
B2	7.6	3.2	3.3	1.6	1.5	1.7	1.8
BC1	5.3	2	1.7	0.8	0.9	1.1	1
BC2							
AB-rr	13.2	6.3	7.2	4.1	4.4	5	6.1
Pit 8							
A	13.8	4.3	4.5	2.6	2.8	3.1	3
AB1	6.5	6.9	3.7	4	4.3	4.3	2.1
AB2	14.2	6.4	7.3	4	4.3	4.5	4.5
B	12.4	5.4	5.8	3	3.1	3.3	3.4
Bw	10.2	4.5	4.5	2.2	2.2	2	1.9
C (R?)	9.2	3.8	3.7	1.8	1.9	2.1	1.8
AB1_rr	15.1	6.9	7.5	4.2	4.5	4.8	4.9
Pit 9							
A	4.2	2	2	2.4	3.5	1.6	1.6
Aw	4.6	2	2.8	1.4	1.2	1.1	1.5

Sample ID	**2**	**1.5**	**1**	**0.8**	**0.6**	**0.5**	**0.4**
	1.5	**1**	**0.8**	**0.6**	**0.5**	**0.4**	**0.3**
	Clay	**Clay**	**Clay**	**Clay**	**Clay**	**Clay**	**Clay**
Pit 5							
ABw1	1.9	2.4	1	1	0.7	1	0.9
ABw2	1.9	2.4	1.1	1.1	0.7	0.9	0.8
Bw	1.4	1.5	0.8	0.9	0.6	0.9	1
ABb	1.4	1.9	1.1	1.2	0.6	0.7	0.8
C	1.5	1.7	0.8	1	0.6	0.8	0.9
Bw_rr							
Pit 6							
Aw	0.8	0.4	0.4	0.2	0.3	0.5	0.8
AB	0.9	1.2	0.4	0.3	0.1	0.2	0.3
Ab	1	1	0.3	0.3	0.2	0.4	0.3
ABb	1.1	1.2	0.4	0.3	0.2	0.3	0.4
B	1.1	1.2	0.4	0.5	0.3	0.3	0.4
C	1.2	1.9	0.8	0.8	0.8	1.3	1.5
Pit 7							
A	3.1	3.4	1.3	1.2	0.8	1.1	1.1
AB	2.9	2.9	1.1	1.4	1	1.1	0.9
B1	0.8	0.9	0.5	0.3	0	0	0
B2	0.8	0.5	0.3	0.4	0.1	0.1	0.3
BC1	0.5	0.3	0.1	0	0	0	0.1
BC2							
AB-rr	3.6	3.7	1.5	1.5	0.6	0.7	0.8
Pit 8							
A	1.3	1.3	0.5	0	0	0	0.1
AB1	2.1	0.8	0.7	0.3	0.2	0.2	0.2
AB2	2	2.2	0.8	0.6	0.3	0.3	0.3
B	1.7	1.4	0.4	0.3	0.1	0.1	0.2
Bw	1	1	0.4	0.3	0.1	0	0
C (R?)	0.8	0.8	0.4	0.4	0.1	0	0
AB1_rr	2.6	2.8	1	0.7	0.2	0.2	0.4
Pit 9							
A	0.7	1	0.5	0	0	0	
Aw	1	1.5	0.3	0	0	0	0

Sample ID	0.3 0.2 Clay	Total	Measured Original Wt.	Measured < 300um Wt.	>300um
Pit 5		0			0
ABw1	1.4	94.6	14.43	7.71	6.72
ABw2	0.7	91.1	15.19	6.63	8.56
Bw	0.7	97.2	14.07	10.17	3.9
ABb	0.1	92	14.57	10.79	3.78
C	0.9	97.4	14.62	9.12	5.5
Bw_rr		0	11.2	7.65	3.55
		0			0
		0			0
Pit 6		0			0
Aw		90.8	10.71	8.85	1.86
AB	1.7	93.1	11.22	9.63	1.59
Ab	0	86.8	10.3	7.68	2.62
ABb	0.7	95.8	10.68	6.72	3.96
B	0.5	96.4	10.56	9.96	0.6
C	0	92	13.08	6.85	6.23
		0			0
		0			0
Pit 7		0			0
A	1.2	94.5	10.24	8.87	1.37
AB	1.2	101	8.96	7.71	1.25
B1	0	91.6	12.06	7.39	4.67
B2	0.8	88.7	15.05	6.76	8.29
BC1	0.3	89.8	13.52	6.54	6.98
BC2		0	12.94	6.43	6.51
AB-rr	0.1	99.5	10.81	9.22	1.59
					0
		0			0
Pit 8		0			0
A	1.1	97.9	9.86	8.5	1.36
AB1		94.4	8.01	7	1.01
AB2	0.5	92.2	7.33	6.51	0.82
B	0.5	99	9.48	7.02	2.46
Bw	0	94.4	13.5	6.33	7.17
C (R?)	0	94.6	16.02	5.8	10.22
AB1_rr	0.4	99.4	10.78	9.54	1.24
					0
		0			0
Pit 9		0			0
A		103.4	9.82	6.27	3.55
Aw	0	100.1	13.12	8.02	5.1

Sample ID	Depth (Mid)	LOI	Total Sand % Percentages with >300 um sand added back in	Total Silt %	Total Clay %
B1	34	8.197429	24.58199581	63.56523801	11.85276618
B2	45	20.74312	22.51739405	65.70524984	11.7773561
B3	74		29.8186804	60.34649342	9.834826177
B1_rr			22.15990981	66.9873853	10.85270488
Pit 10	AF2-10				
Aw	3.5	14.84047	35.68713836	56.4336943	7.879167343
Bw	14	26.01193	44.72104044	46.76528032	8.513679238
Ab	31 -		26.24124497	58.52257152	15.23618351
Bb1	48	20.72002	26.96756194	53.67444243	19.35799563
Bb2(Ab2?)	71	11.77541	25.5525908	54.49901445	19.94839475
Bb3	97	11.56039	25.74636552	54.92180589	19.33182858
Bb4	120	12.13282	21.85959497	59.85402639	18.28637864
Ab_rr			31.0450984	51.90074499	17.05415661
Ab_rr2			26.37585388	54.81623107	18.80791506
Pit 11	AF1-11				
O	0.5	73.93955			
A	5	14.02847	31.41442996	53.00162986	15.58394017
AB	13	13.45699	28.46436338	60.15496716	11.38066946
Box	24	6.182812	40.82584506	47.26626944	11.9078855
B1(Ab?)	37	6.394853	54.49989391	34.77106873	10.72903736
B2 (Bb?) - 1	57	9.777198	26.24664396	56.50886632	17.24448972
B2 (Bb?) - 2	71	23.47911	23.96118822	56.95120022	19.08761156
Box_rr			40.90281197	44.71302746	14.38416058
Pit 12	Qt2-12				
A	5	16.89561			
AB	17	13.92915	21.7676761	66.32740504	11.90491885
B	35	12.58343	22.69499184	66.23711052	11.06789764
Ab	50	4.212103	17.07164421	74.18452249	8.743833297
Bb1	75	19.00405	72.04157461	25.83966498	2.118760408
Bb2	107	14.51298	10.04065344	75.22132595	14.73802061
Pit 13	LGM-13				
A	9	10.75493	33.62229538	50.38837908	15.98932553
B1	26	6.581892	58.42408878	22.52881889	19.04709233

Sample ID	Total %	Sand <300 Silt Clay Percentages recalculated to equal 100%			Sand<300um Silt Sedigraph raw percentages	
B1	100	17.6	69.5	13.0	16.8	66.5
B2	100	14.2	72.7	13.0	14.5	74.2
B3	100	13.8	74.1	12.1	14.3	76.7
B1_rr	100	15.7	72.5	11.8	15.5	71.6
					0	0
Pit 10					0	0
Aw	100	10.9	78.2	10.9	11.7	83.8
Bw	100	10.3	75.9	13.8	10.6	78
Ab	100	6.1	74.5	19.4	6.1	74.9
Bb1	100	6.0	69.1	24.9	5.8	67.1
Bb2(Ab2?)	100	4.7	69.8	25.5	4.6	68.3
Bb3	100	5.6	69.9	24.6	5.4	67.9
Bb4	100	6.1	71.9	22.0	6	70.7
Ab_rr	100	6.7	70.2	23.1	6.7	70.3
Ab_rr2	100	4.8	70.9	24.3	4.6	68.2
Pit 11					0	0
O					0	0
A	100	17.9	63.5	18.7	18.4	65.3
AB	100	9.9	75.8	14.3	9.2	70.3
Box	100	11.9	70.4	17.7	10.9	64.7
B1(Ab?)	100	12.6	66.8	20.6	11.7	61.9
B2 (Bb?) - 1	100	10.6	68.5	20.9	9.9	63.9
B2 (Bb?) - 2	100	5.3	70.9	23.8	5.5	73.1
Box_rr	100	9.7	68.3	22.0	9.4	65.9
					0	0
Pit 12					0	0
A					0	0
AB	100	8.9	77.2	13.9	9	78
B	100	8.1	78.7	13.2	8	77.8
Ab	100	10.4	80.1	9.4	10.5	80.6
Bb1	100	36.4	58.8	4.8	34.7	56.1
Bb2	100	7.2	77.6	15.2	7.3	78.6
					0	0
					0	0
Pit 13					0	0
A	100	8.2	69.7	22.1	8.1	68.7
B1	100	9.7	48.9	41.4	8.7	44

Sample ID	Clay	Total	300 250 Medium	250 200 Medium to	200 150 to	150 100 to	100 80 Fine
B1	12.4	95.7	0.2	0.3	0.8	3.2	4
B2	13.3	102	0.2	0.3	0.6	2.6	3.6
B3	12.5	103.5	0.1	0.2	0.6	2.7	3.5
B1_rr	11.6	98.7	0.2	0.3	0.6	2.6	3.7
	0	0					
Pit 10	0	0					
Aw	11.7	107.2	0.2	0.3	0.6	2	2.7
Bw	14.2	102.8	0.2	0.2	0.4	1.5	2.5
Ab	19.5	100.5	0.1	0.1	0.3	1	1.3
Bb1	24.2	97.1	0.1	0.1	0.2	0.9	1.3
Bb2(Ab2?)	25	97.9	0	0.1	0.1	0.7	1
Bb3	23.9	97.2	0.1	0.1	0.2	0.8	1.2
Bb4	21.6	98.3	0.1	0.1	0.2	0.9	1.3
Ab_rr	23.1	100.1	0.1	0.1	0.2	1	1.6
Ab_rr2	23.4	96.2	0.1	0.1	0.2	0.6	1
Pit 11	0	0					
O	0	0					
A	19.2	102.9	0.2	0.4	0.7	3.2	4.6
AB	13.3	92.8	0.1	0.1	0.3	1.4	2.1
Box	16.3	91.9	0.1	0.2	0.5	2.2	2.6
B1(Ab?)	19.1	92.7	0.2	0.3	0.6	2.2	2.7
B2 (Bb?) - 1	19.5	93.3	0	0.3	0.5	1.8	2.2
B2 (Bb?) - 2	24.5	103.1	0	0	0.1	0.8	1.3
Box_rr	21.2	96.5	0.1	0.2	0.4	1.7	2.3
	0	0					
Pit 12	0	0					
A	0	0					
AB	14	101	0.1	0.1	0.3	1.6	2.2
B	13	98.8	0.1	0.2	0.3	1.2	1.8
Ab	9.5	100.6	0.2	0.2	0.5	1.7	2.4
Bb1	4.6	95.4	0.9	1.2	2.4	8.2	8.8
Bb2	15.4	101.3	0.1	0.2	0.3	1.5	1.9
	0	0					
	0	0					
Pit 13	0	0					
A	21.8	98.6	0.1	0.2	0.3	1.5	2
B1	37.2	89.9	0.1	0.1	0.3	1.6	2.2

Sample ID	80 60 Sand	60 50 Silt	50 40 Silt	40 30 Silt	30 25 Silt	25 20 Silt	20 15 Silt
B1	8.3	6.5	8.4	10.3	5.9	6.6	7.6
B2	7.2	5.5	7.3	10	6.5	8	9.7
B3	7.2	5.6	7.4	10	6.6	8.2	9.9
B1_rr	8.1	6.5	8.5	10.9	6.5	7.3	8.4
Pit 10							
Aw	5.9	5.1	7.6	12.3	9.1	11.5	12.8
Bw	5.8	4.9	7.1	11	7.8	9.5	10.8
Ab	3.3	3.2	5.1	8.7	6.7	8.8	10.9
Bb1	3.2	3	4.7	7.8	5.5	6.9	8.7
Bb2(Ab2?)	2.7	2.7	4.5	7.8	5.7	7.3	9.2
Bb3	3	2.9	4.6	7.7	5.7	7.2	8.9
Bb4	3.4	3.2	4.9	7.6	5.5	7.2	9.3
Ab_rr	3.7	3.3	4.9	7.9	5.9	7.9	10.1
Ab_rr2	2.6	2.5	4.1	7.2	5.7	7.7	10
Pit 11							
O							
A	9.3	7.1	9.2	11.3	6.3	6.8	7
AB	5.2	4.7	6.9	10.3	6.8	8	8.9
Box	5.3	4.2	6	8.8	5.7	6.8	8.1
B1(Ab?)	5.7	4.7	6.3	8.4	5.1	5.9	7.3
B2 (Bb?) - 1	5.1	4.5	6.4	8.9	5.5	6.3	7.5
B2 (Bb?) - 2	3.3	3.2	5.3	8.5	5.7	6.8	8.6
Box_rr	4.7	3.9	5.6	8	5.3	6.6	8.3
Pit 12							
A							
AB	4.7	4	6.3	9.9	6.8	8.4	10.5
B	4.4	4.2	6.6	10.4	7	8.7	10.7
Ab	5.5	4.7	6.9	10.5	7.3	9.3	11.6
Bb1	13.2	7.7	8.6	9.9	5.4	5.9	6.8
Bb2	3.3	2.5	4.1	8.7	7.9	11	13
Pit 13							
A	4	3.5	5.7	9.4	6.4	7.7	9
B1	4.4	3.4	4.5	6.1	3.7	4.2	5.1

Sample ID	**15**	**10**	**8**	**6**	**5**	**4**	**3**
	10	**8**	**6**	**5**	**4**	**3**	**2**
	Silt	**Silt**	**Silt**	**Silt**	**Silt**	**Clay**	**Clay**
B1	8.7	4	4.2	2.1	2.2	2.5	3.1
B2	11	4.9	5.4	2.9	3	3.3	3.8
B3	11.7	5.3	5.9	3.1	3	3.1	3.6
B1_rr	9.4	4.3	4.7	2.5	2.6	2.9	3.1
Pit 10							
Aw	11.3	4	4.8	2.7	2.6	2.8	3.2
Bw	11.2	4.6	5.1	2.9	3.1	3.1	3.5
Ab	12.8	5.6	6	3.4	3.7	3.9	4.4
Bb1	11.3	5.4	6	3.6	4.2	4.5	5.4
Bb2(Ab2?)	11.5	5.5	6.2	3.7	4.2	4.5	5.1
Bb3	11.3	5.5	6.2	3.7	4.2	4.8	5.2
Bb4	12.1	5.9	6.8	3.9	4.3	4.6	5
Ab_rr	12	5.4	6.1	3.3	3.5	3.9	4.6
Ab_rr2	12.2	5.6	6.1	3.4	3.7	4.3	4.8
Pit 11							
O							
A	7.3	3.1	3.2	1.9	2.1	2.2	2.3
AB	9.9	4.4	4.9	2.7	2.8	2.5	2.9
Box	9.6	4.4	5	2.9	3.2	3.5	3.7
B1(Ab?)	9.2	4.2	4.8	2.8	3.2	3.5	4
B2 (Bb?) - 1	9.3	4.3	5	3	3.2	3.4	3.8
B2 (Bb?) - 2	11.4	5.3	5.9	4.4	8	12.3	8.3
Box_rr	10.3	5	5.8	3.3	3.8	4.3	4.9
Pit 12							
A							
AB	12.9	5.9	6.3	3.4	3.6	3.9	3.6
B	12.5	5.6	5.9	3	3.2	3.5	3.2
Ab	13.6	5.5	5.5	2.9	2.8	2.6	2.2
Bb1	6.5	2	1.8	0.8	0.7	1.2	1.1
Bb2	13.8	5.8	5.8	2.9	3.1	3.7	3.7
Pit 13							
A	10.3	4.6	5.3	3.2	3.6	4.1	4.3
B1	6.5	2.8	3.3	2	2.4	3.3	4.9

Sample ID	**2**	**1.5**	**1**	**0.8**	**0.6**	**0.5**	**0.4**
	1.5	**1**	**0.8**	**0.6**	**0.5**	**0.4**	**0.3**
	Clay	**Clay**	**Clay**	**Clay**	**Clay**	**Clay**	**Clay**
B1	2	2.1	0.6	0.5	0.2	0.2	0.3
B2	1.7	1.6	0.8	0.9	0.3	0.1	0
B3	1.6	1.5	0.8	0.8	0.4	0.2	0
B1_rr	1.8	1.5	0.5	0.6	0.3	0.4	0.5
Pit 10							
Aw	1.6	1.6	0.8	0.9	0.5	0.3	0
Bw	2	2.1	1	1	0.5	0.6	0.4
Ab	2.4	2.9	1.5	1.7	0.9	0.9	0.9
Bb1	3.2	3.6	1.5	1.7	1	1	1.1
Bb2(Ab2?)	3.2	3.7	1.5	1.9	1.2	1.2	1.1
Bb3	3	3.7	1.6	1.7	0.9	1	1.2
Bb4	2.7	2.9	1.3	1.3	0.7	0.7	0.8
Ab_rr	2.7	3.2	1.6	1.8	0.9	0.9	1.2
Ab_rr2	2.9	3.5	1.6	2	1	1	1.2
Pit 11							
O							
A	1.2	1.2	0	0	0	3.4	6.8
AB	1.7	1.6	0.7	1.1	0.8	0.9	0.8
Box	2	2.6	1.1	1.1	0.7	0.8	0.7
B1(Ab?)	2.4	2.7	1.2	1.5	0.9	0.9	0.8
B2 (Bb?) - 1	2.2	2.6	1.2	1.6	1	1.1	1.1
B2 (Bb?) - 2	1	0.3	0.1	0.4	0.3	0.4	0.6
Box_rr	2.8	2.9	1.2	1.4	0.8	0.8	0.8
Pit 12							
A							
AB	1.8	2	0.7	0.5	0.2	0.5	0.8
B	1.4	1.7	0.8	0.7	0.3	0.4	0.6
Ab	1	1.2	0.5	0.7	0.4	0.5	0.4
Bb1	0.1	0	0	0.6	0.8	0.8	0
Bb2	1.7	2	1	1	0.5	0.6	0.7
Pit 13							
A	2.6	3.4	1.6	1.9	1	1.1	1.3
B1	3.5	5.4	3.1	3.9	2.5	2.9	3.3

Sample ID	0.3 0.2 Clay	Total	Measured Original Wt.	Measured < 300um Wt.	>300um
B1	0.9	95.7	8.33	7.62	0.71
B2	0.8	102	7.75	7	0.75
B3	0.5	103.5	7.54	6.14	1.4
B1_rr	0	98.7	11.36	10.49	0.87
					0
		0			0
Pit 10		0			0
Aw	0	107.2	11.04	7.97	3.07
Bw	0	102.8	12.85	7.92	4.93
Ab	0	100.5	9.22	7.24	1.98
Bb1	1.2	97.1	9.45	7.34	2.11
Bb2(Ab2?)	1.6	97.9	8.82	6.89	1.93
Bb3	0.8	97.2	8.56	6.73	1.83
Bb4	1.6	98.3	8.82	7.34	1.48
Ab_rr	2.3	100.1	11.15	8.24	2.91
Ab_rr2	1.1	96.2	11.2	8.66	2.54
					0
					0
Pit 11		0			0
O		0	8.07	5.34	2.73
A	2.1	102.9	8.92	7.45	1.47
AB	0.3	92.8	7.77	6.17	1.6
Box	0.1	91.9	9.92	6.66	3.26
B1(Ab?)	1.2	92.7	13.27	6.91	6.36
B2 (Bb?) - 1	1.5	93.3	9.09	7.5	1.59
B2 (Bb?) - 2	0.8	103.1	8.03	6.45	1.58
Box_rr	1.3	96.5	10.63	6.96	3.67
					0
		0			0
Pit 12		0			0
A		100.6	7.44	6.25	1.19
AB	0	101	7.51	6.45	1.06
B	0.4	98.8	7.24	6.09	1.15
Ab	0	100.6	7.56	7	0.56
Bb1	0	95.4	16.34	7.18	9.16
Bb2	0.5	101.3	7.53	7.3	0.23
		0			0
		0			0
Pit 13		0			0
A	0.5	98.6	9.79	7.08	2.71
B1	4.4	89.9	12.47	5.74	6.73

Sample ID	Depth (Mid)	LOI	Total Sand % Percentages with >300 um sand added back in	Total Silt %	Total Clay %
B2	42	6.265044	54.0884935	22.74006161	23.17144489
B3	65	6.711955	62.6443465	25.75946722	11.59618627
BC	97	11.02536	77.15449374	6.884186576	15.96131968
C	137	4.235045	88.01468627	3.580228333	8.4050854
Pit 14	Col-14				
A	8	12.92333	28.46601918	53.57502783	17.95895299
AB	21	10.18584	43.37125831	39.59754118	17.03120051
B1	33	8.265601	46.35606597	34.83908243	18.8048516
B2	47	9.641394	55.82846895	29.34820194	14.82332911
BC1	72	8.224396	58.23538981	30.43942413	11.32518606
BC2	105	5.149331			
B2_rr			40.31003889	37.66976664	22.02019447
Pit 15	AF2-15				
A	6	19.3836	19.36676915	66.44105906	14.1921718
AB	20	17.73783	19.38538135	66.38321111	14.23140754
B1	34	12.76053	26.41319472	59.7322433	13.85456199
B2	49	11.86913	33.24762037	55.29057795	11.46180169
BC1	64	6.468106			
BC2	75	5.0164	53.26657062	42.77812611	3.955303268
BC2_rr			57.00690844	38.19475545	4.798336112
Pit 16	AF2-16				
A	4	47.29375			
Aboxw	13	6.439316	55.11236573	37.25242625	7.635208025
Abw	24	4.505885			
C1 - 1	39	3.684448	56.95115109	35.24658605	7.802262857
C1 - 2	49	2.765028	68.21862348	26.51697673	5.264399791
C2 - 1	62	4.730958	54.89580221	37.23403091	7.870166882
C2 - 2	75	3.498134			
Pit 17	GT-17				
AB	8	14.36571	32.59391068	57.53824417	9.867845154
B1		12.78437			
B2	37	10.71603	34.07516404	56.58845378	9.336382173
B3	52	10.69222	35.48419657	54.12588079	10.38992264
B4	73	8.622254	40.58332459	49.04337738	10.37329803

Sample ID	Total %	Sand <300 Silt Clay Percentages recalculated to equal 100%			Sand<300um Silt Sedigraph raw percentages	
B2	100	10.5	44.4	45.2	8.7	36.9
B3	100	12.0	60.7	27.3	11.5	58.2
BC	100	6.4	28.2	65.4	5.6	24.8
C	100	8.0	27.5	64.5	6.8	23.3
					0	0
					0	0
Pit 14					0	0
A	100	7.1	69.5	23.3	7.3	71
AB	100	5.1	66.4	28.5	5	65.1
B1	100	5.9	61.1	33.0	5.7	59.1
B2	100	5.9	62.5	31.6	5.6	59
BC1	100	6.8	67.9	25.3	6.4	63.7
BC2					0	0
B2_rr	100	5.0	60.0	35.1	4.5	54.4
					0	0
Pit 15					0	0
A	100	4.1	79.0	16.9	3.8	73.5
AB	100	4.3	78.8	16.9	4	73.7
B1	100	5.3	76.8	17.8	5	72
B2	100	6.2	77.7	16.1	6.1	76.7
BC1					0	0
BC2	100	15.3	77.5	7.2	13.9	70.3
BC2_rr	100	18.9	72.0	9.0	15.7	59.7
					0	0
Pit 16					0	0
A					0	0
Aboxw	100	27.2	60.4	12.4	27.2	60.5
Abw					0	0
C1 - 1	100	19.7	65.8	14.6	19.3	64.6
C1 - 2	100	17.5	68.8	13.7	17.3	68
C2 - 1	100	17.4	68.2	14.4	17.5	68.6
C2 - 2					0	0
					0	0
					0	0
Pit 17					0	0
AB	100	8.0	78.5	13.5	8.1	79.3
B1					0	0
B2	100	9.6	77.6	12.8	9.8	79.4
B3	100	9.6	75.8	14.6	9.8	77.1
B4	100	7.5	76.4	16.2	7.3	74.7

Sample ID	Clay	Total	300 250 Medium	250 200 Medium	200 150 to	150 100 to	100 80 Fine
B2	37.6	83.2	0.2	0.2	0.5	1.9	2.1
B3	26.2	95.9	0.1	0.2	0.5	2.4	2.9
BC	57.5	87.9	0.1	0.2	0.4	1.2	1.4
C	54.7	84.8	0.2	0.2	0.5	1.5	1.7
	0	0					
	0	0					
Pit 14	0	0					
A	23.8	102.1	0.1	0.1	0.3	1.2	1.7
AB	28	98.1	0.1	0.1	0.1	0.6	1.1
B1	31.9	96.7	0.1	0.1	0.2	0.9	1.3
B2	29.8	94.4	0.1	0.2	0.3	0.9	1.2
BC1	23.7	93.8	0.1	0.1	0.3	1.1	1.5
BC2	0	0					
B2_rr	31.8	90.7	0	0.1	0.1	0.7	1.1
	0	0					
Pit 15	0	0					
A	15.7	93	0	0	0	0.5	0.9
AB	15.8	93.5	0	0	0.1	0.7	1
B1	16.7	93.7	0.1	0.1	0.2	0.7	1.1
B2	15.9	98.7	0.1	0.2	0.4	1.4	1.5
BC1	0	0					
BC2	6.5	90.7	0.5	0.6	1.2	4.4	3.8
BC2_rr	7.5	82.9	0.2	0.4	0.8	3.1	3.7
	0	0					
Pit 16	0	0					
A	0	0					
Aboxw	12.4	100.1	0.5	0.7	1.8	6.6	6.8
Abw	0	0					
C1 - 1	14.3	98.2	0.4	0.6	1.3	4.2	4.6
C1 - 2	13.5	98.8	0.3	0.4	0.8	3.4	4.2
C2 - 1	14.5	100.6	0.3	0.4	0.8	3.6	4.4
C2 - 2	0	0					
	0	0					
	0	0					
Pit 17	0	0					
AB	13.6	101	0.1	0.1	0.2	1.3	2
B1	0	0					
B2	13.1	102.3	0.1	0.1	0.3	1.8	2.4
B3	14.8	101.7	0.1	0.3	0.6	1.8	2.3
B4	15.8	97.8	0.1	0.1	0.1	0.8	1.7

Sample ID	80	60	50	40	30	25	20
	60	50	40	30	25	20	15
	Sand	Silt	Silt	Silt	Silt	Silt	Silt
B2	3.8	2.9	3.9	4.8	2.4	2.4	3.2
B3	5.4	3.9	4.9	6.1	3.7	4.4	5.2
BC	2.3	1.5	1.9	2.8	1.7	1.8	2.2
C	2.7	1.8	2.2	2.7	1.6	1.9	2.3
Pit 14							
A	3.9	3.5	5.3	8.5	6.2	8	10.1
AB	3	3	4.8	7.8	5.4	6.7	8.5
B1	3.1	2.7	4	6.3	4.5	6	7.9
B2	2.9	2.6	3.9	6.2	4.4	5.6	7.4
BC1	3.3	2.9	4.4	7.1	5	6.3	8.1
BC2							
B2_rr	2.5	2.1	3.3	5.2	3.7	4.8	6.5
Pit 15							
A	2.4	2.3	3.9	7.5	6.4	9	11.4
AB	2.2	2.1	3.8	7.6	6.4	9	11.7
B1	2.8	2.7	4.4	7.2	5.4	7.6	10.3
B2	2.5	1.7	3.1	7.9	7	9.3	11.8
BC1							
BC2	3.4	1.2	4.5	15.2	11.2	10.5	9.1
BC2_rr	7.5	5.9	7.7	9	5	6	7.4
Pit 16							
A							
Aboxw	10.8	6.9	8	9.6	5.6	6.1	6.3
Abw							
C1 - 1	8.2	5.8	7.6	10.2	6.2	6.8	7.4
C1 - 2	8.2	6.2	8.1	10.5	6.3	7.1	7.9
C2 - 1	8	5.8	7.7	10.2	6.2	7.4	8.4
C2 - 2							
Pit 17							
AB	4.4	4	6.4	10.7	7.7	9.5	11.1
B1							
B2	5.1	4.2	6.2	9.9	6.9	8.6	11
B3	4.7	3.9	6	9.3	6.4	8	10.3
B4	4.5	4.1	6.1	9.1	5.9	7.1	9.5

Sample ID	15 10 Silt	10 8 Silt	8 6 Silt	6 5 Silt	5 4 Silt	4 3 Clay	3 2 Clay
B2	5.7	3.3	3.8	2.1	2.4	3.4	5
B3	6	2.9	4.5	5.5	11.1	14.8	6.6
BC	3.2	1.8	2.7	2.1	3.1	4.6	7.6
C	2.9	1.7	2.3	1.6	2.3	3.5	5.9
Pit 14							
A	11.8	5	5.6	3.3	3.7	4.2	5
AB	10.8	5	5.7	3.4	4	4.7	5.5
B1	9.9	4.6	5.6	3.5	4.1	4.8	6
B2	10	4.9	5.9	3.7	4.4	5.1	6.2
BC1	10.8	5.3	6.2	3.6	4	4.3	4.8
BC2							
B2_rr	9.1	4.8	6.2	4	4.7	5.5	6.8
Pit 15							
A	13.1	5.9	6.5	3.6	3.9	4	4.5
AB	13.6	6	6.4	3.5	3.6	3.6	3.9
B1	13	6.2	7.1	3.9	4.2	4.4	4.6
B2	15.3	6.8	6.8	3.4	3.6	3.7	4
BC1							
BC2	9.4	3.7	3.2	1.2	1.1	1.1	1.4
BC2_rr	7.7	3	3.7	2.2	2.1	1.9	2.7
Pit 16							
A							
Aboxw	7.6	3.4	3.2	1.7	2.1	2.7	2.9
Abw							
C1 - 1	8.4	3.8	4	2.1	2.3	2.9	3.1
C1 - 2	9	3.9	4.2	2.3	2.5	2.9	3.1
C2 - 1	9.2	4.2	4.5	2.4	2.6	3	3.2
C2 - 2							
Pit 17							
AB	12.4	5.5	5.7	3	3.3	3.5	3.5
B1							
B2	13.6	6.1	6.4	3.2	3.3	3.4	3.2
B3	13.2	6.2	6.7	3.5	3.6	3.6	3.8
B4	12.8	6.2	6.6	3.5	3.8	4.3	4.6

Sample ID	**2**	**1.5**	**1**	**0.8**	**0.6**	**0.5**	**0.4**
	1.5	**1**	**0.8**	**0.6**	**0.5**	**0.4**	**0.3**
	Clay	**Clay**	**Clay**	**Clay**	**Clay**	**Clay**	**Clay**
B2	3.6	5.6	3.4	4.4	2.6	3.1	3.7
B3	0	0.2	0.4	0.8	0.6	0.9	1.2
BC	5.8	8.6	5.1	6.8	4.3	4.8	4.9
C	4.4	6.7	4.5	7	4.9	5.7	5.7
Pit 14							
A	2.9	3.4	1.7	2	1.1	1	0.8
AB	3.4	4.3	2.2	2.5	1.4	1.4	1.2
B1	3.9	4.9	2.3	2.7	1.6	1.7	1.5
B2	3.6	4.5	2.4	2.8	1.6	1.7	1.4
BC1	2.5	3.1	1.6	1.9	1.2	1.4	1.3
BC2							
B2_rr	4.1	5.1	2.4	2.6	1.5	1.8	1.6
Pit 15							
A	2.2	1.7	0.9	1	0.4	0.3	0.4
AB	2.1	2.5	1.2	0.9	0.4	0.3	0.3
B1	2.4	2.7	1	0.7	0.2	0.2	0.4
B2	2.2	2	0.7	0.7	0.3	0.2	0.3
BC1							
BC2	0.8	0.7	0.3	0.2	0.2	0.3	0.2
BC2_rr	1.7	0.9	0	0	0	0.2	0.1
Pit 16							
A							
Aboxw	1.2	0.9	0.3	0.9	0.7	0.8	1.1
Abw							
C1 - 1	1.3	1.6	0.5	0.5	0.5	0.7	0.9
C1 - 2	1.3	1.7	0.9	1	0.4	0.2	0.4
C2 - 1	1.5	1.4	0.6	0.7	0.6	0.9	1.2
C2 - 2							
Pit 17							
AB	1.6	2	1	0.9	0.3	0.2	0.3
B1							
B2	1.4	1.8	1.2	0.9	0.1	0	0.3
B3	1.8	1.6	1	1	0.2	0.1	0.6
B4	1.8	1.9	1	1.1	0.4	0.3	0.4

Sample ID	0.3 0.2 Clay	Total	Measured Original Wt.	Measured < 300um Wt.	>300um
B2	2.8	83.2	14.14	7.25	6.89
B3	0.7	95.9	15.62	6.63	8.99
BC	5	87.9	17.5	4.27	13.23
C	6.4	84.8	26.17	3.41	22.76
		0			0
		0			0
Pit 14		0			0
A	1.7	102.1	9.67	7.45	2.22
AB	1.4	98.1	10.91	6.51	4.4
B1	2.5	96.7	12.35	7.04	5.31
B2	0.5	94.4	14.46	6.79	7.67
BC1	1.6	93.8	14.68	6.58	8.1
BC2		0	12.28	5.19	7.09
B2_rr	0.4	90.7	10.62	6.67	3.95
		0			0
Pit 15		0			0
A	0.3	93	7.03	5.91	1.12
AB	0.6	93.5	7.54	6.35	1.19
B1	0.1	93.7	7.77	6.04	1.73
B2	1.8	98.7	9.22	6.56	2.66
BC1		0	12.25	6.75	5.5
BC2	1.3	90.7	12.52	6.91	5.61
BC2_rr	0	82.9	10.37	5.5	4.87
					0
		0			0
Pit 16		0			0
A		0			0
Aboxw	0.9	100.1	10.27	6.33	3.94
Abw		0	14.22	6.57	7.65
C1 - 1	2.3	98.2	13.83	7.41	6.42
C1 - 2	1.6	98.8	16.3	6.28	10.02
C2 - 1	1.4	100.6	12.71	6.94	5.77
C2 - 2		0	17.33	6.88	10.45
		0			0
		0			0
Pit 17		0			0
AB	0.3	101	9.32	6.83	2.49
B1		0	8.75	6.35	2.4
B2	0.8	102.3	8.49	6.19	2.3
B3	1.1	101.7	8.67	6.19	2.48
B4	0	97.8	9.36	6.01	3.35

Sample ID	Depth (Mid)	LOI	Total Sand % Percentages with >300 um sand added back in	Total Silt %	Total Clay %
Pit 18	Col-18				
A	4	15.99168			
AB	16	9.876411	46.7693356	34.45332198	18.77734242
B1	31	12.03369	53.79652897	34.79110289	11.41236814
B2	50	9.831084	48.04752824	40.89082108	11.06165069
Cr	70	12.37506			
Pit 19	LGM-19				
A	8	16.18863	36.90845372	45.26132668	17.8302196
AB	22	10.33304	41.70596709	35.60239594	22.69163697
B1	38	8.908453	43.0284899	36.12347763	20.84803246
B2	61	10.46722	46.08650741	37.28710939	16.6263832
B3	81	8.156607	48.45714869	37.38206794	14.16078336
BC	95	6.734632	57.64604811	0	

Sample ID	Total %	Sand <300 Silt Clay Percentages recalculated to equal 100%			Sand<300um Silt Sedigraph raw percentages	
					0	0
					0	0
Pit 18					0	0
A					0	0
AB	100	5.6	61.1	33.3	5.6	61.1
B1	100	12.5	65.9	21.6	11.9	62.8
B2	100	10.6	70.4	19.0	9.9	65.8
Cr					0	0
					0	0
					0	0
Pit 19					0	0
A	100	5.6	67.7	26.7	5.5	66
AB	100	7.6	56.4	36.0	7.4	54.6
B1	100	8.6	57.9	33.4	8.2	55.1
B2	100	9.0	63.0	28.1	8.7	61
B3	100	9.5	65.6	24.9	9	62.3
BC					0	0

Sample ID	Clay	Total	300 250 Medium	250 200 Medium to	200 150 to	150 100	100 80 Fine
	0	0					
	0	0					
Pit 18	0	0					
A	0	0					
AB	33.3	100	0	0.1	0.1	0.8	1.4
B1	20.6	95.3	0.2	0.3	0.5	2.2	2.8
B2	17.8	93.5	0.1	0.2	0.4	2	2.5
Cr	0	0					
	0	0					
	0	0					
Pit 19	0	0					
A	26	97.5	0.1	0.1	0.2	0.9	1.3
AB	34.8	96.8	0.1	0.1	0.3	1.3	1.8
B1	31.8	95.1	0.1	0.1	0.3	1.5	2.1
B2	27.2	96.9	0.1	0.1	0.3	1.7	2.2
B3	23.6	94.9	0	0.1	0.4	1.8	2.2
BC	0	0					

Sample ID	80	60	50	40	30	25	20
	60	50	40	30	25	20	15
	Sand	Silt	Silt	Silt	Silt	Silt	Silt
Pit 18							
A							
AB	3.2	2.8	4.1	6.6	4.6	5.8	7.7
B1	5.9	4.8	6.7	9.4	5.6	6.2	6.9
B2	4.7	3.6	5.4	8.6	5.9	6.8	8.1
Cr							
Pit 19							
A	2.9	2.6	4.2	7.6	5.8	7.5	9.3
AB	3.8	3	4.2	6	4.1	5.1	6.4
B1	4.1	3.2	4.5	6.3	4	4.8	6.3
B2	4.3	3.3	4.6	6.7	4.7	5.9	7.5
B3	4.5	3.9	5.3	6.8	4.2	5.6	7.8
BC							

Sample ID	15 10 Silt	10 8 Silt	8 6 Silt	6 5 Silt	5 4 Silt	4 3 Clay	3 2 Clay
Pit 18							
A							
AB	10.5	5.2	6	3.6	4.2	5	6.2
B1	8.5	4.1	4.6	2.8	3.2	3.6	4
B2	10.6	4.9	5.3	3.1	3.5	3.4	3.5
Cr							
Pit 19							
A	10.6	5.1	5.9	3.4	4	4.7	5.6
AB	8.3	4.6	5.5	3.3	4.1	5.2	6.6
B1	8.7	4.6	5.6	3.3	3.8	4.9	6.3
B2	10.1	5	5.9	3.4	3.9	4.7	5.5
B3	10.7	5.2	5.8	3.3	3.7	4.4	5.2
BC							

Sample ID	2	1.5	1	0.8	0.6	0.5	0.4
	1.5	1	0.8	0.6	0.5	0.4	0.3
	Clay	Clay	Clay	Clay	Clay	Clay	Clay
Pit 18							
A							
AB	3.8	4.8	2.3	2.6	1.5	1.6	1.9
B1	2	2.4	1.6	1.8	1	1.2	1.6
B2	1.9	2	1.3	1.3	0.7	1	1.5
Cr							
Pit 19							
A	3.1	4	1.9	1.9	0.9	0.9	1
AB	4	5.5	2.8	3	1.4	1.4	1.9
B1	3.9	5.1	2.7	3.1	1.5	1.4	1.4
B2	2.8	3.7	2	2.3	1.2	1.3	1.6
B3	2.5	3.4	1.8	1.9	0.9	0.8	1
BC							

Sample ID	**0.3**				
	0.2		**Measured**	**Measured**	
	Clay	**Total**	**Original Wt.**	**< 300um Wt.**	**>300um**
		0			0
		0			0
Pit 18		0			0
A		0	11.69	6.68	5.01
AB	3.6	100	11.74	6.62	5.12
B1	1.4	95.3	12.16	6.42	5.74
B2	1.2	93.5	12.03	6.99	5.04
Cr		0	11.05	5.89	5.16
		0			0
		0			0
Pit 19		0			0
A	2	97.5	10.17	6.8	3.37
AB	3	96.8	10.9	6.88	4.02
B1	1.5	95.1	10.65	6.64	4.01
B2	2.1	96.9	10.67	6.32	4.35
B3	1.7	94.9	10.73	6.11	4.62
BC		0	11.64	4.93	6.71
		0			
		0			

APPENDIX G – SOIL PROFILES

Photographs for all pit profiles examined in the field. The locations of all pits can be found in Johnson et al. (2010). The scale for all pictures in this appendix is centimeters. All description material can be found in Appendix E.

Pit 1 - Pgt

Pit 2 - Pgt

Pit 3 - PHcol

Pit 4 – PHaf1

Pit 5 – Haf2

Pit 6 – Hft2

Pit 7 – Pft1

Pit 8 - Pgt

Pit 9 – Hft2

Pit 10 – Haf2

Pit 11 - PHaf1

Pit 12 – Hft2

Pit 13 - LGM

Pit 14 - PHcol

Pit 15 – Haf2

Pit 16 – Haf2

Pit 17 - Pgt

Pit 18 - Pcol

Pit 19 - LGM